POLITECNICO
MILANO 1863

SCUOLA DI INGEGNERIA INDUSTRIALE
E DELL'INFORMAZIONE

End-to-end deep neural network and virtual sensing techniques: An Arterial blood pressure waveform reconstruction using Soundi® device

Tesi di Laurea Magistrale in
Biomedical Engineering - Ingegneria Biomedica

Author: **Federico Petraccia**

Student ID: 952887
Advisor: Prof. Pietro Cerveri
Co-advisors: Ing. Mattia Sarti
Academic Year: 2022-23

Abstract

Arterial pressure is a physiologically significant parameter in monitoring human health. It provides crucial insights into the functioning of the cardiovascular system and can reveal pathological conditions such as hypertension, hypotension, and other related diseases. This is a key factor in preventing cardiovascular diseases. It is often referred to as a "silent killer" since it does not cause visible symptoms but can lead to premature death. Significant efforts are being directed towards studying new techniques that allow for simple monitoring of these parameters due to the difficulties associated with traditional invasive and non-invasive monitoring methods. Traditionally, arterial pressure measurement has been performed using non-invasive devices, such as mercury manometers or sphygmomanometers. However, these methods have limitations in terms of practicality and the ability to continuously monitor pressure. In recent years, the advent of artificial neural networks and machine learning has opened up new perspectives in the non-invasive prediction and monitoring of arterial pressure. Deep Neural Networks (DNNs) are particularly suited to handle complex data and learn patterns from physiological signals. In this study, deep learning-based neural networks are employed to create an end-to-end approach for arterial pressure monitoring using a set of signals recorded with the Soundi® device. This allows for the acquisition of a dataset comprising physiological signals including Photoplethysmography (PPG), Phonocardiogram (PCG), Electrocardiogram (ECG), and Seismocardiogram (SCG) without the need for initial subject calibration. Consequently, a dataset consisting of recordings from 25 subjects is created, which is utilized to train three different DNN models: U-Net, GRU, and 3GRU-Net. Specifically, a subject-dependent analysis is conducted using only the recordings subject00. Among the proposed models, the 3GRU-Net model exhibits the best performance. It incorporates three different encoder branches, which account for the varying frequency content of the input signals, resulting in superior arterial pressure waveform reconstruction. It achieves a mean absolute error of 10.5 mmHg, while the U-Net and GRU-Net models achieve mean absolute errors of 11.5 mmHg and 11.31 mmHg, respectively. Comparing these results to a regression model based on specifically calculated Pulse Transit Time (PTT), the Deep Neural Networks models demonstrate significantly better performance, as the mathemat-

ical model yields considerably higher mean absolute errors. The great advantage of this technique concerns its ability to avoid the initial calibration performed on the subject, as is done with classical mathematical methods, thus opening the doors to a possible subject-independent analysis. For this analysis, a model with three different branches, 3GRU-ResNet, is used, yielding mean absolute error values of 15.583 mmHg. The calculation of the BHS index reveals that the models perform reasonably well in reproducing the waveform for subject-dependent studies but fail in subject-independent studies, showing considerably lower percentages. Through the utilization of this technique, it becomes possible to establish a novel approach to arterial pressure monitoring that does not require initial calibration during the recording phase and eliminates the preprocessing steps necessary in the implementation of classical mathematical models based on Pulse Wave Velocity.

Keywords: Deep Learning, End-to-end, PPG, Arterial Blood Pressure, soundi®, 3GRU-Net, GRU-Net

Abstract in lingua italiana

La pressione arteriosa è un parametro fisiologicamente significativo nel monitoraggio della salute umana. Fornisce indicazioni cruciali sul funzionamento del sistema cardiovascolare e può rivelare condizioni patologiche come l'ipertensione, l'ipotensione e altre malattie correlate. Questo è un fattore chiave nella prevenzione delle malattie cardiovascolari. Spesso viene definita come un "killer silenzioso" poiché non causa sintomi visibili ma può portare a morte prematura. Sono stati compiuti sforzi significativi nello studio di nuove tecniche che consentano il monitoraggio semplice di questi parametri a causa delle difficoltà associate ai metodi tradizionali di monitoraggio invasivo e non invasive. Tradizionalmente, la misurazione della pressione arteriosa è stata effettuata utilizzando dispositivi non-invasivi come i manometri a mercurio o gli sfigmomanometri. Tuttavia, questi metodi presentano limitazioni in termini di praticità e possibilità di monitorare la pressione in maniera continua. Negli ultimi anni, l'avvento delle reti neurali artificiali e dell'apprendimento automatico ha aperto nuove prospettive nella previsione e nel monitoraggio non invasivo della pressione arteriosa. Le Reti neurali profonde (DNN) sono particolarmente adatte per gestire dati complessi e apprendere modelli dai segnali fisiologici. L'uso del deep learning ha acquisito una rilevanza sempre maggiore nella medicina moderna, specialmente nel campo dell'imaging medico, dove è diventato uno strumento chiave per il supporto diagnostico. In questo studio, sono impiegate reti neurali basate su apprendimento profondo per creare un approccio end-to-end per il monitoraggio della pressione arteriosa utilizzando un insieme di segnali registrati con il dispositivo soundi®. Questo consente l'acquisizione di un insieme di segnali fisiologici tra cui la Fotopletismografia (PPG), la Fonocardiografia (PCG), l'Elettrocardiografia (ECG) e la Seismocardiografia (SCG), senza la necessità di una calibrazione iniziale sul soggetto. In questo modo è stato realizzato un dataset composto dalle registrazioni di 25 soggetti, utilizzato per trainare i tre differenti modelli di DNN proposti: U-Net, GRU, 3GRU-Net. In particolare viene effettuata un analisi Soggetto-dipendente, utilizzando unicamente le registrazioni del soggetto00. Dei modelli proposti, le performance migliori sono raggiunte dal modello 3GRU-Net, che presenta tre divversi rami di encoder che tengono conto del diverso contenuto in frequenza dei segnali in input, ottenendo risultati migliori nella ricostruzione della waveform di pressione arte-

riosa. Infatti raggiunge valori di errore medio assoluto pari a 10.5 mmHg, mentre con gli altri due modelli si raggiungono valori di 11.5 mmHg per la U-Net e 11.31 mmHg per la GRU-Net. Confrontanto questi risultati anche un modello regressivo basato su PTT appositamente calcolato, si vede come le prestazioni delle DNN siano notevolmente migliori, infatti con il modello matematico si ottengono errori medi assoluti notevolmente più alti. Il grande vantaggio di questa tecnica riguarda la capacità di evitare la calibrazione iniziale effettuata sul soggetto, come avviene con il classici metodi matematici, aprendo le porte ad una possibile analisi soggetto-indipendente. Per questa analisi viene utilizzato il modello con tre differenti branch, 3GRU-ResNet, con cui si ottengono valori di mean absolute error pari a 15.583 mmHg. Il calcolo dell'indice BHS mostra come i modelli riescano abbastanza bene nella riproduzione della waveform per uno studio soggetto-dipendente ma falliscono per uno studio soggetto-indipendente avendo percentuali decisamente inferiori. Grazie all'utilizzo di questa tecnica è possibile realizzare un nuovo approccio di monitoraggio della pressione arteriosa, che non richieda una calibrazione iniziale durante la fase di recording e che eviti la parte di preprocessing necessaria nell'implementazione dei classici modelli matematici basati su la velocità di propagazione dell'onda di polso (PWV).

Keywords: Deep Learning, End-to-end, PPG, Arterial Blood Pressure, soundi®, 3GRU-Net, GRU-Net

Contents

1 | Introduction

1.1. Arterial Blood Pressure

Continuous blood pressure monitoring is an important tool for assessing hypertension, which is one of the major risk factors for cardiovascular disease (CVD). Blood pressure variability is also an important indicator associated with risky cardiovascular events. Studies have shown that hypertension often goes undetected because it is a "silent killer", meaning that it has no visible symptoms but can lead to premature death. According to the World Health Organization, hypertension represents a global public health crisis, and more than 4 million people die of cardiovascular diseases every year only in Europe, with more than 17 million worldwide [4, 14]. Therefore, early detection and continuous monitoring of blood pressure can be essential in preventing cardiovascular diseases and saving lives.

1.1.1. Traditional monitoring techniques

There are two clinical gold standards available to measure arterial blood pressure [31]:

- **Invasive catheter system:** The invasive catheter system, illustrated in Figure 1.1 involves the insertion of a catheter into an artery and is primarily used in intensive care units to accurately monitor blood pressure and obtain arterial blood gas samples. This procedure can be performed only by physicians and specialized nurses and is often painful despite the use of anesthetics to alleviate discomfort and prevent vasospasm.

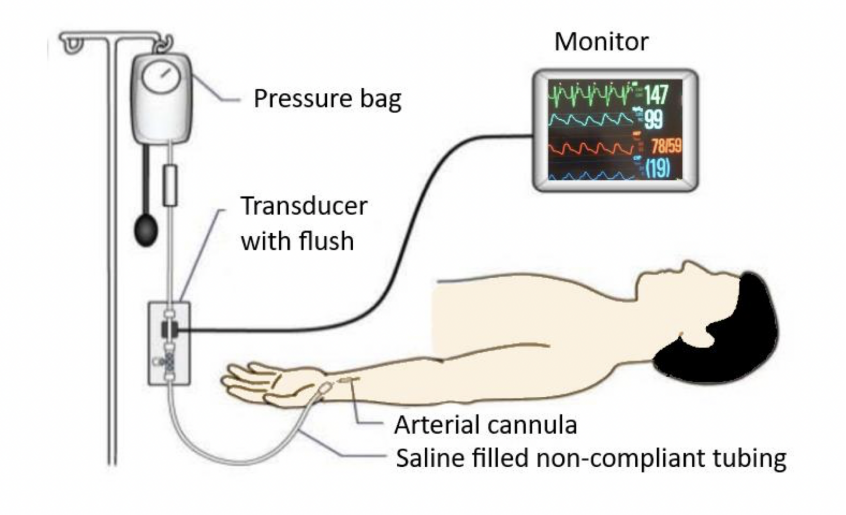

Figure 1.1: ABP monitoring with invasive technique

- **Noninvasive sphygmomanometer-based cuff:** Intermittent blood pressure monitoring, illustrated in figure Figure 1.2, a sphygmomanometer, which is an arm cuff that occludes artery, is used. Blood pressure can be obtained manually by auscultation of Korotkoff sounds or palpation, or automatically through oscillometry. The Holter blood pressure monitor (HBPM) allows for periodic readings at intervals of 15 or 30 minutes over a duration of up to 48 hours. Although cuff-based devices are commonly recommended by physicians, due to their high accuracy in indirectly measuring blood pressure, they have some drawbacks: one limitation is that the cuff sizes are often too small, which can result in diagnostic errors [48, 49]. Additionally, these devices require active mechanical stimulation, wired connections, and expensive equipment, which can limit their usefulness for daily activities and overnight monitoring [53].

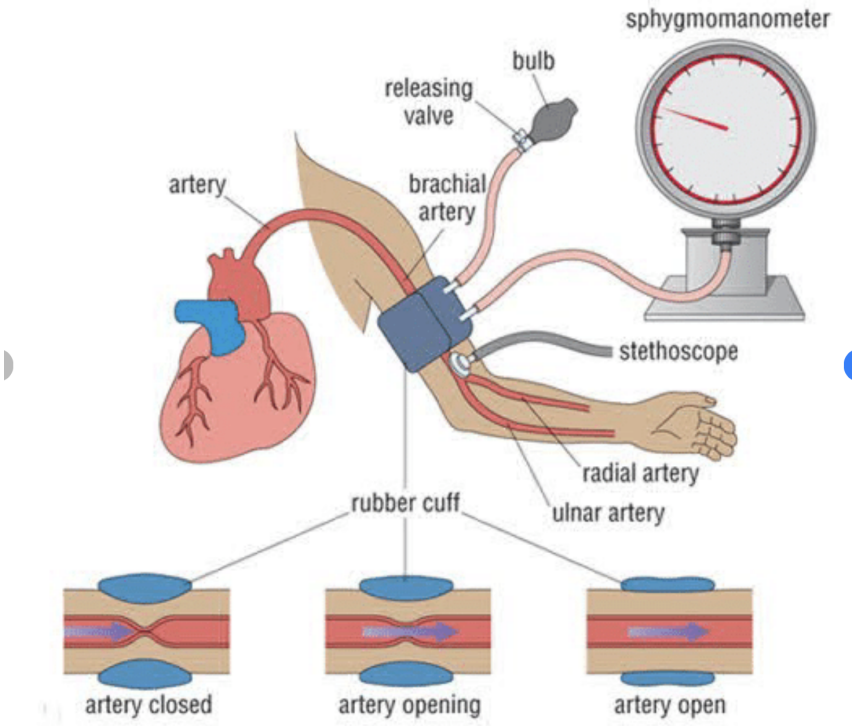

Figure 1.2: Noninvasive sphygmomanometer-based cuff

1.2. Non-invasive techniques

Recently, the introduction of wearable devices capable of unobtrusively measuring electrocardiographic (ECG), photoplethysmography (PPG), Phonocardiogram (PCG), and Seismocardiograph (SCG) signals have significantly improved non-invasive blood pressure monitoring [7, 11, 12]: the calculation of ABP using these signals is a key focus of research. Several studies have addressed this problem using a range of techniques, with the majority utilizing PPG either alone or in combination with other biological signals like ECG. Many techniques are related to the calculation of physiological parameters from the pressure signal, such as systolic, diastolic, and mean pressure. Many of these do not involve waveform processing. There are three main techniques for the reconstruction of the arterial blood pressure waveform:

- Pressure-Based Method
- Ultrasound-Based Method
- Deep-Learning-Based Methods

1.2.1. Pressure-Based Method

In the literature, two main pressure-based techniques can be found for the reconstruction of the arterial blood pressure waveform:

- **Volume clamp method:** This technique, also known as the Vascular Unloading Technique, is based on the method developed by Penaz (Penaz, 1992) that allows for the calculation of the arterial pressure waveform by linearizing the internal pressure using an external transducer, thereby maintaining a constant volume at the measurement point. Instruments based on this measurement method utilize a cuff and a plethysmographic sensor for monitoring blood volume through PPG (Photoplethysmography). The cuff is applied to the finger and contains an internal plethysmograph, connected to an external microcontroller that regulates the cuff pressure. During the systolic phase, the blood volume in the finger increases, and the microcontroller increases the cuff pressure. During the diastolic phase, the cuff pressure decreases. This keeps the PPG signal constant and equalizes the internal pressure. A manometer is used to continuously measure the pressure on the cuff, enabling the tracking of the arterial pressure signal. An example is shown in Figure 1.3a. This technique allows for continuous non-invasive monitoring of pressure and waveform reproduction, and it is employed by many commercial devices. However, it has certain limitations associated with the measurement procedure and the cuff, such as skin temperature, density, and finger size, which can affect the calculation parameters of the pressure

- **Arterial Tonometry:** Arterial tonometry is a technique used to measure arterial pressure in a non-invasive manner. In this technique, a pressure sensor is applied to a superficial artery, usually the radial artery, and the pulsatile pressure signal is recorded during the cardiac cycle. The pressure signal is then processed to obtain various parameters, including systolic, diastolic, and mean pressure. The most common technique is called Applanation Tonometry, where pressure is applied to the radial artery using a tonometer, and the arterial pressure signal is reconstructed using pressure sensors such as strain gauges or piezoelectric sensors. The pressure due to the opening and closing of the cardiac valves is calculated from the reflected waves. Once the pressure is applied and the tonometer is stabilized as shown in Figure 1.3b, the pressure applied by the deformation of the arterial walls is converted into an electrical signal by the strain gauges located at the tip of the device, thus recording the arterial pressure signal. This technique does not require the use of a cuff and is therefore less sensitive to geometric constraints compared to a volume

clamp. However, it is difficult to apply in overweight individuals and requires the subject to remain still during the measurement.

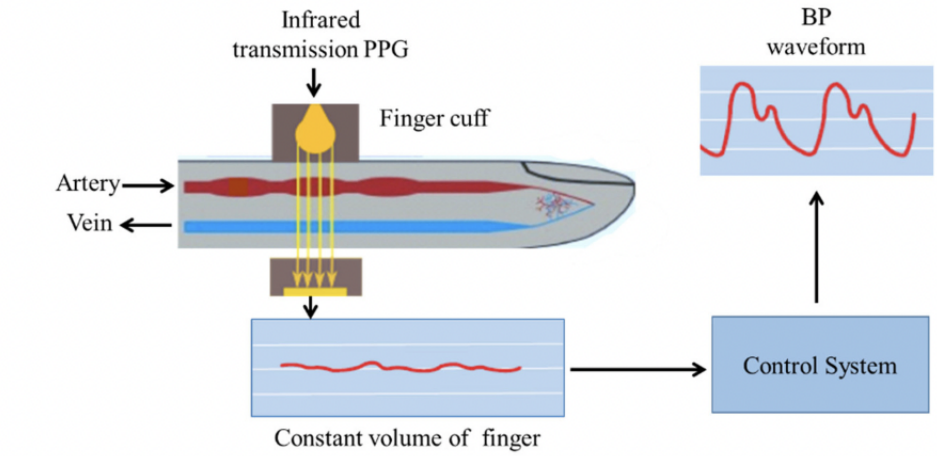

(a) Volume Clamp Prcedure.

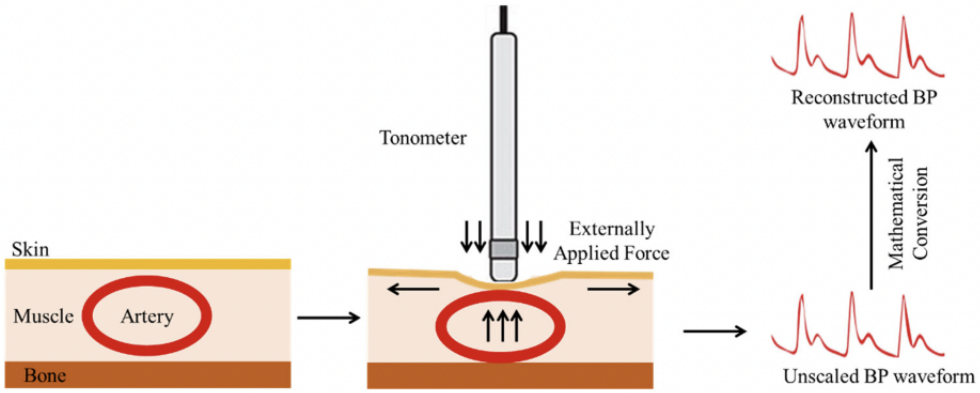

(b) Tonometry procedure.

Figure 1.3: a) Volume Clamp Procedure for ABP waveform extraction, b) Tonometry-based Procedure

1.2.2. Deep Learning and Mathematical approach

Research also have investigated the relationship between the rate of blood flow and blood pressure, with Pulse Wave Velocity (PWV) being a popular parameter for assessing blood flow rate. PWV determines the time delay required for blood pulses to reach the periphery of the body from the heart, which is referred to as Pulse Transit Time (PTT) Defined as the temporal distance between the R peak of the ECG and the peak of the PPG. Pulse

Arrival Time (PAT) and Pre-Ejection Period (PEP) are other PPG fiducial points, in particular, PEP is the time between the electrical systole (ECG Q wave) and the initial opening of the aortic valve. Mathematical models have been developed based on these parameters to estimate blood pressure values. On the other hand, PAT is defined as the sum of PTT and PEP. [2, 9, 10, 39, 50, 55]. Other non-invasive methods utilize physiological quantities such as the R-wave peak detected in ECG or cardiac sounds detected from PCG. The first cardiac sound (S1) has been proposed as a proximal timing for PTT estimation to avoid the pre-ejection period (PEP). For the distal timing, fiducial points such as the foot, the maximum slope, and the systolic peak detected in the PPG waveform may be used. Several models have been studied to relate blood pressure to PTT, including inverse models and analytical functions, particularly the Moens-Korteweg (M-K) model. Accurate identification of events and fiducial points in signals is critical to ensuring reliable estimates of BP-related parameters [16, 33, 36]. For an estimation of BP-related parameters, it is essential to accurately and automatically identify events and fiducial points in signals. Nevertheless, traditional algorithmic methods have been widely documented to fail due to their sensitivity to noise, inter-subject and pathological variability [11, 23]. To accurately compute these features, algorithms typically require the signals to be in near-ideal condition at all times, which is not practical. In recent years, a few studies have attempted to address these issues by utilizing various deep learning techniques, such as 1D segmentation [29, 43], variational autoencoders (VAEs) [37], and CycleGAN [45], to estimate or reconstruct arterial blood pressure (ABP) waveforms from PPG and/or ECG signals. Thus using raw physiological signals as inputs for deep networks it is possible to directly generate continuous systolic and diastolic pressure outputs or try to reconstruct the entire waveform of ABP [29, 43]. Leveraging the deep end-to-end network paradigm, non-invasive blood pressure assessment has been reframed as a regression problem to determine the complete waveform of arterial blood pressure from network outputs. To achieve this, a sensor-fusion approach was pursued by utilizing various signals including ECG, PPG, PCG, SCG, and bioimpedance along with body and ambient temperature signals, which were all captured by a chest-worn device. The deep network was then trained to produce brachial BP time series outputs using reference waveforms obtained from the Finometer® device (Finapres Medical Systems BV, NL). The network's performance was tested on a cohort of 25 healthy adult subjects, who underwent an alternating rest-cycling protocol that lasted 30 seconds.

1.3. Background

In literature, three different cuff-less and non-invasive techniques have been found, which aim to reconstruct Blood Pressure:

1. Techniques that use mathematical or regression models to reconstruct systolic and diastolic values based on specific parameters including PTT and PAT, in combination with HR fiducial points.
2. Techniques that rely on the use of machine learning models to predict systolic and diastolic pressure, extracting morphological features from the signal. These techniques mainly use PPG.
3. Instead a new approach is based on deep learning and refers to the use of CNN and RNN in order to predict Systolic and Diastolic Blood pressure, directly employing raw signals. They are also able to reconstruct the entire waveform performing continuous monitoring.

1.3.1. Model-based techniques

Model-based techniques are the most explored field of ABP reconstruction, and it is based on the use of mathematical models to reconstruct the values of systolic and diastolic pressure. Among the most commonly used techniques, there are adaptive filtering techniques like Kalman filters, gradient-based analysis, and peak detection [5, 13, 47, 55]. For each method, it is required to select some fiducial point, as in the research of Zhou et al. [55] in which after the selection of the peak of PPG and ECG compute the parameters used in the tested models reported in the study. The statement suggests that certain techniques used in physiological signal processing, such as those based on the correlation between the amplitude and frequency of signals and noise, may not always work effectively when there are systematic perturbations. Zhou et al. [55] and colleagues mentioned that in some studies this type of approach has been found to be unsuccessful. This highlights the importance of developing more robust and adaptable techniques that can handle various types of noise and perturbations, such as machine learning-based methods.

1.3.2. Feature-based techniques

The featured-based procedure is based on the study of the PPG waveform and enables the extraction of various morphological features from the signal, such as [24]:

- **Time domain features**: systole and diastole pack, PPT, Dicrotic Notch, and Inflection Point for the PPG;
- **Frequency domain features**: amplitude and phase of the PPG peak, Power spectrum energy;
- **Statistical features**: Mean, standard deviation, and entropy;
- **Physical features**: height, weight, BMI, HR.

After an extensive pre-processing procedure to extract these features, machine learning models such as Decision trees, Support Vector Machine (SVM), or regression algorithms are trained to predict and reconstruct ABP values, specifically the three values of SBP, DBP, and MAP. This techniques also achieve excellent results, but as reported by Hartmann et al. [23], there are some disadvantages in using the PPG signal, especially due to intra-subject variability conditions such as skin color, physical state, and age of the subjects involved. However, there are issues also with the repeatability of the measurements due to the high correlation between noise introduced by motion and PPG quality, which does not cause flattening of the end of the diastolic phase, but increases the variability of the waveform parameters [21, 34].

1.3.3. End-to-end techniques

"End-to-end" techniques in deep learning refer to the approach of training a single deep neural network model to solve an entire problem, from input data to the desired final output, without the need for using different phases or intermediate models for data pre-processing or post-processing. In other words, the neural network model is trained to learn the input data representations autonomously, without the need for manually engineered features. This approach can simplify the process of model development and training, reduce computational complexity, and improve the overall performance of the system. Research is heading towards this approach which involves a smarter procedure compared to other sophisticated techniques, thus finding a solution to the problems related to the identification of fiducial points and the variability of parameters extracted from morphological analysis. This approach aims to use raw signals, such as only PPG [29, 38] or a bank of raw signals (e.g. PPG and ECG) [8], as input for a deep learning model. In particular, there is the widespread use of networks based on Recurrent Neural Networks (RNN), 1D Convolutional Neural Networks (CNN), Generative Adversarial Networks (GAN), and Autoencoders [6, 14].

1.4. Work contribution

The focus of this study is to introduce a technique for reconstructing the waveform of a pressure signal. To accomplish this, a deep-learning neural network is employed, utilizing a bank of raw signals as its input. The proposed method following the proposed pipeline Figure 1.4 consists of three models that employ both CNN and Gated Recurrent Unit techniques, ultimately creating a GRU-Net. The following are the primary accomplishments of this research:

- demonstration of the complete end-to-end approach to estimate the entire BP waveform
- implementation of a multi-task network predicting the arterial BP exploiting raw physiological signals
- exploitation of sensor-fusion to take advantage of signal redundancy
- comparison with a simple regression model based on Pulse Transit Time (PTT) which is the most popular model for the mathematical computation of arterial blood pressure.

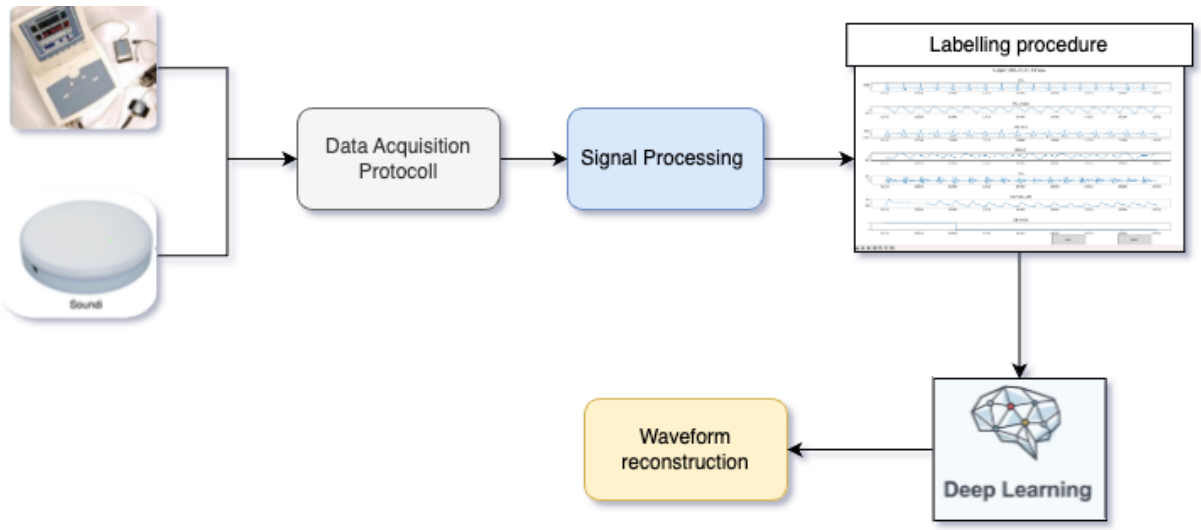

Figure 1.4: Project pipeline

2 | Objectives of the Study

The project was developed in collaboration with Biocubica, the developer of the Soundi® device used for data acquisition, and with Eng. Mattia Sarti for the development of DNN. The device was designed for studying and identifying sleep disorders, enabling overnight data collection. It allows the recording of various physiological and non-physiological signals, which are stored on a micro-USB and subsequently processed. The objective of the study is to create a deep neural network model for the calculation of ABP (Arterial Blood Pressure) waveforms, as well as the main parameters of interest such as SBP (Systolic Blood Pressure), DBP (Diastolic Blood Pressure), and MAP (Mean Arterial Pressure). This approach helps reduce the signal preprocessing phase and the identification of key points of interest required for the development of classical mathematical models based on parameters like PTT (Pulse Transit Time) and PWT (Pulse Wave Transit). Additionally, the unique aspect of this project is that it doesn't solely rely on PPG (Photoplethysmography) and ECG (Electrocardiography) signals, as seen in most recent deep neural network studies. Instead, a range of physiological and non-physiological signals recorded using the Soundi® device is utilized. This technique can leave to the elimination of the calibration phase for ABP monitoring, indeed after the training of the model the network can compute the principal ABP parameters from the reconstructed waveform in a continuous manner without a calibration phase that is not necessary for the device. The proposal involves constructing a new network architecture based on the widely used U-Net in the medical field. Two new models are suggested and compared to the conventional U-Net to evaluate the reconstructive capabilities of the developed model.

3 | Material and Methods

3.1. Soundi®

The device utilized for signal acquisition in this study is Soundi®, a chest-worn sensor developed by Biocubica Srl (Milan, Italy) Figure 3.1. It is capable of simultaneously recording multiple physiological signals, including electrocardiographic, photoplethysmographic, acoustic, accelerometer, bioimpedance, and temperature (both body surface and ambient) for up to 24 hours. The device has a circular shape with a diameter of less than 6 cm and a thickness of approximately 1 cm, weighing no more than 40 grams. It is currently undergoing the CE marking procedure to become a certified medical device of class II, and it has been patented at the European level (Patent No. EP3248541A1). To ensure secure attachment to the chest during use, the device uses medically certified double-sided tape.

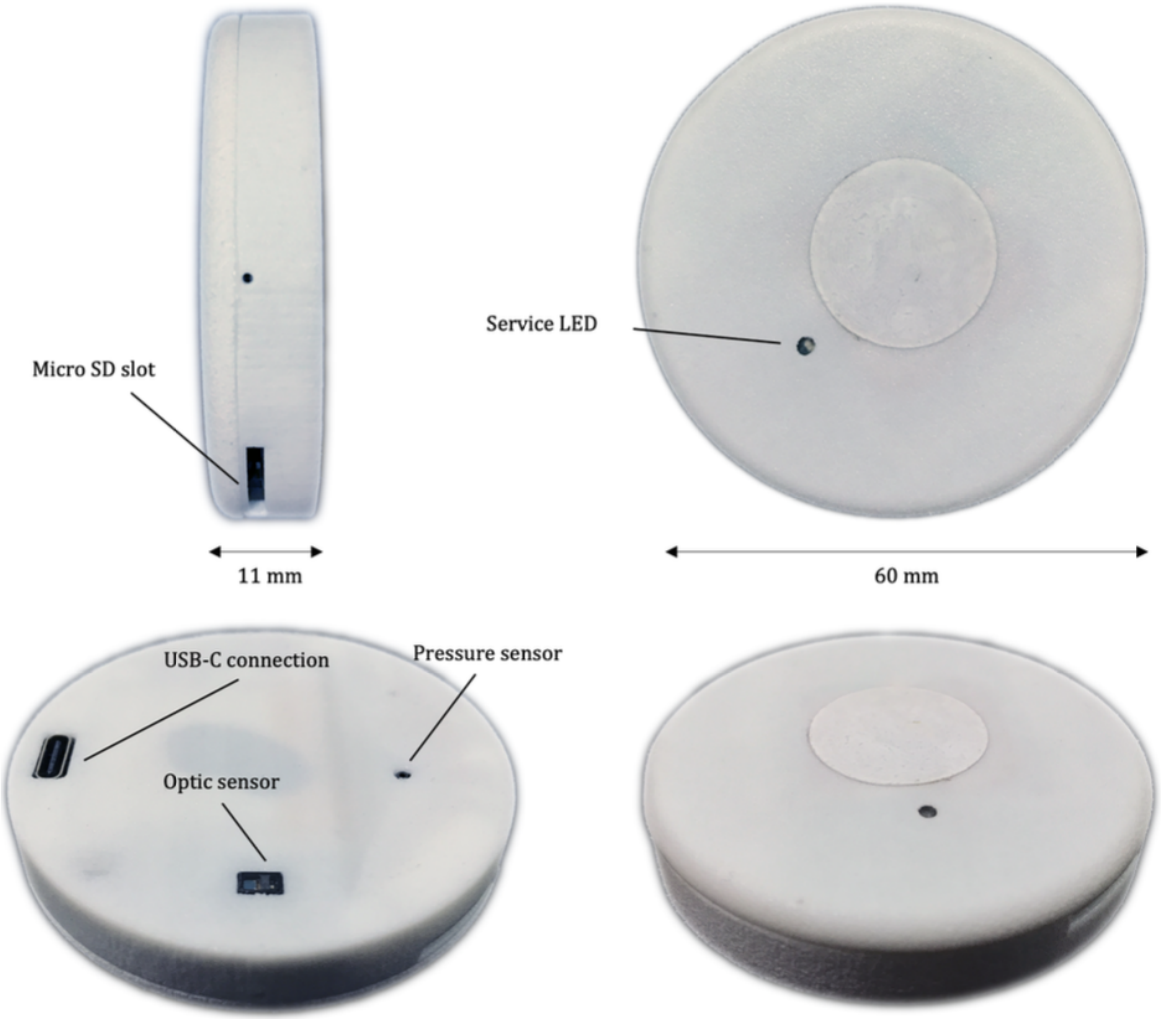

Figure 3.1: Soundi® device and its sensors.

Sensor	**Model**	**Additional info**	**Sampling frequencies (Hz)**
Three-axis accelerometer	BHI160B (Bosh®)		100
Optic sensor	MAXM86161 (Maxim Integrated ®)	Red ($\lambda = 650$ nm) Infrared ($\lambda = 940$ nm) Green ($\lambda = 525$ nm) with 1 photodetector	25
Pressure	SDP32 (Sensirion®)		400

Table 3.1: Soundi's sensors characteristics

in Table 3.1 are displayed the main sensors used by the device to extract the signals. The plethysmographic sensor, which has its characteristics illustrated in Table 3.1, uses the principle of optical reflection to calculate the R parameter and extract the plethysmographic signals from the 3 channels. The PPG waveform exhibits an upward trend in response to increased capillary blood volume resulting from cardiac contraction, and a downward trend in response to decreased capillary blood volume caused by cardiac dilation. This pattern is repeated with each cardiac cycle, where the ascending curve represents the systolic phase of the PPG waveform, while the descending curve represents the diastolic phase of the PPG waveform [42]. Air pressure signals are used to detect heart sounds in order to eliminate ambient noise from the chest. The initial heart sound (S1) is produced by the closure of the mitral and tricuspid (atrioventricular) valves and occurs at the start of ventricular systole. The second sound (S2) is generated by the closure of the aortic and pulmonary valves and takes place at the end of the systolic and diastolic phases [22]. The ECG and Bioimpedance signals indeed are extracted using external electrodes attached respectively to the ankle and on the upper chest part, connected through a jack to the device.

3.2. Finapres Finometer® PRO

The Finapres Medical Systems BV (NL) provides a medically certified device called the Finometer Finapres PRO figure 3.2 and 3.3, which estimates continuous signals in a pulsatile manner of the blood pressure using a finger cuff. Finometer® to reconstruct the waveform use the so-called Volume-Clamp tecnique developed originally by Pena [44]. This equipment was used in the research study to collect reference blood pressure waveforms for training the deep network and validating model predictions. Additionally, the Finometer Finapres PRO device provides hemodynamic parameters such as stroke volume, total peripheral resistance, cardiac output, pulse rate variability, and baroreflex sensitivity analysis. To ensure accuracy, the reconstructed blood pressure was calibrated at set intervals against brachial measurements using an upper arm cuff [3]. For other information about the Finapress Finometer ® Pro refer to Tables 3.2 and 3.3

Figure 3.2: Finapres® device for ABP monitoring

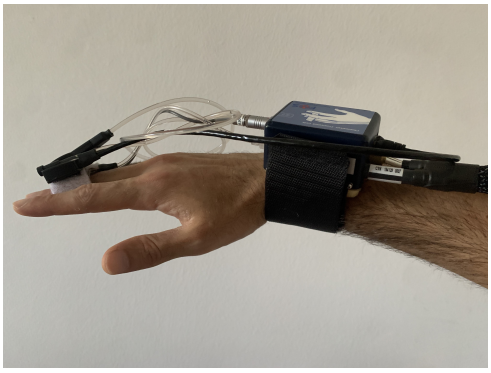

Figure 3.3: Cuff sensor for ABP finger acquisition by plethysmographic sensor

Features	Description
Category	Digital beat-to-beat blood pressure measuring device
Measurement method	The arterial volume-clamp method by J. Peñáz, Physical criteria by K.H. Wesseling, Brachial waveform reconstruction by Bos, Gizdulich, and Wesseling, and the Modelflow method by Wesseling.
Finger cuff pressure	Max 350 mmHg
Weight of the finger cuff	18-23 g
Arm cuff pressure	Max 300 mmHg
The dimensions and weight of the arm cuff	12 x 18 cm, 270 g (cuff Speidel and Keller)
Height sensor	interval: $\pm 128\ mmHg$

Table 3.2: General characteristics.

Accuracy	
Digital Pressure	1%(max 3 mmHg), automatic zero
Brachial pressure	1% (max 3 mmHg), automatic zero
Height corrector	2% (max 3 mmHg), Manual zero
Frequency	(frequency [bpm] / 60)%, 1% at 60 bpm
Interbeat interval	10 ms (On the peak, non-cumulative)
The dimensions and weight of the arm cuff	12 x 18 cm, 270 g (cuff Speidel and Keller)
Height sensor	interval: $\pm 128\ mmHg$

Table 3.3: Accuracy characteristics.

3.3. Software

The presented study was fully implemented using Python 3.7 programming language. The use of a single High-level language, allowed for a unified workflow for all the tools required by the project. Moreover, Python is an open-source language, widely supported by a range of libraries and modules, including Keras, TensorFlow, Scikit-learn, NumPy, Pandas, SciPy, Plotly, and Matplotlib, which were utilized in this project for machine learning and artificial intelligence procedures, high-performance data analysis and dataframe manipulation, advanced computing in signal processing and mathematics, as well as data visualization and interactive figure creation. Since the work was conducted in collaboration, GitHub was used for shared files and update management.

3.4. Acquisition protocol

This study recruited 25 healthy adult volunteers who had no prior clinical conditions of the cardiovascular system. The participants had an average age of 28 years old, with weights and heights ranging respectively from 53-96 kg and 160-201 cm, the Metadata and subject information are illustrated in Figure 3.4. Here are reported the Subject ID, gender, weight, height of each subject, and the achieved pedal speed during the pedaling phase. The study was conducted following the experimental protocol (Opinion 3/2019, dated February 19th, 2019), which received approval from the Politecnico di Milano Ethical Committee. The protocol involved a single 30-minute signal acquisition phase where the subjects wore a Finometer cuff on the finger of their dominant hand, and the Soundi® system was attached to their chest surface. Three electrodes were placed on the thorax surface of each subject, like in Figure 3.5, and connected to the Soundi® to record the

II-lead ECG and bioimpedance signals. The protocol consisted of 5 different periods, including rest and pedaling periods to induce blood pressure variations due to physical exercise:

Subject code	¿/Gen	Age	ght (	ight (	Date of Acquisition	Physical training	Average Speed
Subject_000	M	53	190	92	14/11/2022	Medium	23
Subject_000	M	53	190	92	23/12/2022	Medium	22
Subject_000	M	53	190	92	20/1/2023	Medium	20
Subject_000	M	53	190	92	21/1/2023	Medium	20
Subject_000	M	53	190	92	31/1/2023	Medium	20
Subject_000	M	53	190	92	10/3/2023	Medium	20
Subject_000	M	54	190	94	28/4/2023	Medium	20
Subject_001	F	28	169	50	14/11/2022	Low	21
Subject_002	M	27	179	68	14/11/2022	Low	22
Subject_002	M	27	179	68	20/1/2023	Low	22
Subject_002	M	27	179	68	10/3/2023	Low	22
Subject_003	F	31	154	55	15/11/2022	Low	17
Subject_004	F	25	163	63	16/11/2022	Low	22
Subject_005	M	24	172	72	14/11/2022	Medium	23
Subject_005	M	24	172	72	14/2/2023	Medium	18
Subject_006	M	24	201	96	16/11/2022	High	24
Subject_007	F	21	178	80	16/11/2022	Medium	23
Subject_008	F	26	163	50	16/11/2022	Low	20
Subject_009	M	24	183	75	16/11/2022	Medium	25
Subject_010	M	23	181	72	16/11/2022	Medium	20
Subject_011	M	24	185	75	17/11/2022	Low	23
Subject_012	M	25	185	75	18/11/2022	Medium	24
Subject_012	M	25	185	75	7/3/2023	Medium	20
Subject_013	M	23	162	70	18/11/2022	Medium	23
Subject_014	M	26	182	86	18/11/2022	Low	20
Subject_014	M	26	182	86	23/12/2022	Low	20
Subject_015	M	26	181	78	22/11/2022	High	20
Subject_015	M	26	181	78	14/2/2023	High	16
Subject_016	M	26	185	82	12/1/2023	High	20
Subject_017	M	25	180	63	12/1/2023	Medium	20
Subject_017	M	25	180	63	9/3/2023	Medium	20
Subject_018	F	26	160	56	13/1/2023	Low	20
Subject_019	F	39	170	59	26/1/2023	Medium	18
Subject_019	F	39	170	59	21/2/2023	Medium	20
Subject_019	F	39	170	59	30/3/2023	Medium	20
Subject_020	M	26	170	68	27/1/2023	Low	19
Subject_021	M	29	183	82	15/2/2023	Medium	20
Subject_022	M	25	170	55	20/2/2023	Low	20
Subject_023	M	25	175	54	1/3/2023	Low	20
Subject_024	M	25	174	87	7/3/2023	Low	18
Subject_025	F	34	167	78	14/4/2023	Medium	20

Figure 3.4: Metadata of enrolled subjects for experimental protocol

1. 5 minutes rest.
2. 10 minutes pedaling.
3. 5 minutes rest.
4. 5 minutes pedaling.
5. 5 minutes rest.

Before the tests, all participants were provided with detailed information about the experimental sessions, and they were asked to sign an informed consent form. During the entire acquisition duration, both devices continuously and simultaneously acquired physiological signals. Synchronization was ensured via a repeated digital pulse signal generated during the first 30 and the last 30 seconds of the acquisition by the master computer and recorded by both devices. The Finometer device is able to record finger and brachial arterial pressures, but in this study, we use only the first one.

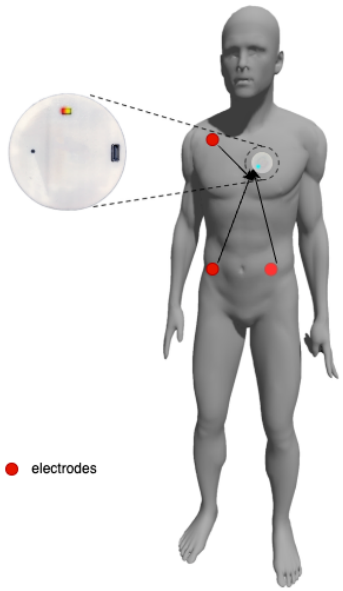

Figure 3.5: Soundi® chest position: in red are reported the ECG electrodes connected through jack

3.5. Signals Processing

To create the dataset, it is necessary first to perform a signal analysis. These signals can be divided into two main blocks, those recorded with the Soundi sensor are:

- Acceleration signals
- Plethysmographic signals
- ECG
- Bioimpedance
- Ambient temperature
- Body temperature

Those recorded by the Finapress are:

- Brachial ABP
- Finger ABP

In addition, a mask is created that will be used in training to exclude segments where the Finapress calibration is present. In this case, only the ABP signal acquired with the finger cuff is analyzed. Respiration signals are also added to these, derived respectively from the acceleration magnitude signal, the plethysmographic signal, and the acoustic signal. The first common operation for signals acquired through Soundi® sensors (IMU, Acoustic sensor, ECG, PPG) is to extract and process the signals saved on the MicroSD. These signals are sampled at different frequencies depending on the sensor with which the signal is acquired, so they are interpolated around the central sampling frequency of 400 Hz. Since the Finapress has a sampling frequency of 1 kHz, it is also resampled at 400 Hz. Signals are processed and divided into 10-second windows without overlapping to be able to eliminate artifacts caused by the device.

3.5.1. Acceleration signal

Acceleration signals, which consist of three main components (Ax, Ay, Az), are processed by applying a Bessel-type bandpass filter. This allows the extraction of acceleration content in the frequency band of 0.05 to 1 Hz, while maintaining a linear phase component that preserves the signal waveform. As a result, very low and high frequencies that are affected by respiration movement distortion are removed from the signal. The Magnitude Acceleration Signal is obtained by utilizing all three components of the filtered acceleration signals and applying the formula presented below:

$$A_M = \sqrt{{A_x}^2 + {A_y}^2 + {A_z}^2} \tag{3.1}$$

Then, Hilbert envelops and Savitzky-Golay filtering (151 samples and four coefficients) were sequentially applied to A_M to compute the Seismocardiogram (SCG), which featured two main patterns representing the aortic valve opening and closure respectively, was computed from the acceleration signal Table 3.4.

Signal	FilterType	Order	Low cut-on frequency (Hz)	High cut-off frequency (Hz)
A_x	Bessel	2	0.05	1
A_y	Bessel	2	0.05	1
A_z	Bessel	2	0.05	1
A_M	Bessel	2	0.05	1

Table 3.4: Filtering parameters adopted for Acceleration signals

3.5.2. Pletismographic (PPG) signal

PPG is an optical technique that is simple and low-cost, used for detecting blood volume changes in the microvascular bed of tissue at the skin surface level. As blood absorbs light more readily than tissue, changes in light intensity can be transduced as changes in blood flow. The sensor's high sensitivity allows for even minor changes in blood volume to be detected. The PPG waveform comprises alternating (AC) and direct (DC) components.

- The AC component represents the blood volume cardiac variation in each heartbeat, attributed to the pulsatile behavior of the heart.
- The DC component is highly correlated to central and peripheral venous pressure [42]. The average blood volume experiences gradual changes over an extended period; however, abrupt fluctuations can arise due to multiple factors such as breathing, the presence of disease, vasomotor activity, sympathetic nervous system activity, and thermoregulation.

The Pletismographic (PPG) signal is collected by the optic sensor located at the bottom of the Soundi® device, utilizing three different light sources (Green, Red, and Infrared). This results in the availability of three channels for the PPG. Subsequently, all signals are filtered using a Bessel bandpass filter with a frequency band ranging from 0.05 to 10 Hz Table 3.5.

Signal	FilterType	Order	Low cut-on frequency	High cut-off frequency
Green	Bessel	2	0.05	10
Red	Bessel	2	0.05	10
Infrared	Bessel	2	0.05	10

Table 3.5: Filtering parameters adopted for PPG signals

3.5.3. Electrocardiogram and Bioimpedance signals

Acquiring the ECG signal is a non-invasive procedure that provides a visual representation of the electrical and chemical activity of cardiac muscle fibers during the cardiac cycle. The QRS complex, which comprises three waves (Q, R, and S), is produced by ventricular depolarization following atrial depolarization and plays a crucial role in this process. By using external biomedical electrodes attached to three different regions of the chest and connected to the Soundi® device through a jack hub, the Electrocardiogram signal with II-Lead and Bioimpedance signal is collected. In order to refine the signals, a Bessel bandpass filter is applied between 5 and 25 Hz to extract the content of the ECG signal. After that, a cascade of notch filters at 36 and 50 Hz is applied to eliminate noise from the ECG signal Table 3.6.

Signal	FilterType	Order	Low cut-on frequency	High cut-off frequency
ECG	Bessel	2	5	25
	Notch	2	36	/
BioImp	Bessel	2	0.05	10

Table 3.6: Filtering parameters adopted for ECG and Bio signals

3.5.4. Arterial Blood Pressure (ABP)

The signal of arterial blood pressure shows the pressure wave traveling through arteries, exhibiting various rates of diffusion and morphology based on the artery's cross-sectional area. Arterial blood pressure is the pressure that the blood exerts on the walls of arteries and is a crucial vital sign in clinical practice. In the intensive care unit (ICU), it is regularly measured to monitor the cardiovascular health of critically ill patients. Physiologically, a pressure wave moving through a viscoelastic tube weakens progressively with an exponential reduction in speed. In this project, a cuff signal is utilized as a reference, excluding the brachial one. To eliminate high-frequency noise and smoothen the signal, a lowpass Bessel filter with a linear phase at central frequencies of 25 Hz is employed in Table 3.7.

Signal	FilterType	Order	Low cut-on frequency	High cut-off frequency
ABP	Bessel	2	25	/

Table 3.7: Filtering parameters adopted for ABP signals

3.5.5. Phonocardiogram (PCG)

The acoustic sound produced by the opening and closing of heart valves, especially the Mitral and Aortic valves, is recorded by PCG signal. The PCG signal is reconstructed using the acoustic sensor in the sound device, and a bandpass filter is applied to remove breath and external noise. Specifically, a Butter filter with a range of 10 to 40 Hz is used in Table 3.8.

Signal	FilterType	Order	Low cut-on frequency	High cut-off frequency
PCG	Butter	2	10	40

Table 3.8: Filtering parameters adopted for PCG signals

3.5.6. Respiration signals

The respiration signal is obtained by applying various filters to the Acoustic, Plethysmographic, and Magnitude Acceleration signals. To obtain the first part, a Bessel bandpass filter is applied to the Magnitude Acceleration signal in the frequency range of 0.05 to 1 Hz. The second part is obtained by filtering the Acoustic signal in the same way. Finally, the Bioimpedance signal is filtered using a Bessel bandpass filter to obtain the last part of the respiration signal Table 3.9.

Signal	FilterType	Order	Low cut-on frequency	High cut-off frequency
Resp1	Bessel	2	0.05	1
Resp2	Bessel	2	0.05	1
Resp3	Bessel	2	0.05	1

Table 3.9: Filtering parameters adopted for Respiration signals

3.6. Labelling process

After processing the signals, a labeling procedure is performed using a straightforward interface developed in Python Figure 3.6. With this tool is possible to save or delete the displayed chunks of signals: ECG, PPG, SCG, and PCG recorded with the Soundi®, the Arterial Blood Pressure (ABP) target signal, recorded with the Finapress. The last is the ABP_{Mask} that identify the activation of the Calibration window; During the procedure, all signals collected from the 25 volunteers are analyzed through 10-second windows,

and only those that exhibit good patterns among those listed before are saved. The ABP_{Mask} signal allows the inclusion of the temporal instances in which calibration is active. If saved, these chunks with High activation Mask will be used by the network but will not affect the *loss* calculation. Priority is given to ECG, PPG, and target ABP signals in the labeling procedure, as several studies have highlighted their importance in reconstructing the arterial blood pressure signal. Among them, ECG and especially PPG have a strong influence on the model's performance compared to the other signals. Indeed, the deep learning model can learn the complex relationship between these two signals and the ABP signal by combining them. Since the PPG signal is influenced by changes in blood pressure and blood flow, while the ECG signal reflects the heart's activity and cardiac output, these signals allow the model to estimate the ABP signal with higher accuracy [35]. Other studies only use the PPG signal to reconstruct the ABP [6]. Once the bank of six signals is saved, the remaining signals of Acceleration, Bioimpedance, ambient temperature, and body temperature are also concatenated. This block of signals is transformed into *tf.records* through a Tensorflow library, allowing an increase in the model's performance with a direct impact on the training speed. The annotated file is split between training, validation, and test sets with a fixed probability of 0.1% for the test set, 0.2% for the Validation set, and 0.7% for the Training set.

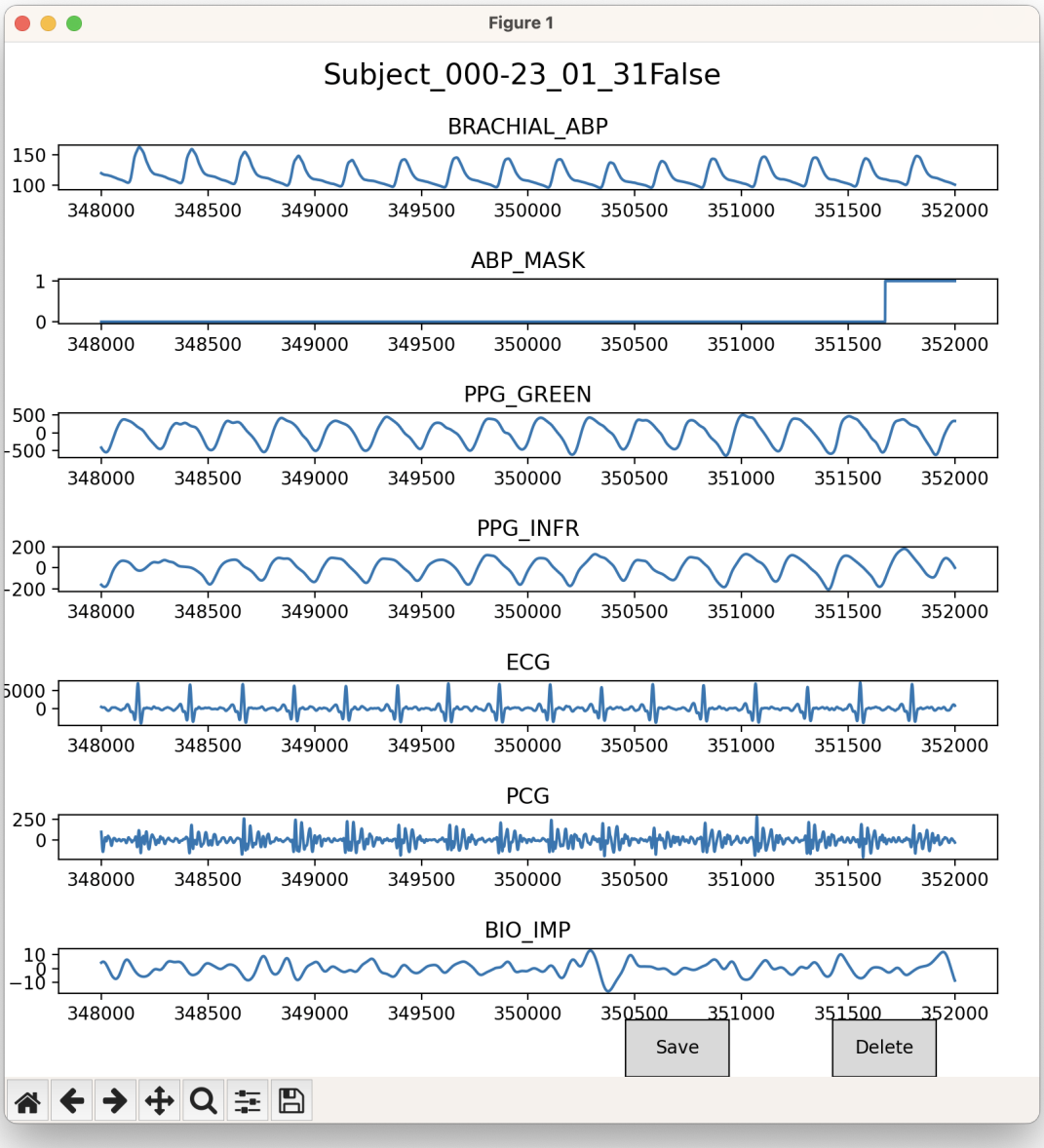

Figure 3.6: Labelling interface

3.7. Data Augmentation

To enhance model performance and increase its generability, Data Augmentation is performed. This technique enables the expansion of the dataset by generating new samples from the original dataset. Various techniques are utilized for Time Series Data Augmentation, including:

- Jittering: This technique involves adding noise with a Gaussian distribution, where the standard deviation determines the extent of change in the predicted sample.
- Scaling: This involves reducing the magnitude of the signal while maintaining its duration.
- Time Warping: This technique enables the modification of the signal's velocity along its duration, distorting it from its initial form.

Among these techniques, it has been chosen to use Jittering first, introducing noise with a scale of 0.01 to the signal. Next, the signal was scaled and time-warped, effectively doubling the initial dataset by adding the newly processed signals. An example of the procedure is shown in the diagram below. In Figure 3.7, an example of Data Augmentation performed on the signal is depicted. In particular, the python library *tsaug* is used, which allows for the application of the main algorithms previously described. In Figure 3.7, we see the modified signal in blue and the original signal in orange. Noise is first added, and the signal is then slightly drifted to avoid modifying the physiological conditions of the signal. The parameters used are shown in Table 3.10[30].

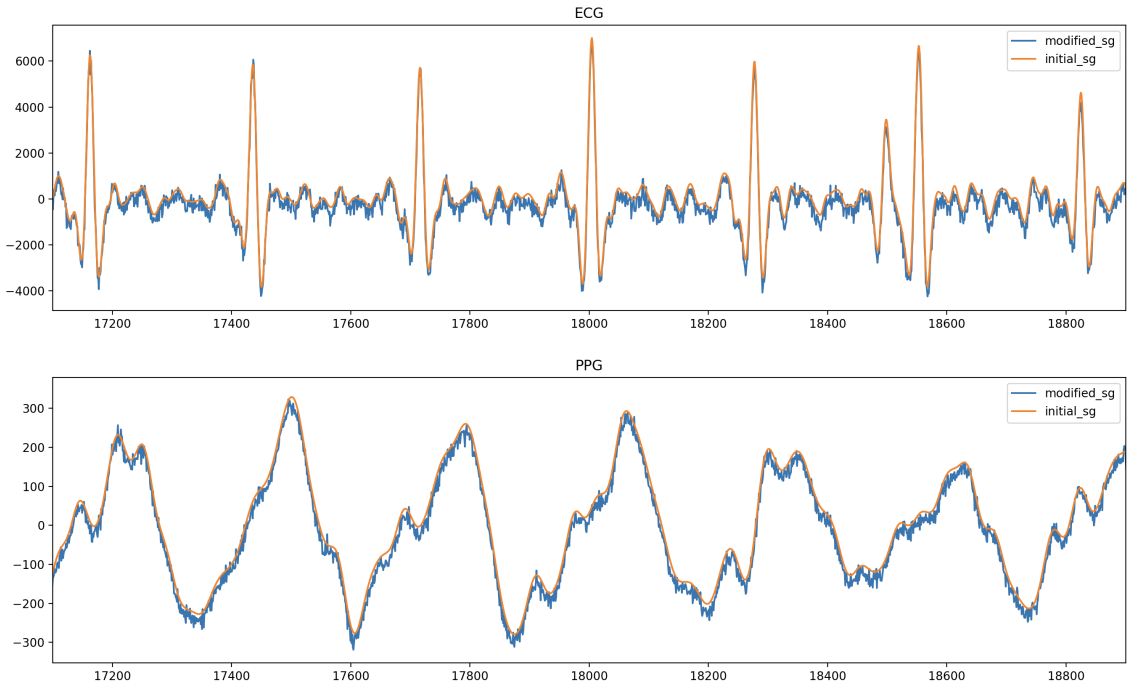

Figure 3.7: Example of Data Augmentation procedure applied on PPG and ECG signals

type	Algorithm	Scale	max drift	drift point
Jittering	tsaug.AddNoise	0.02	/	/
Drift	tsaug.Drift	/	0.03	1

Table 3.10: *tsaug* parameters for Data augmentation

3.8. Dataset Description

Once the signal acquisition procedure is completed, the dataset used to train the network is constructed. Table 3.11 presents the subject metadata:

Item	Value
N° of subjects	25
Gender	
Woman	7 subjects
Man	18 subjects
Age	
Mean	26 years
STD	20 years

Table 3.11: Subject Information

In Table 3.12, the average values of systolic, diastolic, and mean pressures of the input pressure signals for the entire dataset are reported. The values exhibit a high standard deviation as they account for both resting measurements and measurements during the pedaling phase. Obtaining a dataset of 664.0 minutes, which is then divided as previously described into training, validation, and test sets.

	Max(mmHg)	Min(mmHg)	Mean(mmHg)	STD(mmHg)
SBP	200.103	83.882	130.726	22.00
DBP	117.584	49.054	81.545	14.754
MBP	163.586	62.565	97.839	17.556

Table 3.12: Dataset description of all subjects enrolled

In Table 3.13, the values for Subject00 are reported, for which six different recordings were performed, totaling 134.5 minutes. The two distinct datasets are used for dual analysis: subject-dependent analysis on Subject 00 and subject-independent analysis on all twenty-five enrolled subjects. It is notable that while the diastolic and mean pressure values have a low standard deviation, the standard deviation is significantly higher for the systolic values. During the acquisition phase, there were moments when the instrument recorded values that were well outside the acceptable physiological range, particularly for systolic pressure values. This could potentially have a negative impact on the performance of the proposed models.

	Max(mmHg)	**Min(mmHg)**	**Mean(mmHg)**	**STD(mmHg)**
SBP	170.80	81.973	135.36	18.90
DBP	113.18	59.86	87.39	12.07
MBP	131.15	67.23	103.38	13.71

Table 3.13: Dataset description of Subject00

3.9. Evaluation Metrics

In order to evaluate the performance of the proposed models, characteristic parameters of the Arterial Blood Pressure (ABP) signal were chosen and computed for each prediction chunk:

- Systolic Blood Pressure (SBP) :

$$SBP = mean(ABP_{peak}) \tag{3.2}$$

- Diastolic Blood Pressure (DBP) :

$$DBP = mean(ABPpeak_{peak}) \tag{3.3}$$

- Mean Blood Pressure (MBP) :

$$MBP = (2 * DBP + SBP)/3 \tag{3.4}$$

- Standard Deviation (STD):

$$STD = \sqrt{\frac{1}{N}\sum_{i=1}^{N}(ABP_i - \overline{ABP})^2} \tag{3.5}$$

In particular, the standard deviation described in the equation 3.5 allows calculating Blood Pressure Variability (BPV): the higher it is, the better the reconstruction quality. [41]. Therefore, SBP, DBP, MBP, and STD are selected as target parameters to evaluate the quality of the extracted ABP signal.

3.9.1. Extracion of target value

Once the model is trained, the predictions made on the test set are exported to a JSON file and subsequently processed. The ID, target signal, and predicted signal are reported, each with a duration of 10 seconds. The fiducial points that will be used for model evaluation are described in Equations 3.2, 3.3, and 3.4. These, along with the standard deviation in Equation 3.5, will indicate the level of evaluation for the developed method. To identify these fiducial points, in each chunk, the respective fiducial points are detected, as visible in Figure 3.8 and 3.9, for the predicted signal and the target signal: the peaks corresponding to the maximum systolic pressure are indicated in orange, and the peaks corresponding to the diastolic pressure are indicated in blue. These peaks are selected at a minimum distance of four hundred samples, which corresponds exactly to one second. The resulting parameter that will be analyzed corresponds to the average value in each chunk, following clinical practice, which calculates SBP and DBP parameters as the average of multiple measurements.

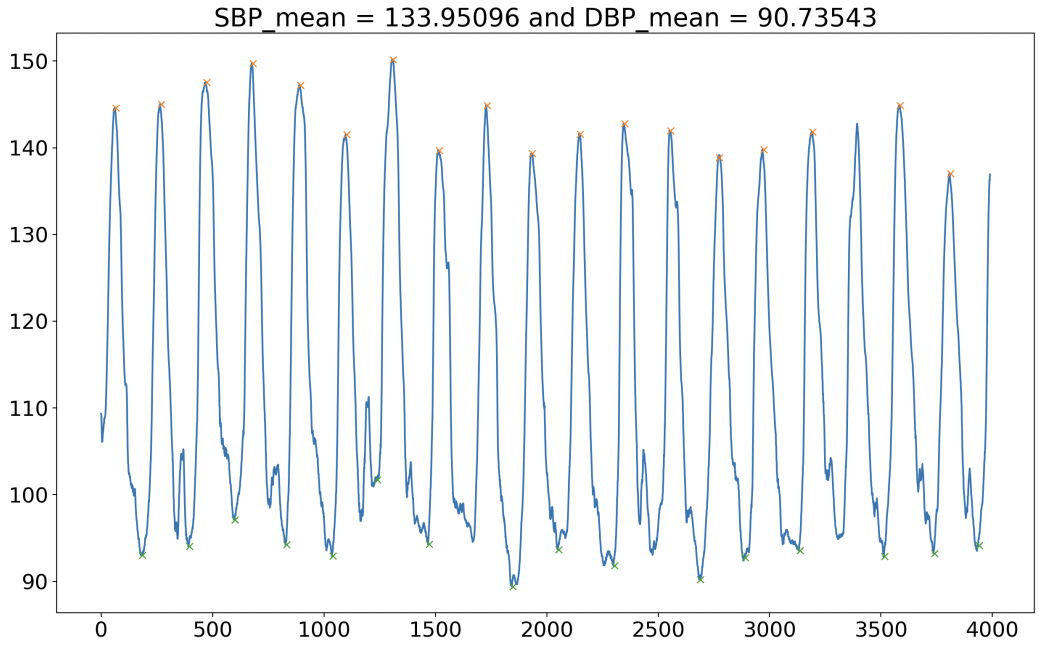

Figure 3.8: Automatic selection of SBP (orange) and DBP (green) peaks in prediction chunk of 10 seconds

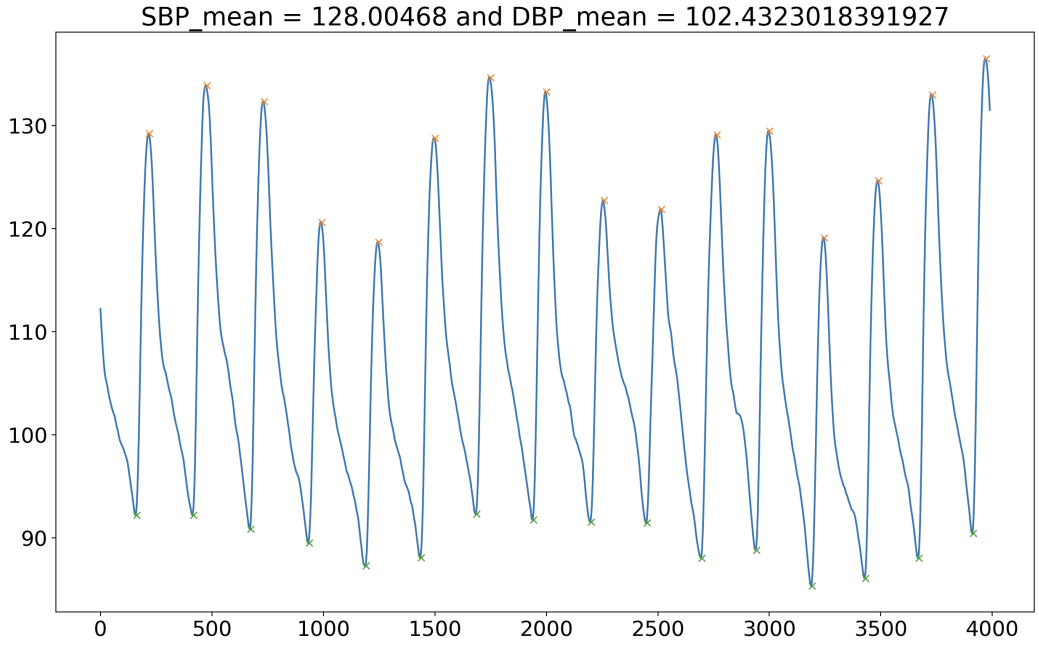

Figure 3.9: Automatic selection of SBP (orange) and DBP (green) peaks in target chunk of 10 seconds

3.10. PTT Models

As described earlier in the introduction, techniques based on the application of models such as those related to PWV are among the most widely used in recent scientific applications. These techniques allow for the prediction of diastolic and systolic pressure values based on the Moens-Korteweg equations [52]. These equations establish a relationship between the propagation velocity of the pressure wave in the arteries (PWV) and characteristics related to the flow and vessels, such as wall elasticity. The Moens-Korteweg equation is provided below:

$$PWV = \frac{L}{PTT} = \sqrt{\frac{E * h}{2 * r * \rho}} \tag{3.6}$$

The parameter L refers to the length of the vessels, representing the segment over which the pressure is calculated. The PTT (Pulse Transit Time) is the time it takes for the pressure pulse to travel along the length L. The radius of the vessels is denoted by r, and their wall thickness is represented by h. The variables E and ρ correspond to the elastic modulus of the vessels and the density of blood, respectively. This equation highlights how PWV is connected to physiological parameters, which also reflects a limitation of this technique. The elastic modulus of the vessels (E), as reported in various scientific studies, has been found to be correlated with factors such as age, arterial stiffness, and vascular health. The density of blood (ρ) remains relatively constant and is not subject to significant physiological variations. Therefore, the primary factors influencing PWV are the vessel properties (such as elasticity and dimensions) and the length over which the pulse wave propagates. [27]:

$$E = E_0 * e^{\alpha * p} \tag{3.7}$$

In Formula 3.7, α represents a constant, *E0* represents the initial modulus of the vessel walls, and P denotes the pressure within the vessels. By combining equations (3.6) and (3.7), it can be observed that pressure has a logarithmic dependence on the Pulse Transit Time (PTT), as illustrated in Formula 3.8:

$$BP = -\frac{2}{\alpha} * \ln PTT + \frac{\ln \frac{2 * r * \rho * L^2}{h * E_0}}{\alpha} \tag{3.8}$$

which can be simplified to:

$$ABP = a * \ln PTT + b \tag{3.9}$$

If the variation of ABP with respect to r is small enough to be negligible, then the second term in equation (3.9) can be ignored. We can therefore extract the linear relationship:

$$ABP = \alpha * PTT + b \tag{3.10}$$

.

Based on Equation (3.10), several variations of models have been developed. In particular looking at the research presented at the 2019 5th Iranian Conference on Signal Processing and Intelligent Systems in Int [1], three different models have been proposed [26]:

- **Linear Model**

$$\begin{cases} BP = \alpha_s * PTT + b_s \\ DBP = \alpha_d * PTT + b_d \end{cases}$$

- **Inverse Model**

$$\begin{cases} SBP = \alpha_s * \frac{1}{PTT} + b_s \\ DBP = \alpha_d * \frac{1}{PTT} + b_d \end{cases} .$$

- **Quadratic Model**

$$\begin{cases} SBP = \alpha_s * \frac{1}{PTT^2} + b_s \\ DBP = \alpha_d * \frac{1}{PTT^2} + b_d \end{cases} .$$

3.10.1. Regression Models

A simple algorithm is implemented in Matlab for estimating the parameters α and b using the previously described linear, inverse, and quadratic models. Following the pipeline illustrated in Figure 3.10, a prediction is made for Diastolic and Systolic pressure values, and the mean absolute error is calculated to evaluate the accuracy.

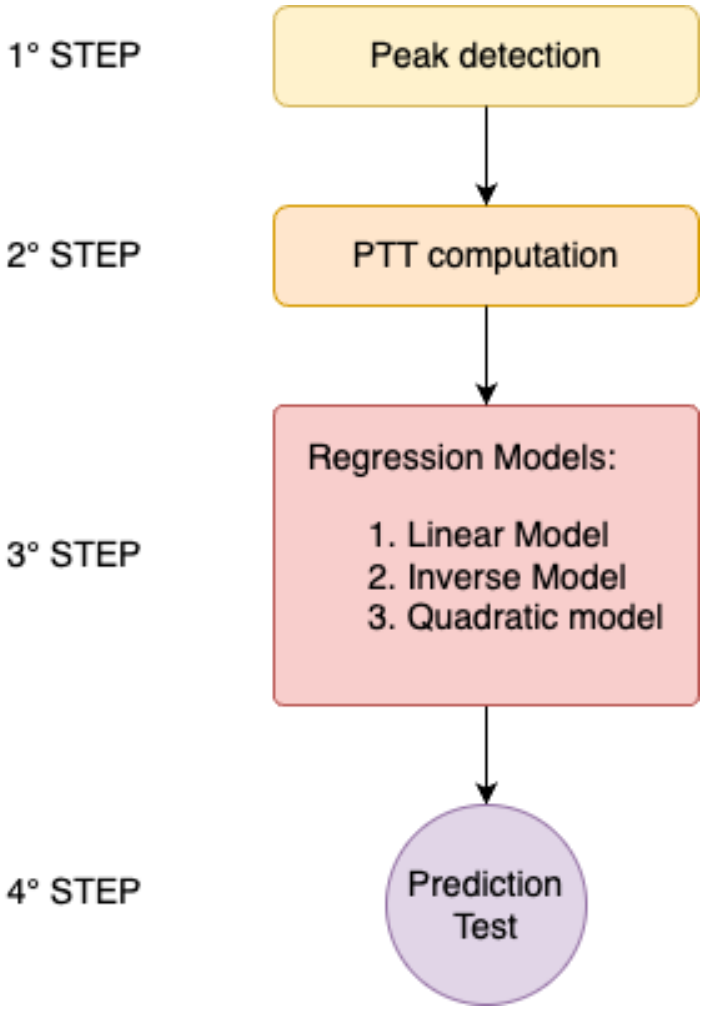

Figure 3.10: Description of Regression model pipeline

The procedure used for estimating the parameters α and b of the models consists of four main steps:

- **1st Step**: Manual selection of corresponding R-peaks for ECG and peak maxima for PPG is performed. This peak labeling procedure is carried out on filtered and aligned signals, considering only the recordings of Subject 00. Once the maxima and minima of the ABP target signal recorded by Finapress are identified, a CSV file is created that includes the occurrence in seconds of the R-peaks and PPG peaks, along with their corresponding systolic and diastolic pressure values.
- **2nd Step**: The time difference in seconds between the ECG and PPG peaks is calculated, indicating the time delay it takes for the impulse to travel from the heart to the index finger, where the PPG is acquired.
- **3rd Step**: A simple algorithm is created using Matlab to implement the regres-

sion using the different described models. Specifically, the Deep Learning Toolbox is used, which includes the function *"fitml"* for implementing a linear model and returning the respective parameters α and b.

- **4th Step**: Predictions are made using the respective models on 1/3 of the dataset created for parameter estimation. This allows for the calculation of prediction errors and the estimation of Mean Absolute Error (MAE) for each model.

3.10.2. PTT Computation

The Pulse Transit Time (PTT) indicates the time it takes for the pressure impulse to travel from the heart to a radial artery in the body. This parameter is closely correlated with blood pressure, as previously described. The PTT can be calculated as the time difference between the occurrence of the R-peak in the electrocardiogram (ECG) and the peak maximum in the photoplethysmograph (PPG). The R-peak in the ECG indicates ventricular depolarization and the onset of contraction, which produces the systolic stroke volume. On the other hand, the peak maximum in the PPG, corresponding to the maximum transmitted light intensity, indicates a decrease in blood volume at the analysis site and therefore corresponds to the minimum pressure, the diastolic pressure.

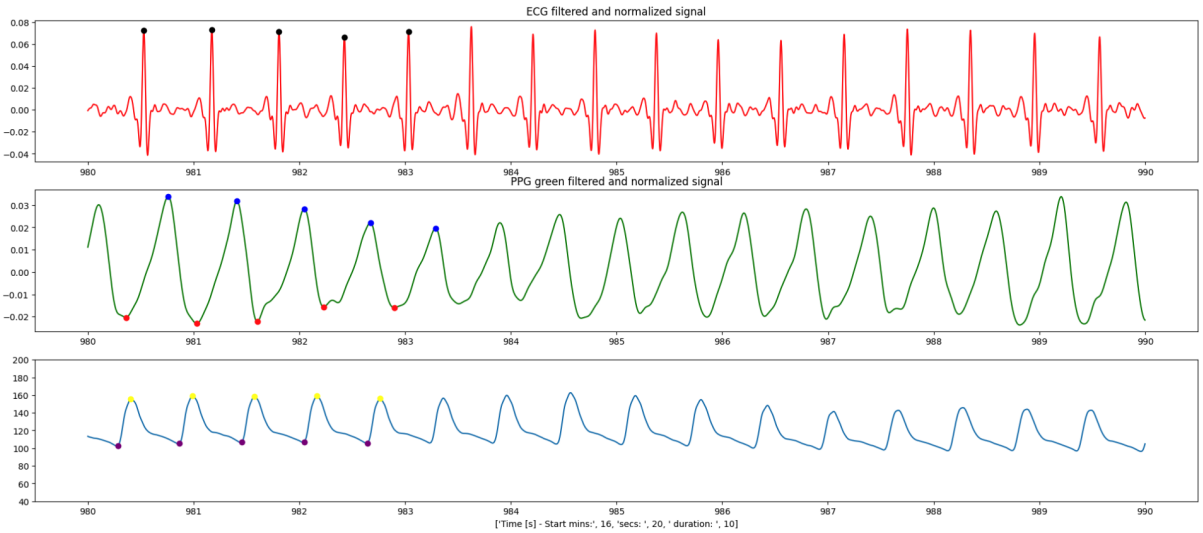

Figure 3.11: Peak selection procedure

In this experiment for the calculation of PTT, the pre-processed and aligned ECG and

green PPG signals from subject 00 were used, following the signal processing procedure described in the signal processing section. For each recording, five specific characteristic points were manually selected for each signal, as highlighted in Figure 3.11:

- R-peak in black
- PPG-peak in blue
- SBP-peak in yellow
- DBP-peak in purple

A total of 100 samples are selected, with 75 samples used for training the parameter estimation model and 25 samples for the test set, from which the accuracy and mean absolute error of the model are derived. Table 3.14 presents the average values of systolic, diastolic, and mean pressure for subject 00 in four out of the six recordings, on which manual feature selection was performed.

	Max(mmHg)	**Min(mmHg)**	**Mean(mmHg)**	**STD(mmHg)**
SBP	167.60	85.363	132.56	14.60
DBP	114.68	60.45	85.19	9.07
MBP	129.55	66.84	105.68	12.17

Table 3.14: Target value of input signals

4 | Artificial Intelligence

After finishing the labeling process, a deep neural network approach was used for Arterial Blood Pressure waveform reconstruction, as mentioned earlier. Defining the input and output of the architecture is the first step. A well-structured procedure must be established to meet computational power and training timing constraints. The network is fed with processed signal chunks to enable it to learn the useful features of the time series and make an accurate signal reconstruction. Sixteen-time series chunks are extracted from the acquisitions and concatenated in the depth dimension:

- Acceleration signals (A_M, A_x, A_y, A_z);
- Plethysmographic signals (Red, Green, Infrared);
- ECG;
- Bioimpedance;
- SeismoCardiogram;
- PhonoCardiogram;
- Respiration;
- Ambient temperature;
- Body temperature;
- ABP Mask;

By concatenating the Finapres-recorded Arterial Blood Pressure target signal to the data, an input of the form $N \times 16 \times M$ is obtained for the convolutional network. Here, N represents the number of samples for the selected chunk length, which is 10 seconds in this case. Sixteen signals are concatenated, and M corresponds to the number of chunks that were saved during the labeling procedure. This input has 16 channels, each representing a separate signal, along with its corresponding ABP target signal. Deep Learning techniques were employed to recreate the ABP signal waveform using signals

obtained with Soundi®. The study specifically examined the use of different architectures that combine Convolutional Neural Networks and Gated Recurrent Unit techniques.

4.1. Gated Recurrent Unit (GRU)

Cho et al. [15] introduced the Gated Recurrent Unit (GRU) in 2014 to tackle the vanishing gradient problem that plagues traditional recurrent neural networks. GRU and Long Short-Term Memory (LSTM) share similarities and can be considered as variations of each other since they both demonstrate similar performance in specific scenarios. GRU overcomes the vanishing gradient issue of regular RNNs by leveraging *update* and *reset* gates that decide which information should be conveyed to the output. The update and reset gates can be trained to preserve relevant data from the past without decaying over time and to filter out irrelevant information that does not contribute to the prediction Figure 4.5.

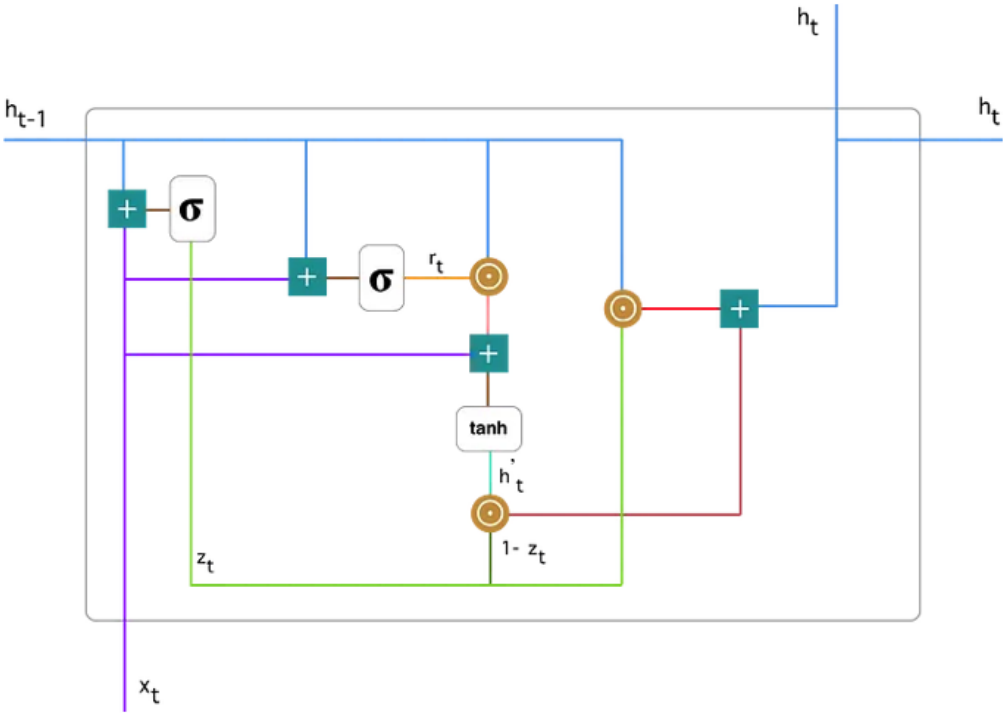

Figure 4.1: Illustration of a single GRU unit.

In Figure 4.1 are reported the GRU's parameters were:

- h$(t-1)$ is the activation function of the previous state;

- x_t is the input at the current time;
- σ is the sigmoid function
- $\circ$ is the Hadamard product;

The *update gate* z_t is a powerful mechanism that allows the model to decide how much of the past information from previous time steps should be carried forward to the future. This capability is particularly useful since the model can choose to retain all the relevant information from the past. The mathematical computation of the Activation is reported in the formula (2) [18]:

$$z_t = \sigma(W_z x_t + U_z h_{t-1}) \tag{4.1}$$

The *reset gate* r_t, on the other hand, determines the amount of past data to discard. The analytical update of the reset gate reported below is similar to update one, but the weight matrix is different (3) [18]:

$$r_t = \sigma(W_r x_t + U_r h_{t-1}) \tag{4.2}$$

4.1.1. GRU layer

To better understand and comprehend the optimal placement of GRU units within convolutional networks such as U-Net, an ablation study was conducted among three different setups using only the recordings from subject 00. Specifically, the following setups were examined:

- **GRU Encoder layer**: The GRU layer is inserted before the bottleneck, taking the output of the last encoder layer as input and transferring the output to the bottleneck. This layer has a number of units equal to the number of output filters from the last encoder layer, which is 128 units.
- **GRU Bottlneck**: In this case, the GRU layer is positioned immediately after the bottleneck and before the decoder. It has a number of units equal to 256.
- **GRU Decoder**: The GRU layer is placed at the output of the network after the last encoder layer. It takes the output of the network as input and produces the ABP wave

The main difficulty in using GRU lies in training, as they require high computational

capacity that can lead to memory saturation. Additionally, like RNNs, GRUs are often affected by the problem of Vanishing or Exploding gradients, which causes training degeneration and makes network training impossible. The ablation study to identify the optimal placement of the GRU layer was conducted on the U-Net with the parameters listed in Table 4.1 .

Models	Loss function	Optimizer	Initial Filter	Epochs
U-Net	MSE	Adam	15	500

Table 4.1: U-Net parameters fo GRU test

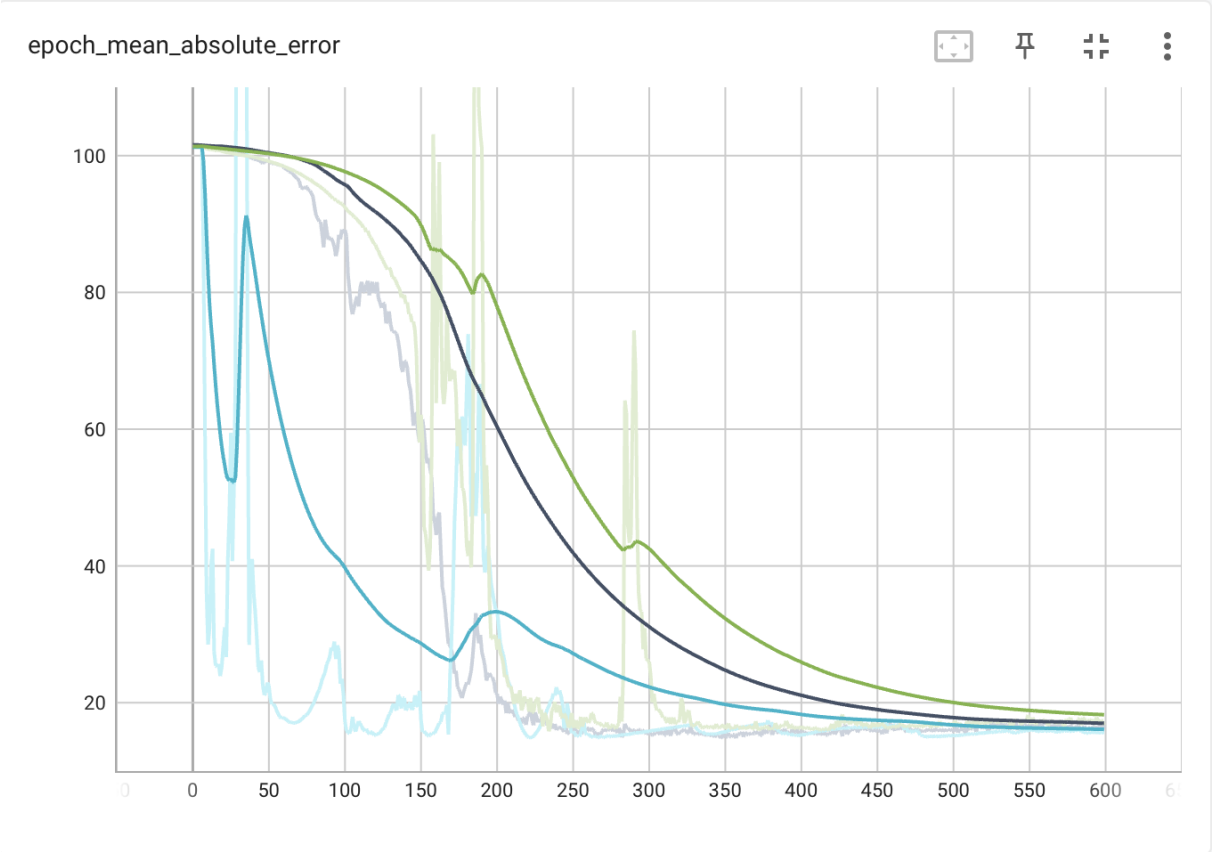

Figure 4.2: In this figure, the different trends of mean absolute metrics are reported for the three different locations of GRU units: green for GRU-Bottleneck, black for GRU-Encoder, and blue for GRU-Decoder.

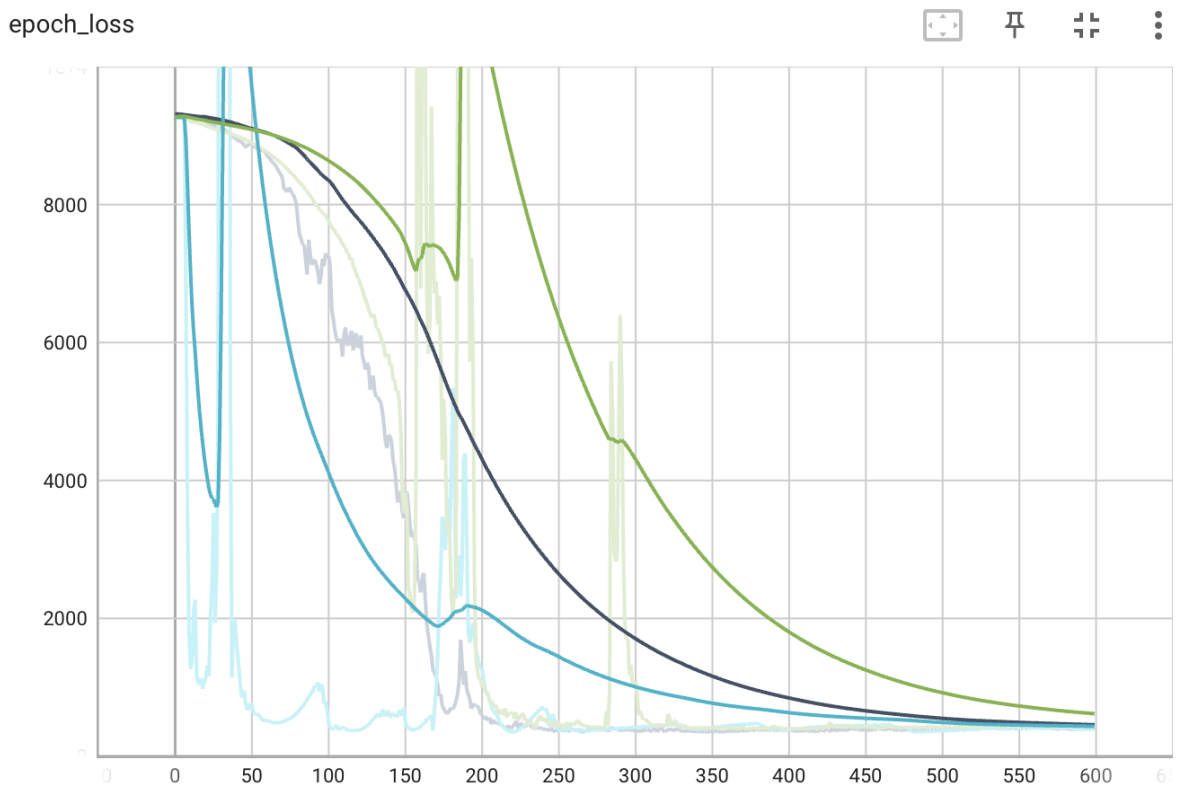

Figure 4.3: In this figure, the different trends of the loss function are reported for the three different locations of GRU units: green for GRU-Bottleneck, black for GRU-Encoder, and blue for GRU-Decoder.

Models	N° units	Activation	Recurrent activation	MAE (mmHg)	Loss
GRU-Encoder	128	linear	sigmoid	14.88	458.6
GRU-Bottleneck	256	linear	sigmoid	15.81	422.5
GRU-Decoder	1	linear	sigmoid	14.79	407.3

Table 4.2: Errors of different GRU positions inside the network

Table 4.2 presents the validation metrics that show how accuracy changes based on the placement of GRU units in a base U-Net. Figures 4.3 and 4.2 show the patterns of the loss function and mean absolute error, respectively. As observed, the position and number of units in the GRU layer greatly influence the network's performance. Placing the GRU layer at the output of the network with a single unit reduces memory usage and the total number of network parameters. In Figures 6.4 and 4.2, the trend on the validation set of the U-Net with GRU in the decoder is represented in blue, while the encoder and

bottleneck trends are shown in black and green, respectively. The U-Net with the GRU layer in the decoder outperforms the other two setups, as can also be observed from the values of the mean absolute error reported in Table 4.2, where it achieves a value of 14.79 mmHg compared to 14.88 and 15.81 mmHg achieved with GRU in the encoder and bottleneck, respectively.

4.2. Convolutional Neural Network (CNN)

CNNs have been widely used in image recognition tasks, but they have also been successful in various other fields, including natural language processing and speech recognition. In recent years, the application of 1D CNNs has gained popularity in processing sequential data such as time series signals. 1D CNN operates on one-dimensional input data and learns a set of filters to capture different features at different scales. The use of 1D CNNs can help capture local patterns in the data, which makes them useful in tasks such as wave reconstruction how in this case, where the features of interest may occur at different time scales. An important aspect of 1D CNNs is the ability to downsample the input data while retaining the relevant information, which is done through the use of pooling layers. This allows the network to learn features at different resolutions and speeds up the training process by reducing the dimensionality of the data [54]. U-Net is widely recognized as one of the most frequently used convolutional neural networks in medical image processing, particularly in the areas of image classification and segmentation using deep learning based on CNN. It is considered one of the most important semantic segmentation frameworks for CNN, according to a report by Du et al. [20]. Numerous studies have also demonstrated that deep learning can be used to achieve physiological signal segmentation and analysis. For example,Oh et al. [40] utilized a modified version of U-Net to categorize ECG beats. Chuang et al. [17] employed deep learning to segment and classify lung nodules in CT images, providing another illustration of its potential in the medical field[17, 40].

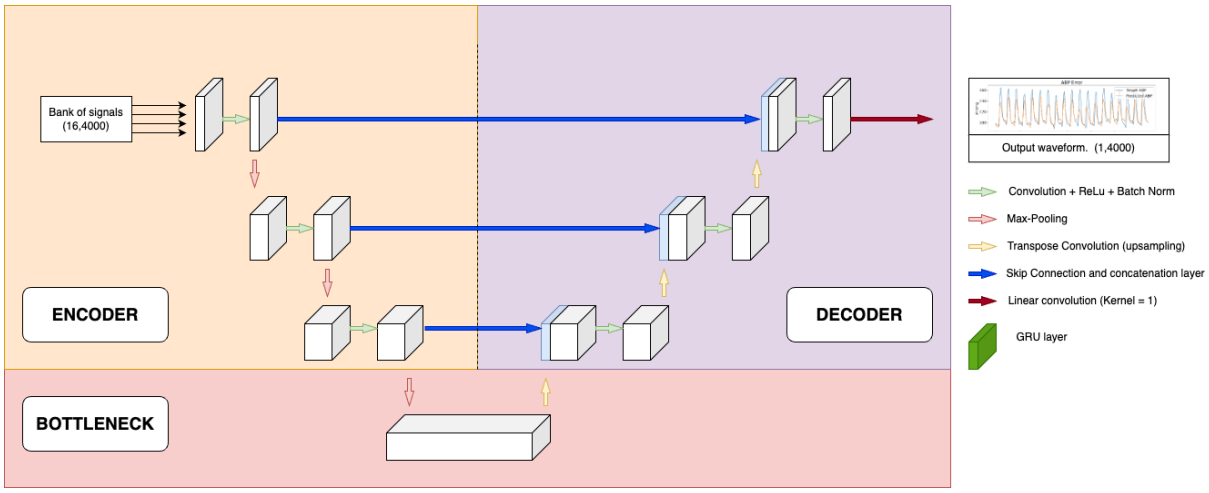

Figure 4.4: In this Figure is reported the classical architecture of U-Net

Model	Output Shape	N° Parameters
U-Net	(None, 4000, 1)	71593

Table 4.3: U-Net parameters

Models	Loss function	Optimizer	Initial Filter	Epochs	Batch size
U-Net	MSE	Adam	15	500	64

Table 4.4: U-Net Hyperparameters

In Figure 4.4 is reported the U-Net architecture and in Table 4.3 its parameters. The U-Net architecture is symmetric, having an Encoder part in orange that extracts spatial features from the image, and a Decoder part in purple that constructs the segmentation map from the encoded features. Indeed in red, there is a bottleneck part that constructs the latent image, which is the main part of the deep network. The Encoder follows the typical formation of a convolutional network. It involves a sequence of two 3×3 convolution operations, which is followed by a max pooling operation with a pooling size of 2×2 and stride of 2. This sequence is repeated four times, and after each downsampling the number of filters in the convolutional layers is doubled. Finally, a progression of two 3×3 convolution operations connects the Encoder to the Decoder. the Decoder first up-samples the feature map using a 2×2 transposed convolution operation, reducing the feature channels by half. Then again a sequence of two 3×3 convolution operations is performed. Similar to the Encoder, this succession of up-sampling and two convolution

operations is repeated four times, halving the number of filters in each stage. Finally, a 1×1 convolution operation is performed to generate the final segmentation map. All convolutional layers in this architecture except for the final one use the ReLU (Rectified Linear Unit) activation function; the final convolutional layer uses a Sigmoid activation function. The most ingenious aspect of the U-Net architecture is the introduction of skip connections. In all four levels, the output of the convolutional layer, prior to the pooling operation of the Encoder is transferred to the Decoder. These feature maps are then concatenated with the output of the upsampling operation, and the concatenated feature map is propagated to the successive layers. These skip connections allow the network to retrieve the spatial information lost by pooling operations [19, 46]

4.3. Proposed Models

Within the literature, there are multiple studies that investigate the prediction of blood pressure values or waveform by utilizing other physiological signals like ECG and PPG. Ibtehaz et al. [29] conducted a study where they attempted to reconstruct the blood pressure waveform solely from the plethysmographic signal. They accomplished this using a deep neural network inspired by U-Net and a Res-Net to refine the signal, yielding outstanding outcomes. Additionally, Baker et al. [8] present a hybrid approach in their study where a neural network is created for the continuous and non-invasive estimation of blood pressure by analyzing electrocardiogram and photoplethysmogram waveforms. This hybrid neural network involves utilizing a Convolutional Neural Network for 1D segmentation and a Long Short-Term Memory for signal dynamics analysis, resulting in a Deep Neural Network that reconstructs the blood pressure signal from ECG and PPG. Another study conducted by Cheng et al. [14] describes the development of a fully convolutional neural network for monitoring arterial pressure. Based on these studies, two different models utilizing Deep Neural Networks have been created. In particular, the classic U-Net design was taken and modified by adding Gated Recurrent Networks.

4.3.1. Basic Unit

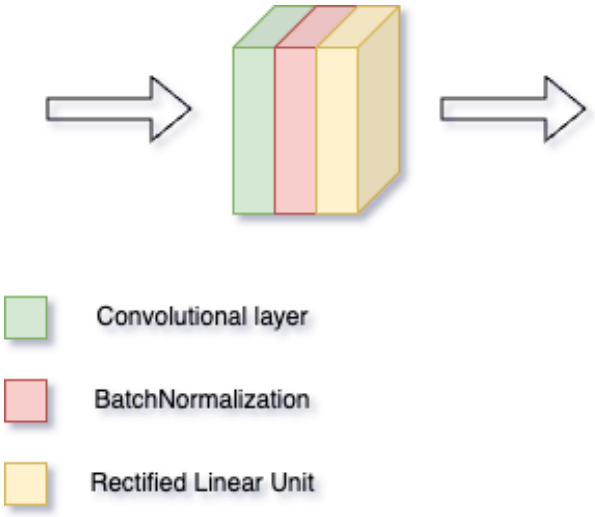

Figure 4.5: Basic Unit of Encoder-Decoder layer.

To create the networks model, the study starts with the definition of the basic unit used in the network's levels. As shown in the Figure 4.5 there are three layers respectively:

- Convolutional layer
- Batch Norm Layer
- Rectified Linear Unit

The convolutional layer enables image segmentation and the extraction of feature maps that capture the salient characteristics of signals. The output from this layer is then fed into the subsequent layer, which applies batch normalization [32]. The training of Deep Neural Networks is complicated by the fact that the distribution of inputs for each layer changes during training, as the parameters of the previous layers are updated. This causes a slowdown in training by necessitating lower learning rates and careful parameter initialization and makes it notoriously difficult to train models with saturating nonlinearities. This phenomenon is referred to as internal covariate shift, and it is addressed by normalizing the inputs to each layer. The approach of the presented study incorporates normalization as part of the model architecture and performs it for each training mini-batch. Batch Normalization allows for much higher learning rates and reduces the need for meticulous initialization. The final basic element is the Rectified Linear Unit (ReLU), a linear activation function that outputs the input directly if it is positive; otherwise, it

outputs zero. This function has become the default activation function for many types of neural networks due to its easiness of training and ability to achieve superior performance.

4.3.2. Single branch GRU-Net

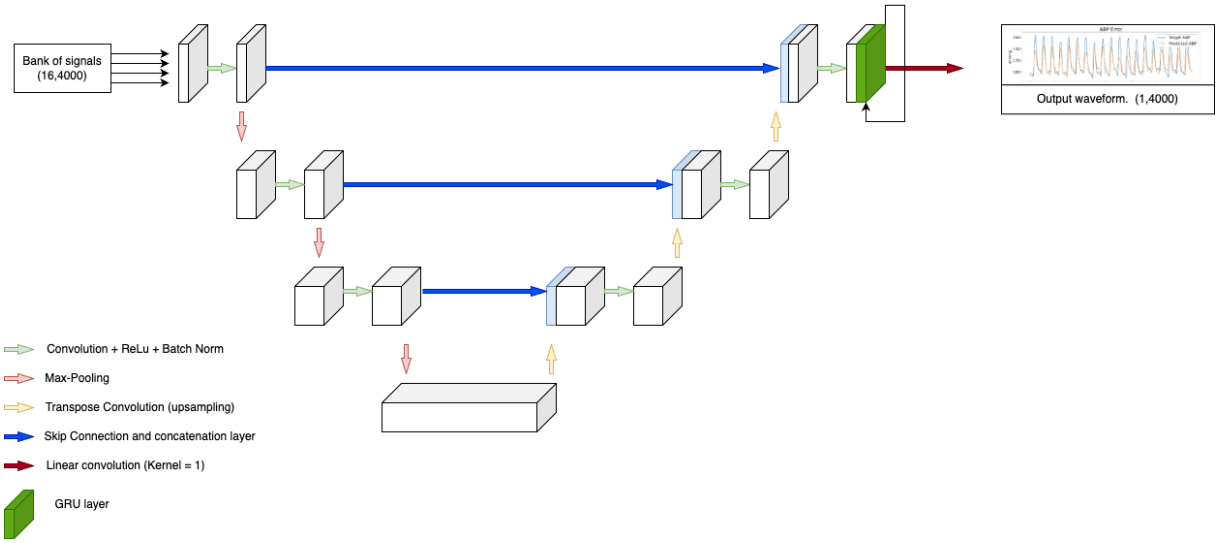

Figure 4.6: developed diagram of GRU-Net

Model	Output Shape	N° Parameters
GRU-Net	(None, 4000, 1)	149970

Table 4.5: GRU-Net parameters

Models	Loss function	Optimizer	Initial Filter	Epochs	Batch size
GRU-Net	MSE	Adam	15	500	64

Table 4.6: GRU-Net Hyperparameters

A simple diagram of the network developed for the reconstruction of the ABP signal is shown in Figure 4.6, and in Table 4.5, the parameters of the network and the output shape are reported. As can be seen, it has the structure of a classic U-Net, with an Encoder as the first part, followed by a Bottleneck, and finally the Decoder. The structure of the encoder is almost identical to that of a normal U-Net, while there are significant differences in the other two parts. In particular, there is *Gated Recurrent Networks* in the respective levels of the decoder, which allow the signal dynamics to be taken into account by storing

the main features using *reset gate and update gate*, as described earlier. The input sample initially passes through the three levels of the encoder until it reaches the output of the bottleneck part. The output is then concatenated in the concatenation layer with the respective skip connection, thus entering the lower level of the Decoder. The output is then concatenated in the concatenation layer with the respective skip connection, thus entering the lower level of the Decoder, which is also enriched with an output GRU layer. From the results, it can be seen that the use of GRU significantly speeds up the network training procedure, improving its final accuracy.

4.3.3. Triple branch 3GRU-Net

An ad-hoc neural architecture was developed to tackle the multiscale multi-modal problem. The primary goal was to learn useful features from all input signals. This was achieved using a multi-path strategy that involved convolutional neural network layers. Thanks to this strategy, it became possible for each of the paths to learn unique features at different scales from the input signals. For instance, while the SpO2 signal had a very slow trend, the high-frequency signal contained finer details that were crucial for learning.

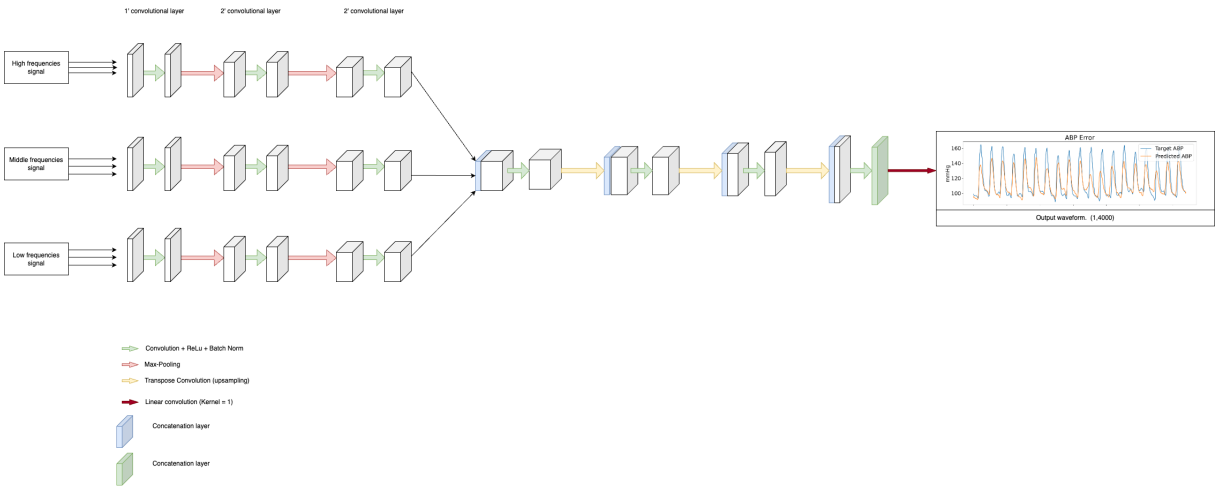

Figure 4.7: Developed diagram of 3GRU-Net

Model	Output Shape	N° Parameters
3GRU-Net	(None, 4000, 1)	251050

Table 4.7: 3GRU-Net parameters

Models	Loss function	Optimizer	Initial Filter	Epochs	Batch size
3GRU-Net	MSE	Adam	15	500	64

Table 4.8: 3GRU-Net Hyperparameters

This model is still inspired by the U-Net, but it focuses on the frequency band of the different input signals. So each branch has the same structure of a U-Net encoder, but each of them receives input different signals. For this reason, the use of this model requires an additional preprocessing step that involves dividing the signals based on their frequency content, in particular, they are grouped as follows:

- **high frequencies**: electrocardiogram and phonocardiogram
- **mead frequencies**: plethysmographic, seismographic, acceleration, bioimpedance
- **low frequencies**: temperature and respiration

Therefore, an alternative encoder consisting of three different branches is developed, one pattern for each signal bank, corresponding to the main frequency. In this way, each branch of the encoder encodes specific aspects of the signal that depend on its main frequency. Each part of the encoder follows a typical convolutional network structure, consisting of a sequence of two 6×6 convolution operations, followed by a 2×2 max pooling operation with a stride of 1. This sequence is repeated three times, with the number of filters in the convolutional layers doubling after each downsampling, specifically using 64, 128, 256, and 512. This is repeated for all three branches. The outputs are concatenated and connected to the decoder by a bottleneck layer composed of two convolutional layers with 512 filters. The decoder first upsamples the feature map, reducing the number of feature channels. Then, a sequence of two 6×6 convolution operations is performed, similar to the encoder. This sequence of upsampling and two convolution operations is repeated three times, halving the number of filters in each stage. A final 1×1 convolution operation is performed to generate the segmentation map. The ReLU activation function is used in all convolutional layers except for the final one, which uses a Linear activation function.

4.3.4. Res-Net

Once the intermediate pressure signal is obtained using the network, a Res-Net is cascaded that reflects the structure proposed by He et al. [25] and Ibtehaz and Rahman [28]. In

particular, to realize the MultiResU-Net, basic units called MultiRes-Blocks are used, as shown in Figure 4.8.

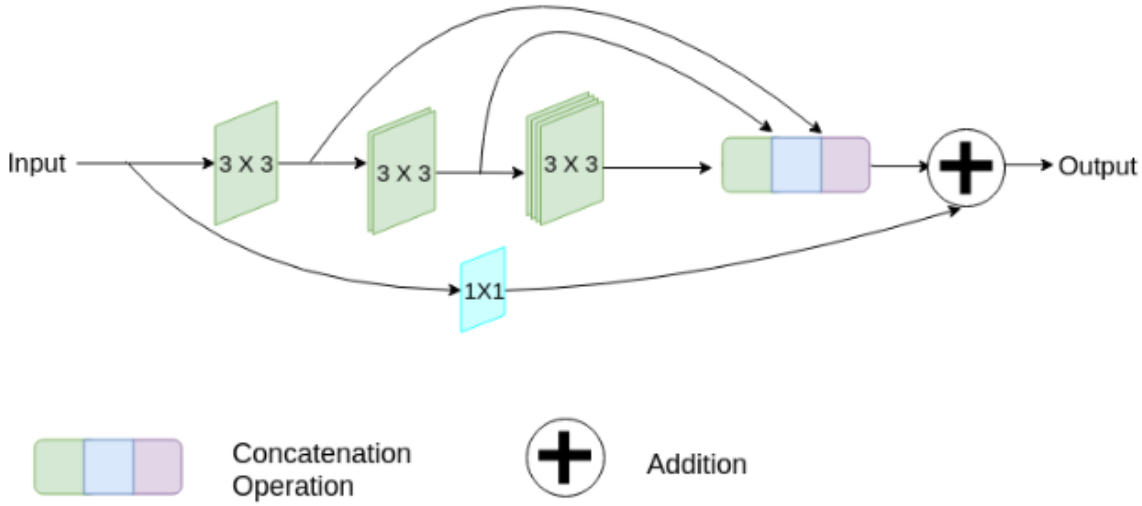

Figure 4.8: Proposed MultiResBlock

As reported in the paper, this setup avoids memory problems compared to the classic Res-block, which involves using an increasing kernel in the various convolutional layers. To overcome this issue, a growing number of filters are inserted into each convolutional layer, and a residual connection with a kernel of 1x1 is added to retrieve spatial information. Then the tensor is passed to the Batchnorm layer and ReLu unit. In addition, an alternative connection to the classic skip connection is developed, which connects the output of the encoder with the input of the decoder, called Res-path 4.9.

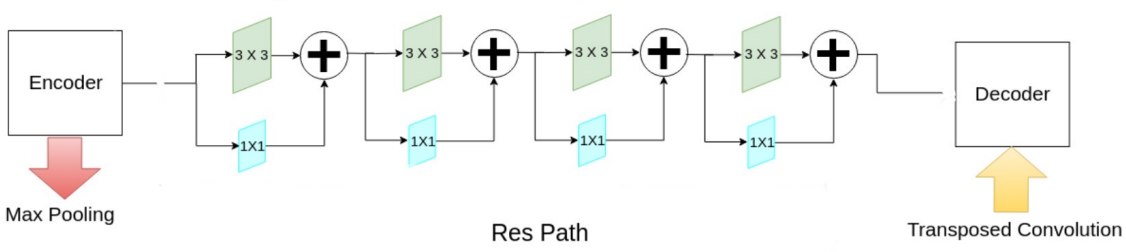

Figure 4.9: Proposed Res-Path

This approach involves the use of a chain of convolutional layers with residual connections

before concatenating the feature maps from the encoder to the decoder, instead of directly concatenating them. These layers use 3×3 filters, and 1×1 filters are incorporated with the residual connections to make learning easier, especially in deep convolutional networks. The number of convolutional blocks in the res path is gradually reduced, with the first layer having 4 blocks, the second layer having 3, and the third layer having 2. The network's final diagram featuring MultiResBlock and Res path is depicted in Figure 4.10, which facilitates fine-tuning the ultimate signal by decreasing noise during reconstruction and realigning the prediction, thereby enhancing the predicted intermediate pressure signal achieved through either the GRU-Net or the 3GRU-Net.

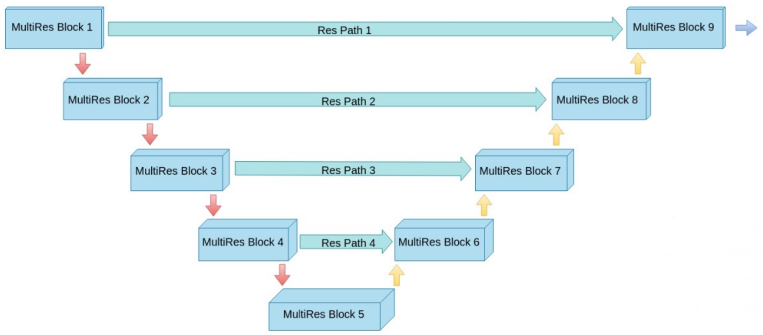

Figure 4.10: Proposed MultiResNet

Model	Output Shape	N° Parameters
Res-Net	(None, 4000, 1)	9244

Table 4.9: Res-Net parameters

Models	Loss function	Optimizer	Initial Filter	Epochs	Batch size
Res-Net	MSE	Adam	32	500	64

Table 4.10: Res-Net Hyperparameters

The effect of cascaded ResNet is immediately visible in Figures 4.11 and Table 4.11, which show the trends of metrics on the training and validation sets for both U-Net and U-Net with cascaded ResNet, calculated over 500 epochs, as well as the values of

validation metrics. It can be observed that the overall mean absolute error significantly decreases with the addition of cascaded ResNet, improving the model reconstruction. Specifically, the mean absolute error decreases from 17.53 mmHg to 13.11 mmHg. In Figure 4.11, it can be seen that the trend on the validation set reaches lower values with 500 epochs, improving the training speed. Additionally, it is noticeable that the model without ResNet quickly tends to overfit. The blue line represents the training metric trend, while the red line represents the validation metric trend for the simple U-Net. Based on these observations, the subsequent analyses are performed using the respective models with cascaded ResNet.

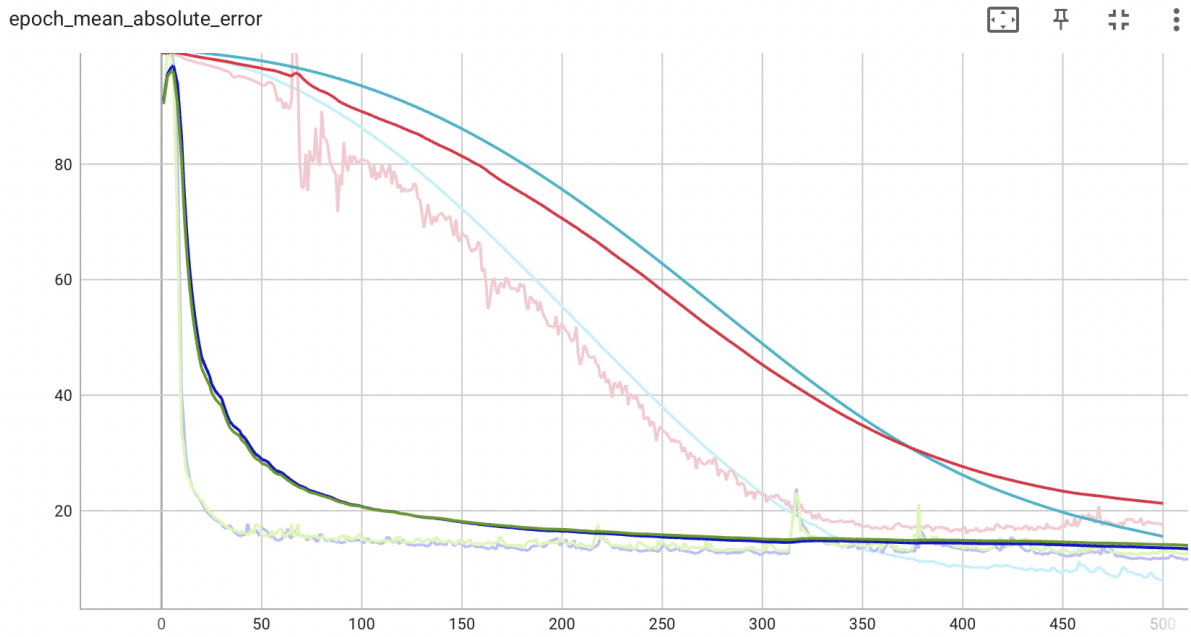

Figure 4.11: Plot of the MAE trend metrics: U-Net over validation set (light blue); U-Net over training set (Red); U-Net+ResNet over validation set (Green); U-Net+ResNet over training set (Blue)

Models	**Loss Value**	**MAE (mmHg)**	**Epochs**
U-Net	464.3	17.53	500
U-Net+ResNet	291.6	13.11	500

Table 4.11: metrics of the developed models: evaluation of target metrics over the validation set.

4.3.5. Summary of proposed models

Three different deep neural network models based on U-Net are developed, introducing the Gated Recurrent Unit (GRU). Tables 4.12 and 4.14 display the parameters of the networks with cascaded ResNet. As observed, in terms of computational complexity, the 3GRU-Net is much more demanding than the simple GRU-Net, as the three branches of the 3GRU increase the complexity of the network. However, this ensures better robustness of the network, as it seems to fit the task better and allows for a more accurate prediction of the waveform.

Model	Output Shape	N° Parameters
U-Net	(None, 4000, 1)	140714
Res-Net	(None, 4000, 1)	9244
Complete model	(None, 4000, 1)	149958

Table 4.12: U-Net + ResNet parameters

Model	Output Shape	N° Parameters
GRU-Net	(None, 4000, 1)	140726
Res-Net	(None, 4000, 1)	9244
Complete model	(None, 4000, 1)	149934

Table 4.13: 3GRU-Net + ResNet parameters

Model	Output Shape	N° Parameters
3GRU-Net	(None, 4000, 1)	241806
Res-Net	(None, 4000, 1)	9244
Complete model	(None, 4000, 1)	251014

Table 4.14: GRU-Net + ResNet parameters

Models	Loss function	Optimizer	Initial Filter	Epochs
U-Net	MSE	Adam	15	500
GRU-Net	MSE	Adam	15	500
3GRU-Net	MSE	Adam	15	500
Res-Net	MSE	Adam	15	500

Table 4.15: Summary of model's Hyperparameters

5 | Experimental session

In this section, an analysis of the different components of the experimental setup is reported, as well as the outcomes of the ablation studies that help in identifying the optimal parameters for the deep learning architectures used in the estimation of ABP waveforms from a Bank of signals. The experiment was carried out through the application of the Python programming language for both algorithm development and implementation, and the construction of the neural network models was executed utilizing TensorFlow with a KERAS frontend, then thanks to TensorFlow tools the result are printed with a Tensorboard.

5.1. Hyperparameter tuning

Through an ablation study the optimal hyperparameters for the network are selected, and since each model has a unique structure, it also has a distinct initial setup:

- GRU-Net: The kernel size for each convolutional layer has been chosen to be 6 to account for the presence of various signal trends. Both the Encoder and the Decoder consist of three levels, each with two basic units as previously described, and the number of filters is increased as the depth of the network increases. In the first levels, there is an initial number of 15 filters, which doubles at each level until there are 128 filters in the Bottleneck layer
  Due to the high computational cost of GRU units, only one unit is chosen for the Decoder layers. The network's performance is strongly linked to the units in this layer, as an excessive number of units could decrease the network's capabilities, while a number that is too low may have no effect on performance, thus not justifying its presence.

- 3GRU-Net: Due to its unique structure, this model requires a higher number of hyperparameters. The three encoder branches have the same structure as those present in the GRU-Net. However, in the Bottleneck layer, the number of input

features is tripled because all the maps present at the output of the three branches are concatenated. The number of filters remains unchanged, therefore they are respectively 15, 32, 64, and 128. Due to the high number of parameters and thus the high computational cost in this set-up, only one GRU layer with a single unit is selected in the Decoder.

- Res-Net: To set the hyperparameters of Res-Net, the study relied on information from the study by He et al. [25]. The network consists of three levels of encoders, a bottleneck, and three levels of decoders. In each MultiRes-block (Figure4.8), there are three convolutional layers with an increasing number of filters, respectively 1/6, 1/3, and 1/2 of the total number of filters of the corresponding level. For example, in the first level of the encoder, there will be 64/6, 64/3, and 64/2 for the three convolutional layers. In addition, the number of filters is weighted by a factor of $\alpha = 1.67$. After several attempts, a kernel size of 6 is selected. The Res-Path (Figure4.9), on the other hand, consists of four convolutional layers for the first level of the encoder, three layers for the second level, and two layers for the third level.

5.2. Loss Function

The loss functions used to train deep learning neural networks are mainly based on the use of Mean Absolute Error (MAE) and Mean Squared Error (MSE), reported in the formula below:

- Mean Absolute Error (MAE):

$$MAE = \frac{1}{n}\sum_{i=1}^{n}|y_i - \hat{y}_i| \tag{5.1}$$

The MAE calculates the average of the absolute distance between the target signal and the predicted signal. It is mainly used as an alternative to MSE when there are many outliers. However, when the error decreases, the optimization stops working as there is no defined minimum point.

- Mean Squared Error (MSE):

$$MSE = \frac{1}{n}\sum_{i=1}^{n}(y_i - \hat{y}_i)^2 \tag{5.2}$$

As stated in the formula, MSE calculates the average of the squared error between the predicted signal and the target. The quadratic dependence penalizes large errors and, due to its parabolic trend, it has a minimum point that allows for better optimization of the gradient at the minimum point. However, outlier values can compromise its performance, as values that are much larger or much smaller can cause a significant increase in loss.

In the present project, both loss functions were tested for all three models. From the analysis of the results, it was found that using MSE as the loss function improves the speed and quality of training, as the quadratic dependence on the error speeds up weight updates. However, since the MSE loss is insufficient in constraining local waveform information, an auxiliary function called *Lmax* is introduced to penalize abnormal points in the predicted waveform. In this way, the total loss depends on the mean squared error calculated between the target ABP and the predicted one, plus a term that depends on the absolute value of the error. The *Lmax* function is multiplied by a weighting factor of $\lambda = 0.005$ [14]. The final formula is presented below:

$$L_{total} = L_{mse} + \lambda \cdot (L_{max}) \tag{5.3}$$

$$L_{mse} = \frac{1}{n}\sum_{i=1}^{n}(|ABP_{ref} - ABP_{pred}|)^2 \tag{5.4}$$

$$L_{max} = \max(|ABP_{ref} - ABP_{pred}|) \tag{5.5}$$

the Equation n° 5.5 is the final selected Loss function that improves the regression task and speeds up the training [51].

5.3. Training procedure

The saved chunks are then transformed into *tf.records* format, which as mentioned before, increases model performance. They are then allocated and split into test, validation, and training sets based on a pre-set probability described in the previous section. Each batch sample corresponds to a 10-second window that includes the 16 input channels for the network, including the target signal and mask. Parameter updates for the network occur every 64 batch samples, which is the chosen batch size, and Adam Optimizer s taken as the

optimization method. The selected Loss was Lmse + Lmax, as presented in the reference section, with an initial value of 0.001. Following the pipeline shown in the diagram in Figure5.1, training is first performed on the training set with the indicated signal bank and the target and mask signals as input. The trained model is then tested on the test set to evaluate its final performance.

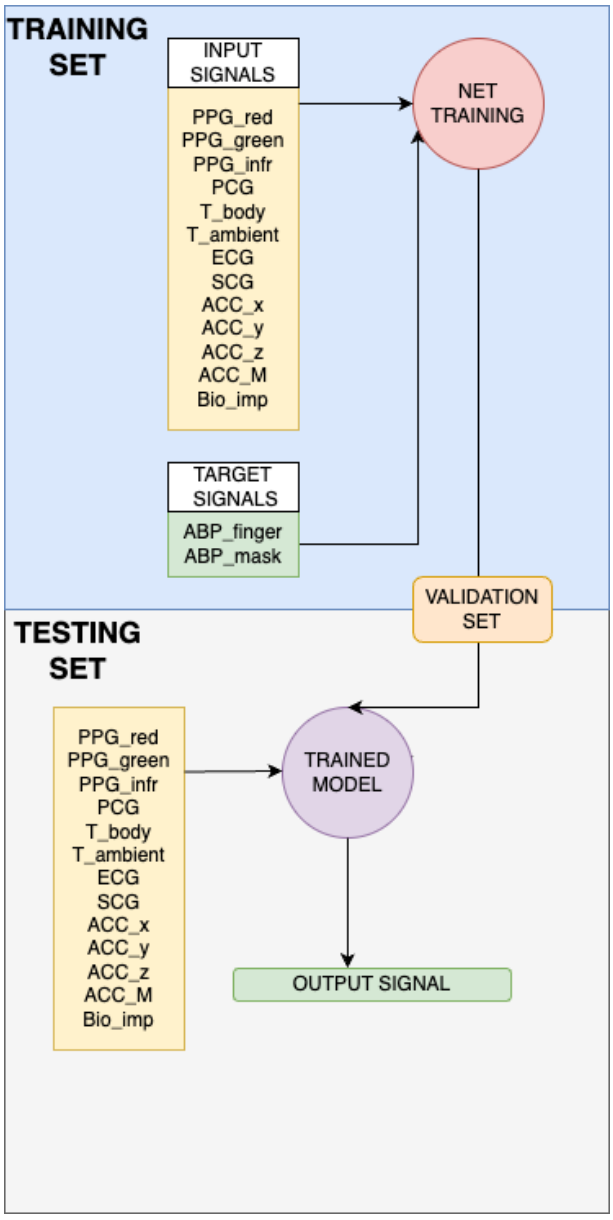

Figure 5.1: Training pipeline

5.3.1. Ablation Study for input signal selection

In the literature, numerous studies attempt to replicate the arterial pressure waveform using deep neural networks, solely relying on the photoplethysmography (PPG) signal, its

derivatives, and the electrocardiogram (ECG). This study leverages various physiological and non-physiological signals recorded through Soundi®. To comprehend the network's behavior based on input signals, an ablation study was conducted using different signal banks as tests. The study focused on the GRU-Net, employing various combinations of input signals. The specific sets experimented with are presented in Table 5.1

channels	Used signals	MAE (mmHg)	Loss value	color
1	PPG green	18.01	542	celeste
1	ECG	18.73	598	fucsia
3	PPG(green, red, infrared)	17.78	499	orange
4	PPG(green, red, infrared)ECG	17.03	469.8	purple
6	PPG(green, red, infrared)ECGPCGSCG	15.02	410	black
16	SignalBank	12.77	293.2	verde

Table 5.1: Ablation study for input signals: the channels refer to the number of the input; MAE is the mean absolute error computed on test set; Loss value refers to the value of the loss function and the indicated *color* The corresponding trend graph is shown in Figure 5.2

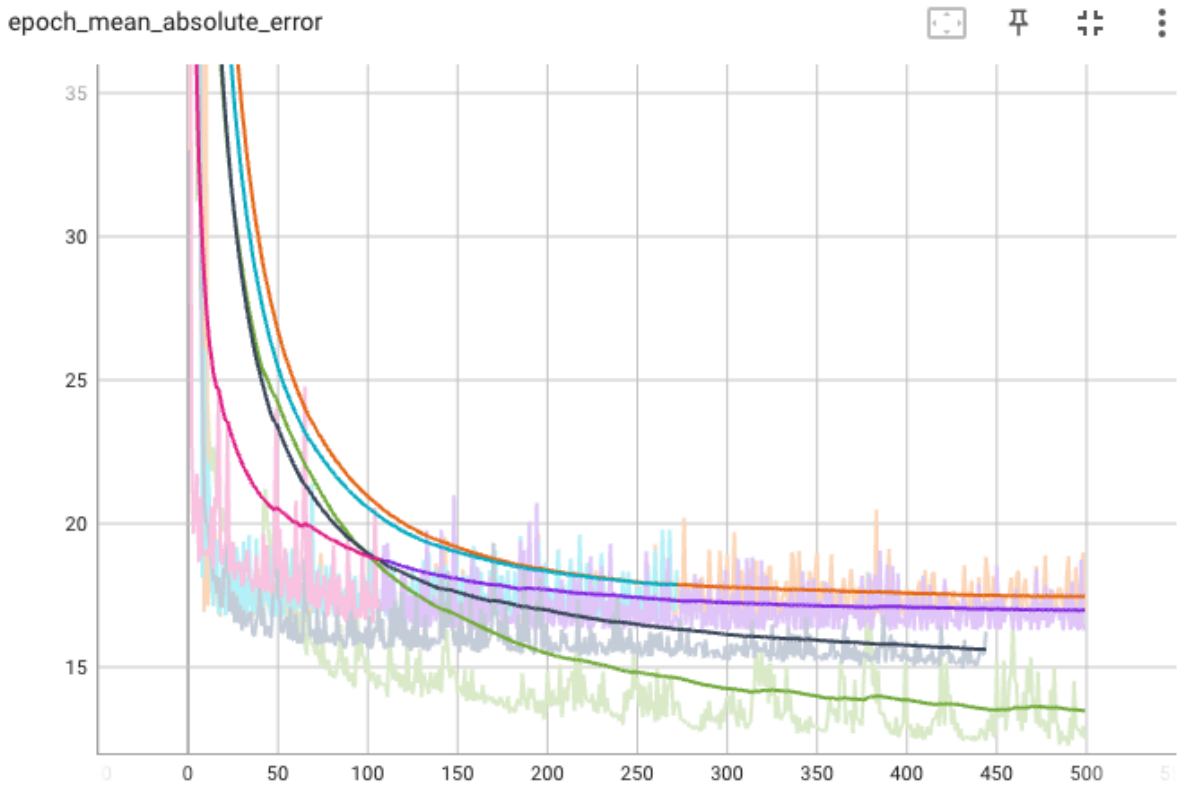

Figure 5.2: The trends of the U-Net with different smoothed input patterns are depicted.

From the results of the different tests shown in Table 5.1, it can be observed that the network performs better in reconstructing the input when all signals are given as input, achieving a mean absolute error of approximately 12.77 mmHg compared to other input combinations. For this reason, all sixteen signals are utilized, resulting in an improved reconstruction of the arterial pressure waveform.

6 | Results

6.1. Subject-dependent analysis

In this section, the results of the network performance and PTT regression models with a discussion of the evaluation metric are presented. The proposed models are compared with the principal model utilized in literature for the computation of the blood pressure waveform, and their performance is evaluated through the analysis of metrics and characteristic parameters. Then a BHS computation explains the evaluation of the developed method. In particular, a subject-dependent analysis is performed through an ablation study and compared with the developed classical mathematical model.

6.1.1. Models performance

For this analysis, the 6 recordings of Subject00 are used, on which data augmentation is performed as described above. The average values of systolic pressure, diastolic pressure, and mean arterial pressure (MAP) of the target input signals are presented in Table 3.13. In total, there are 135.40 minutes of recordings, divided into 10-second windows. Based on this dataset, the various architectures were tested, and a comparison was made between them. In Tabella 6.1 is reported the dataset characteristic for a subject-dependent analysis. The characteristic parameters of the ABP signal, the Loss function, and the trend of the evaluation metric are evaluated to assess the reconstructed waveform, using the metrics described above. Subsequently, the values of systolic pressure, diastolic pressure, and mean arterial pressure (MAP) were calculated for the 10-second chunks.

N° of acquisition	**Sex**	**Age [years]**	**Height [cm]**	**Weight**	**Duration [min]**
6	Male	53	190	92	135.40

Table 6.1: Description of Input Dataset for Subject-dependent analysis

To understand the behavior of the three different models discussed earlier, a subject-dependent analysis is performed to analyze their performance on the input dataset. The

first model under analysis is the U-Net with the cascaded ResNet. The hyperparameters used for initializing the network are listed in Table 6.2

Models	Loss function	Optimizer	Initial Filter	GRU Units	Epochs
U-Net+ResNet	MSE	Adam	15/5	1	1200

Table 6.2: U-Net+ResNet initialization parameters for the complete model

The Mean Squared Error, as described previously, is used as the loss function. After several tests, Adam was selected as the primary optimizer for the models because, although slower than Stochastic Gradient Descent, it proved to be better as it allows for automatic adaptation of the learning rate during training. The initial number of filters for the U-Net is set to 15, while for the ResNet it is set to 5. Additionally, considering a large amount of data, an initial minibatch size of 64 is chosen.

In Figure 6.1, 6.2, and 6.3, the trends of the loss function, Mean Absolute Error and Mean Signed Error are depicted for the U-Net with the cascaded ResNet. The TensorBoard tool of TensorFlow is utilized to visualize the parameter trends across epochs. The validation set trend is highlighted in blue, while the training set trend is shown in black. It can be observed that the network tends to exhibit slight overfitting after 100 epochs. In Figure 6.3, the Mean Signed Error of the validation set approaches zero, following the trend of the training set. Table 6.3 reports the values of Mean Absolute Error (MAE) for both the training set and the validation set, as well as the value of the loss function.

UNet+ResNet			
Training set		Validation set	
Loss value	MAE [mmHg]	Loss value	MAE [mmHg]
193.34	9.80	257.90	11.55

Table 6.3: U-Net+ResNet initialization parameters for the complete model

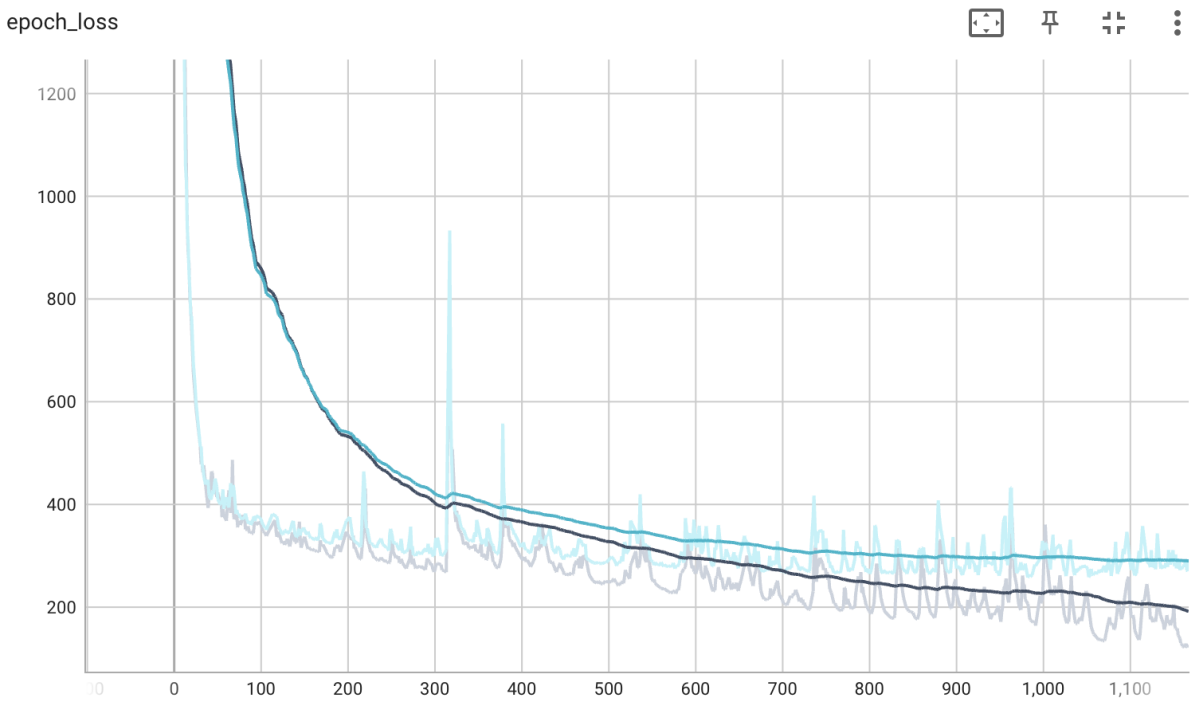

Figure 6.1: Trend fro U-Net loss function vs epochs: Blue for the validation set and black for the training set

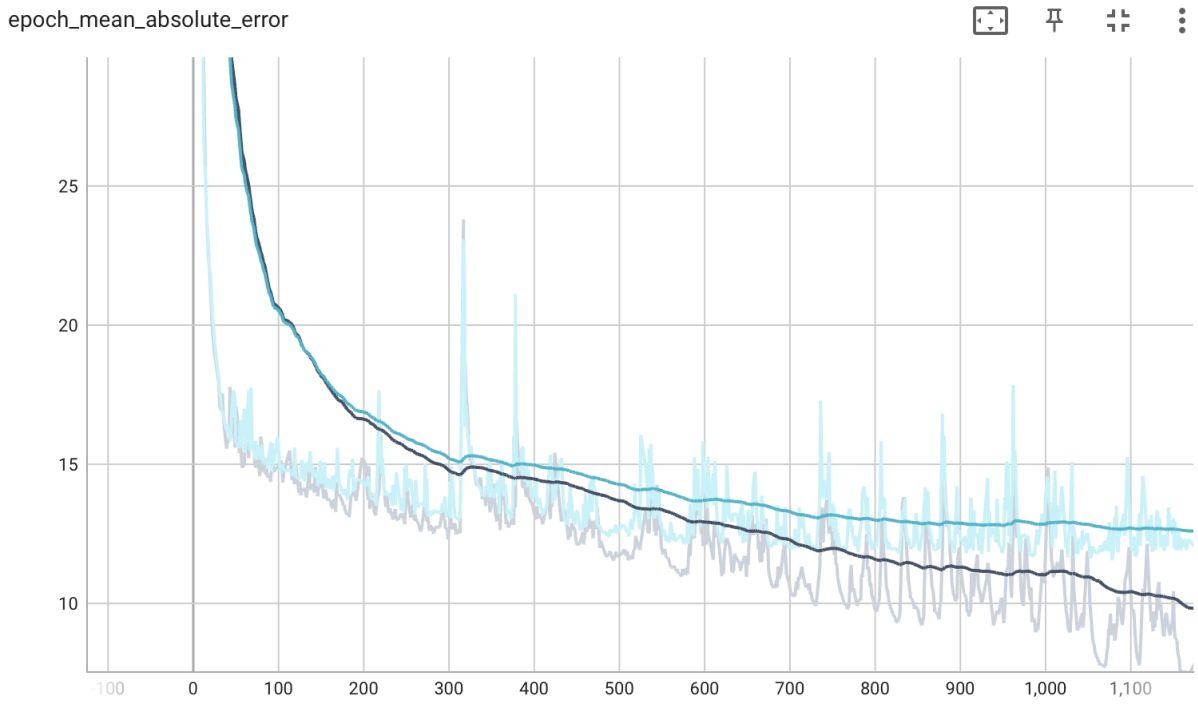

Figure 6.2: Trend fro U-Net MAE metric function vs epochs: Blue for the validation set and black for the training set

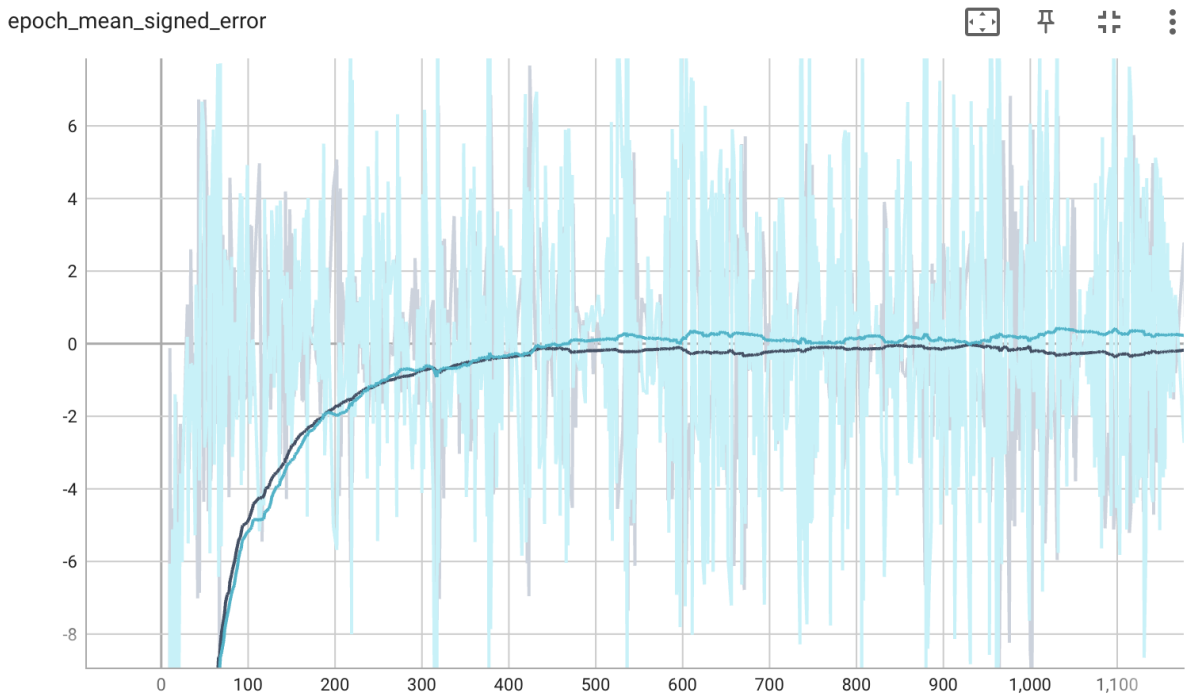

Figure 6.3: Trend fro U-Net MAE mean signed error function vs epochs: Blue for the validation set and black for the training set

Next, the GRU-Net with the cascaded ResNet was tested using the same dataset. The initialization parameters for the network are listed in Table 6.4. It can be observed that the optimizer and loss function remain the same, but there is a new parameter indicating the number of units for the GRU layer, which is set to 1 in this case. In Figure 6.4, 4.2, and 6.6, the trends of the loss function, Mean Absolute Error (MAE), and Mean Signed Error, respectively, are shown.

Models	Loss function	Optimizer	Initial Filter	GRU Units	Epochs
GRU-Net+ResNet	MSE	Adam	15/5	1	1200

Table 6.4: GRU-Net+ResNet initialization parameters for the complete model

GRU+ResNet			
Training set		Validation set	
Loss value	MAE [mmHg]	Loss value	MAE [mmHg]
157.42	9.78	218.21	11.31

Table 6.5: GRU-Net+ResNet value complete model

As shown in Table 6.5, the values of the loss function and MAE are lower compared to the model without the GRU layer. This is also supported by the trends depicted in the figures, which reach slightly lower values.

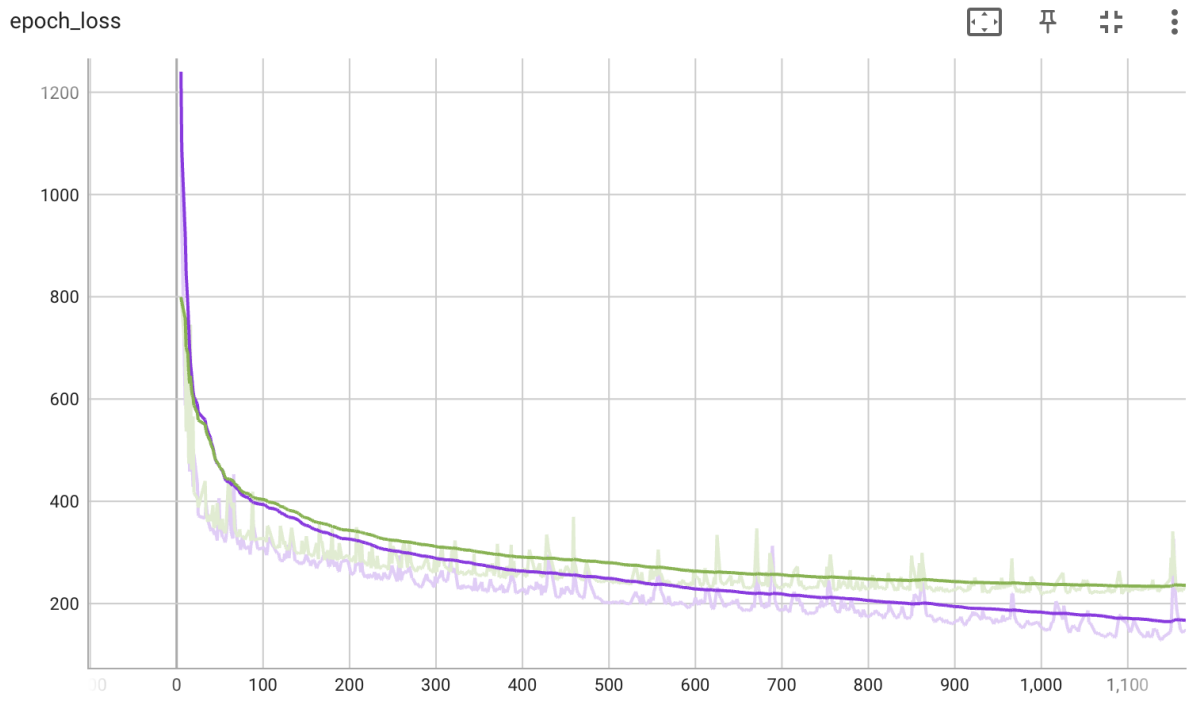

Figure 6.4: Trend fro GRU-Net loss function vs epochs: green for the validation set and purple for the training set

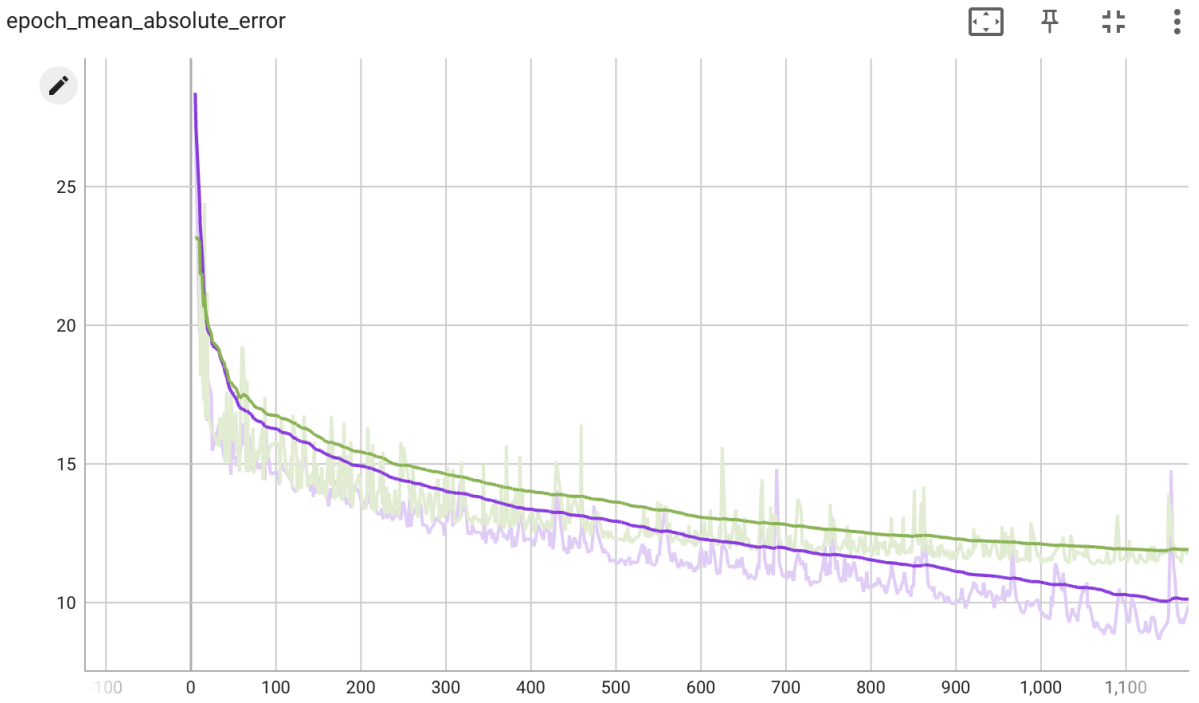

Figure 6.5: Trend fro GRU-Net metric function vs epochs: green for the validation set and purple for the training set

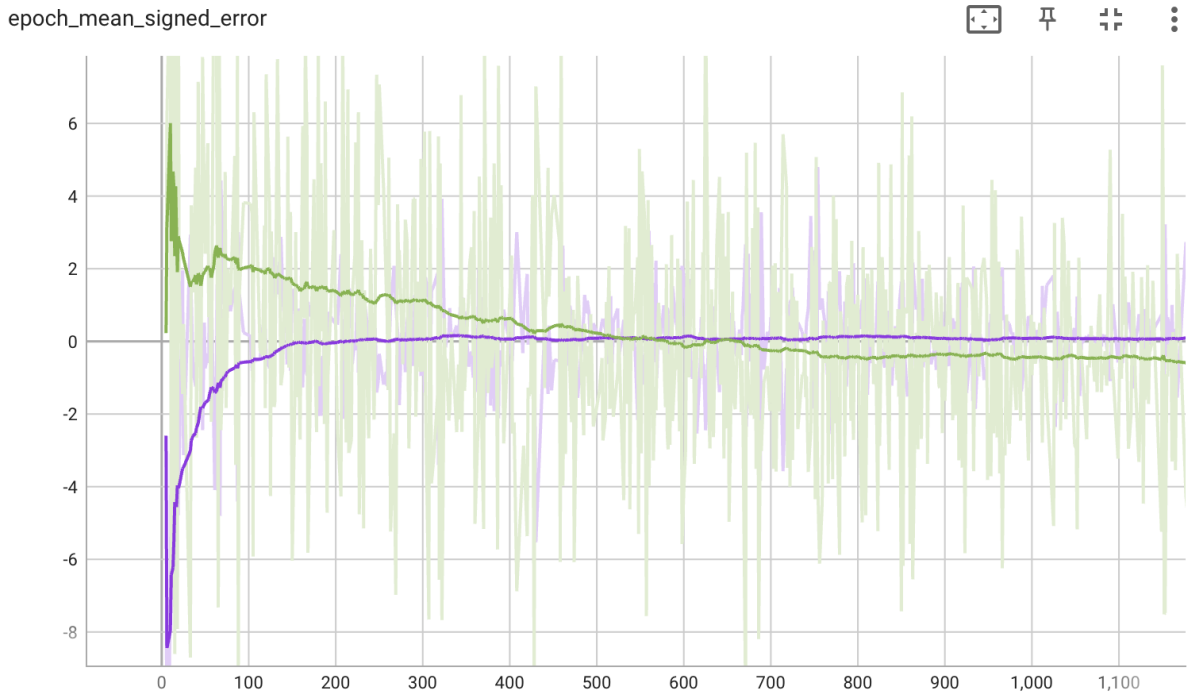

Figure 6.6: Trend fro GRU-Net mean signed error function vs epochs: green for the validation set and purple for the training set

The last model tested is the 3GRU-Net, which consists of three different branches based on the type of input signal, as described earlier. Table 6.6 presents the initialization parameters for the 3GRU-Net and ResNet. In this case, the initial number of filters is set to the same for all three branches. Table 6.7 reports the values of the loss function and MAE. Compared to the previous models, the 3GRU-Net achieves lower Mean Absolute Error values, indicating improved predictive capability. In Figures 6.7, 6.8, and 6.9, the trends of the evaluation parameters on the training and test sets are shown.

Models	Loss function	Optimizer	Initial Filter	GRU Units	Epochs
3GRU-Net+ResNet	MSE	Adam	15/5	1	1200

Table 6.6: 3GRU-Net+ResNet initialization parameters for the complete model

3GRU-ResNet			
Training set		Validation set	
Loss value	MAE [mmHg]	Loss value	MAE [mmHg]
96.56	7.07	194.81	10.53

Table 6.7: 3GRU-Net+ResNet value complete model

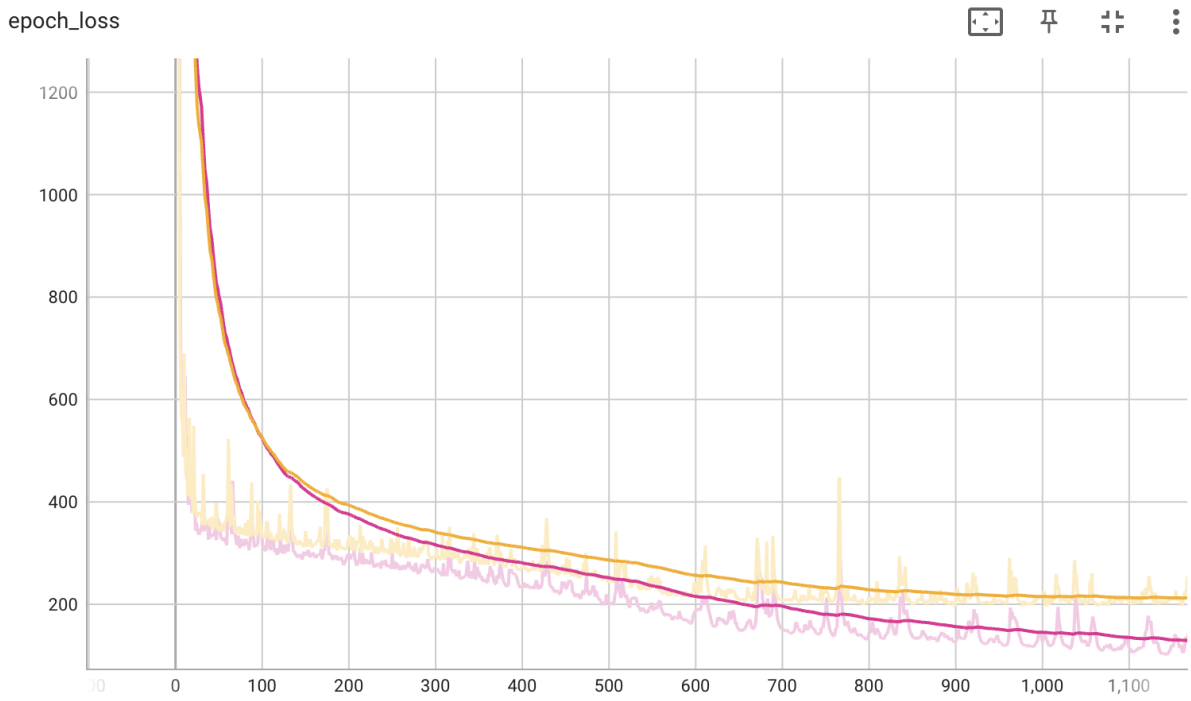

Figure 6.7: Trend fro 3GRU-Net loss function vs epochs: orange for the validation set and magenta for the training set

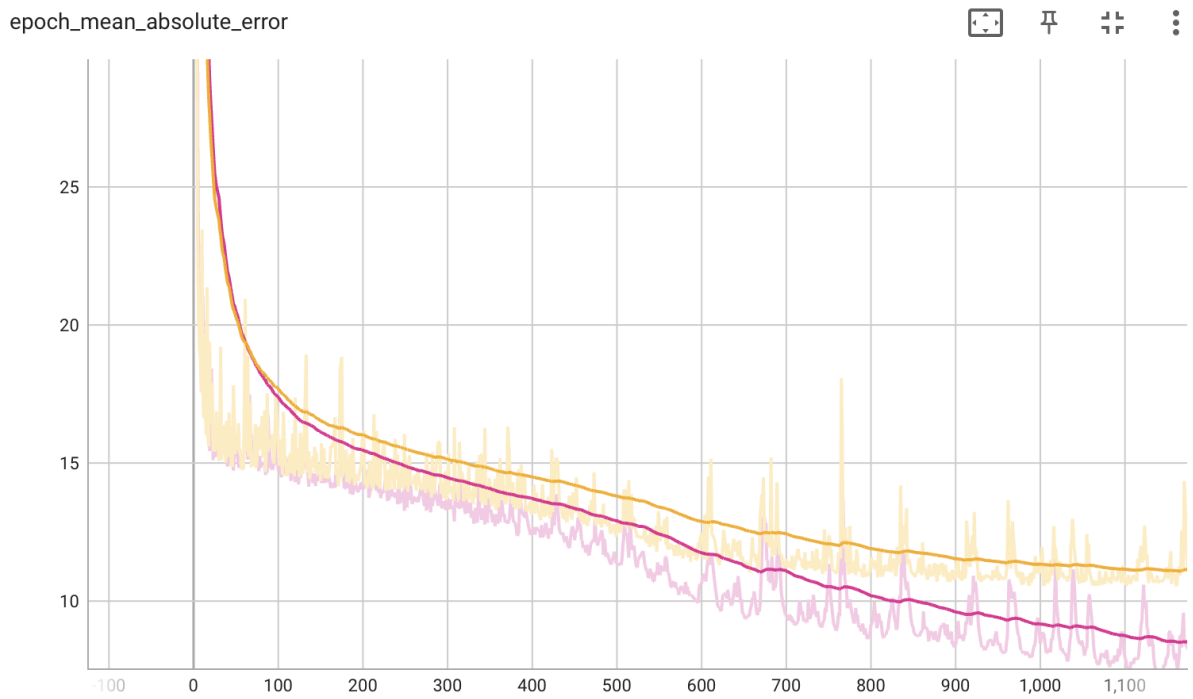

Figure 6.8: Trend fro 3GRU-Net MAE metric function vs epochs: orange for the validation set and magenta for the training set

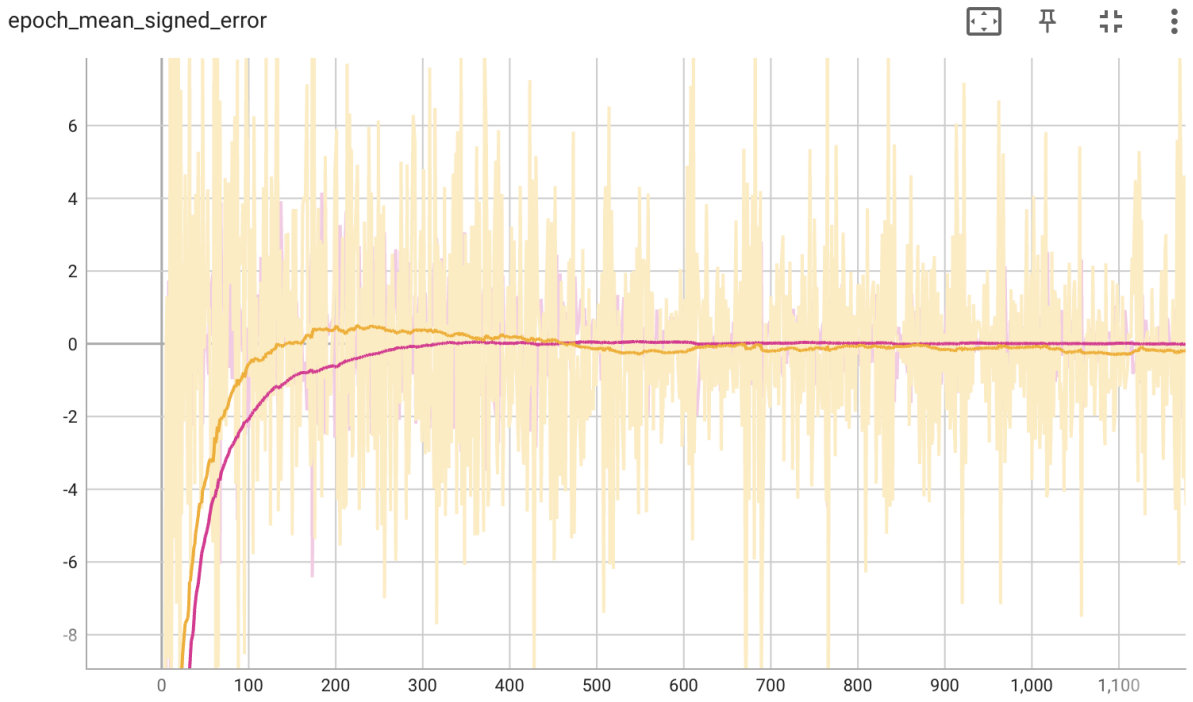

Figure 6.9: Trend fro 3GRU-Net MAE mean signed error function vs epochs: orange for the validation set and magenta for the training set

Among the three models, as seen in Figures 6.10, 6.11, and 6.12, which illustrate the trends of the loss function, mean absolute error, and mean signed error, it appears that the model with three branches (3GRU-Net) exhibits a better trend compared to the other two models. In Table 6.7, the values for the 3GRU-Net model are reported, showing lower values compared to the other models, with an MAE of 10.53 mmHg on the validation set. A recap of the MAE and loss values for each model is presented in Figure 6.11 and 6.10, where the U-Net is represented in blue, the GRU-Net in green, and the 3GRU-Net in orange. It can be observed that the 3GRU-Net achieves lower loss values and a lower MAE value. This is further confirmed by Table 6.8, which provides a summary of the loss and MAE values for all the models in both the training and validation sets.

	Training set		**Validation set**	
Model	**Loss value**	**MAE [mmHg]**	**Loss value**	**MAE [mmHg]**
U-Net	193.34	9.80	257.90	11.55
GRU-Net	157.42	9.78	218.21	11.31
3GRU-Net	96.56	7.07	194.81	10.53

Table 6.8: metrics of the developed models

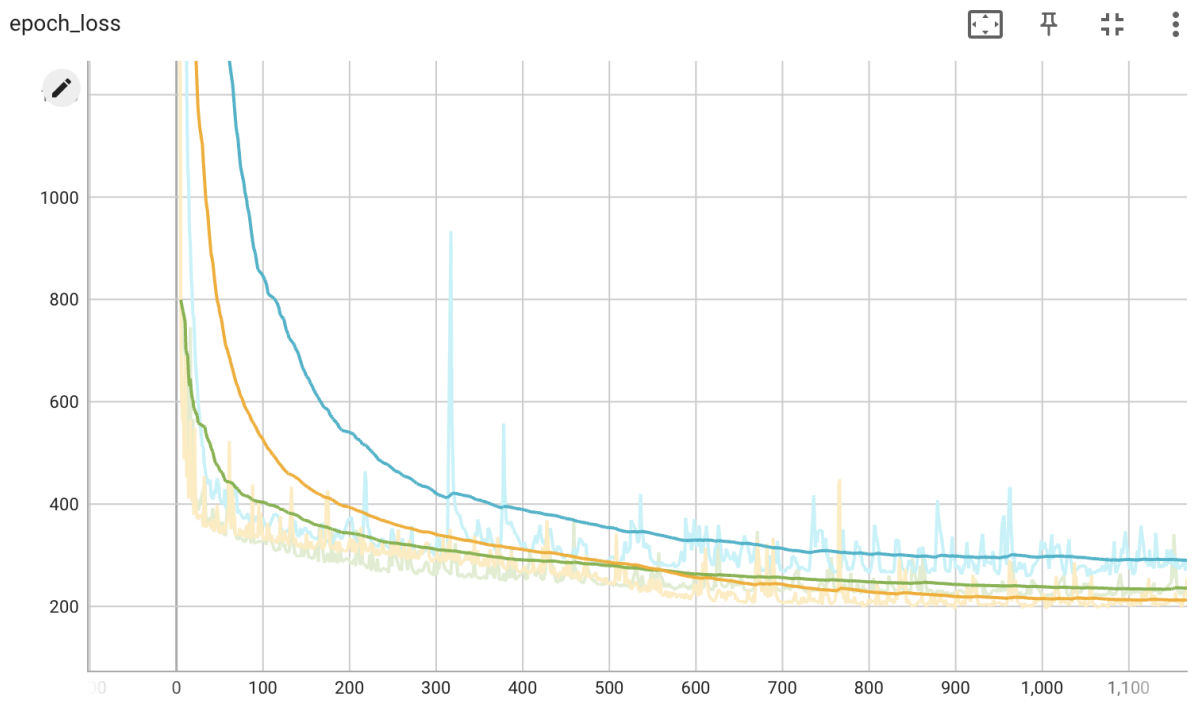

Figure 6.10: Trend of loss function for the three models: orange for 3GRU, green for GRU-Net, and blue for U-Net

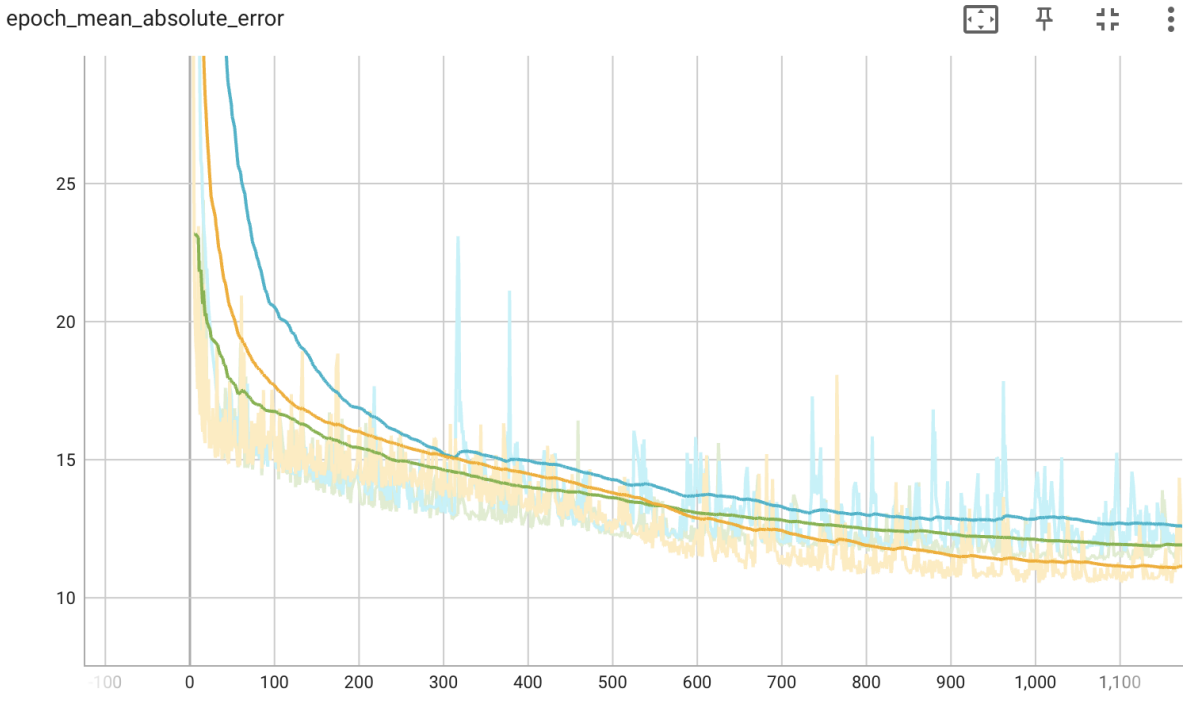

Figure 6.11: Trend of Metrics function for the three models: orange for 3GRU, green for GRU-Net, and blue for U-Net

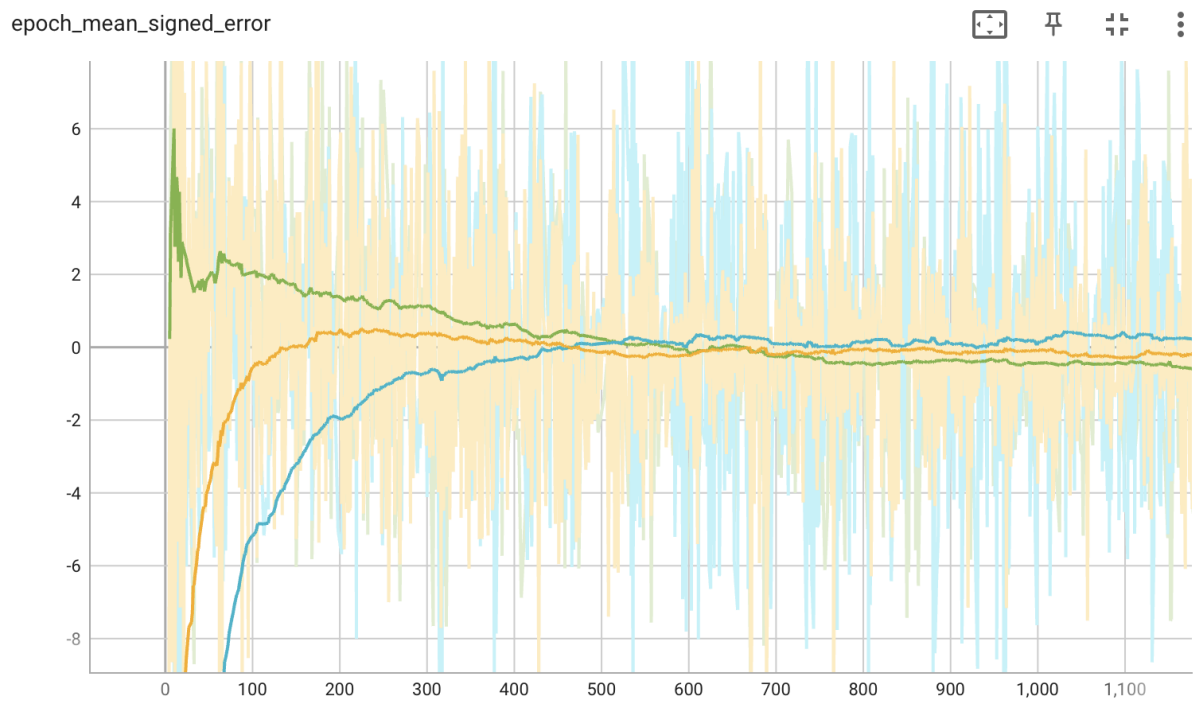

Figure 6.12: Trend of mean signed error function for the three models: orange for 3GRU, green for GRU-Net, and blue for U-Net

Finally, to complete the study, the target parameters, which serve as indicators of the signal reconstruction quality, are computed for each model. For each 10-second chunk, the systolic and diastolic pressure peaks are extracted, one per second, resulting in 10 samples of systolic and diastolic pressure for each chunk, as described previously. The Mean Absolute Error (MAE), Mean Squared Error (MSE), and Root Mean Squared Error (RMSE) are then calculated for each of the evaluated reference parameters. The SBP, DBP, MBP, and STD values, computed over the test set for each analyzed model, are reported in Tables 6.9 and 6.10 for the U-Net and GRU-Net models, and in Table 6.11 for the 3GRU-Net. It can be observed that the models with the presence of the GRU layer exhibit lower error values compared to the regular model using the classic U-Net. Specifically, for the values of systolic, diastolic, and mean pressure, better results are achieved using the GRU layer.

	MAE + STD [mmHg]	MSE + STD [mmHg]	RMSE + STD [mmHg]
SBP	11.78 ± 5.35	167.22 ± 5.31	12.93 ± 5.22
DBP	6.35 ± 5.06	66.04 ± 5.83	8.12 ± 5.10
MAP	5.49 ± 3.56	42.89 ± 6.54	6.54 ± 3.67
STD	6.61 ± 3.51	54.26 ± 3.23	7.36 ± 3.22

Table 6.9: Parameters computation for U-Net over the Test set

	MAE + STD [mmHg]	MSE + STD [mmHg]	RMSE + STD [mmHg]
SBP	11.19 ± 6.29	165.02 ± 6.36	12.84 ± 6.19
DBP	5.30 ± 4.15	45.41 ± 5.55	6.73 ± 4.20
MAP	5.52 ± 4.83	53.90 ± 7.23	7.34 ± 4.77
STD	6.01 ± 2.58	42.90 ± 2.58	6.55 ± 2.80

Table 6.10: Parameters computation for GRU-Net over the Test set

	MAE + STD [mmHg]	MSE + STD [mmHg]	RMSE + STD [mmHg]
SBP	11.35 ± 8.71	204.88 ± 9.13	14.31 ± 8.60
DBP	4.68 ± 4.22	39.78 ± 5.36	6.30 ± 4.19
MAP	6.27 ± 5.33	67.78 ± 7.82	8.23 ± 5.40
STD	5.78 ± 3.15	43.37 ± 3.14	6.58 ± 3.24

Table 6.11: Parameters computation for 3GRU-Net over the Test set

The comparison among these metrics highlights that 3GRU-Net and GRU-Net perform well with respect to the normal U-Net model. Analyzing the reconstructed waveform with the different methods, as shown in Figure 6.13, it can be seen that the normal U-Net, compared to the other two models, presents more noise and a more pronounced shift, failing to fully reproduce the waveform. With the GRU-Net and the addition of MultiResU-Net in cascade, the shift is reduced and the shape improves. Finally, with the 3GRU-Net, there is a significant reduction in noise and the prediction improves slightly compared to the previous one. In the next paragraph are discussed the error analysis to better understand the behavior of the models.

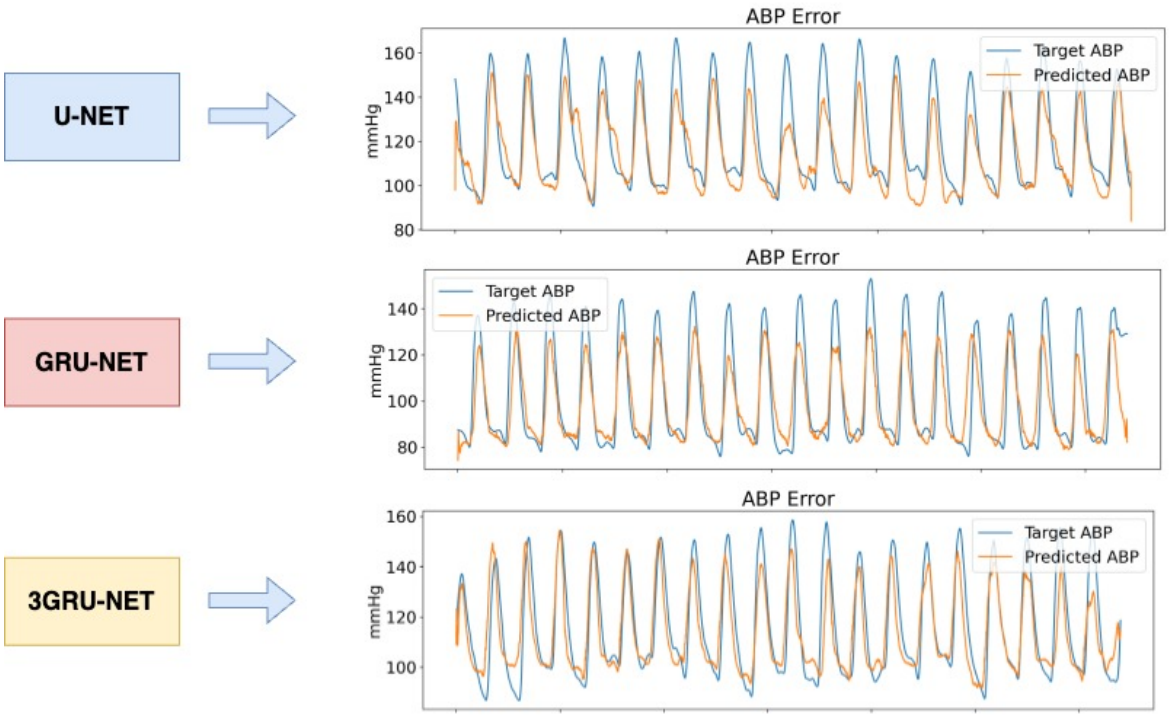

Figure 6.13: Waveform reconstruction with the relative method

6.1.2. Error analysis

In this section, an analysis and comparison of the errors in the calculation of the clinical parameters of interest are presented. Specifically, as in clinical practice, the calculation of average parameters over the ten-second prediction period is reported. In Figures 6.14, 6.15, and 6.16 are depicted plots of the analyzed parameters, including SBP, DBP, and MAP for the employed models. These figures provide visual representations of the predicted values compared to the ground truth values for each model.

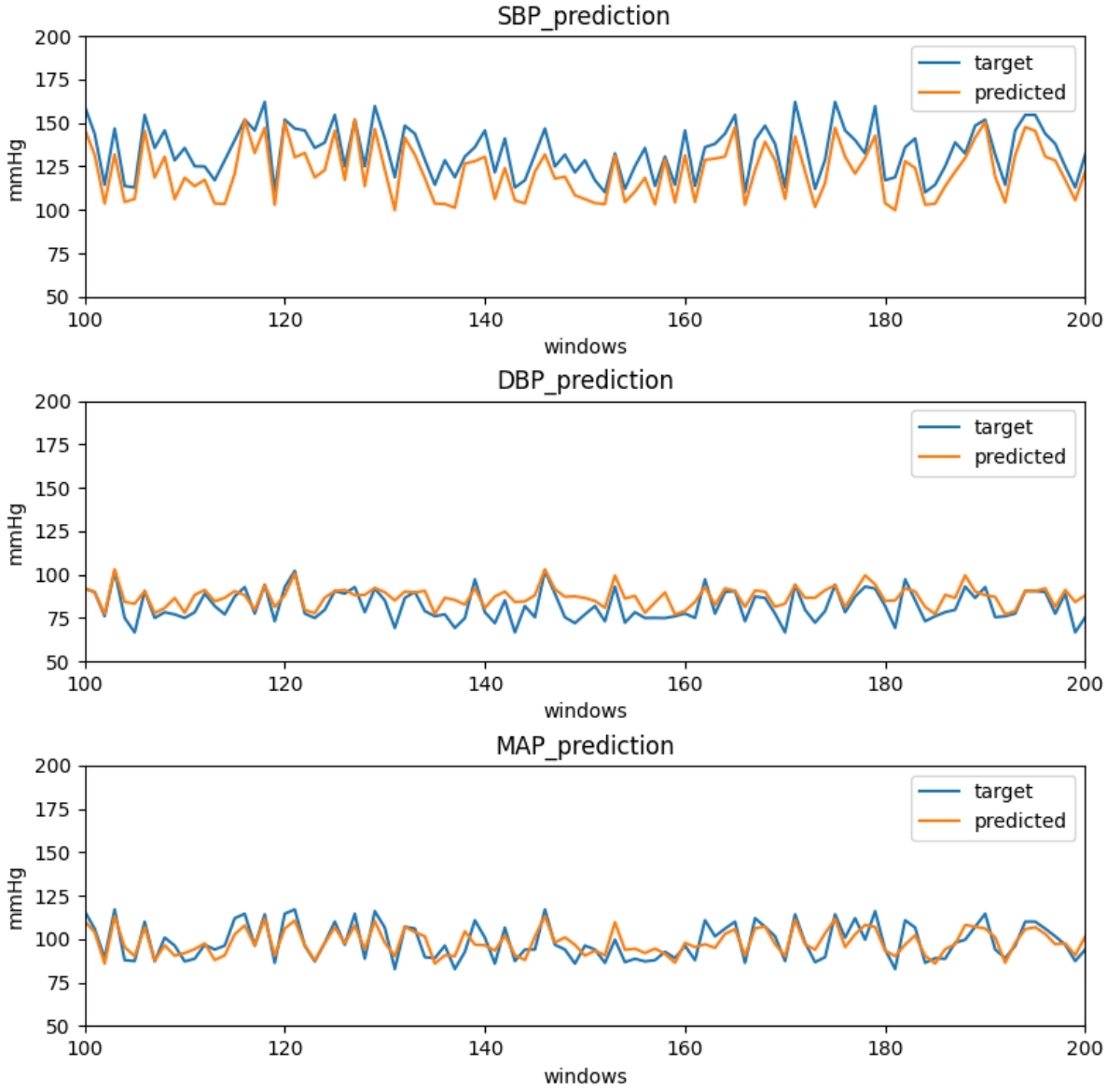

Figure 6.14: Prediction of characteristic parameters for U-Net model: SBP, DBP, MBP, STD

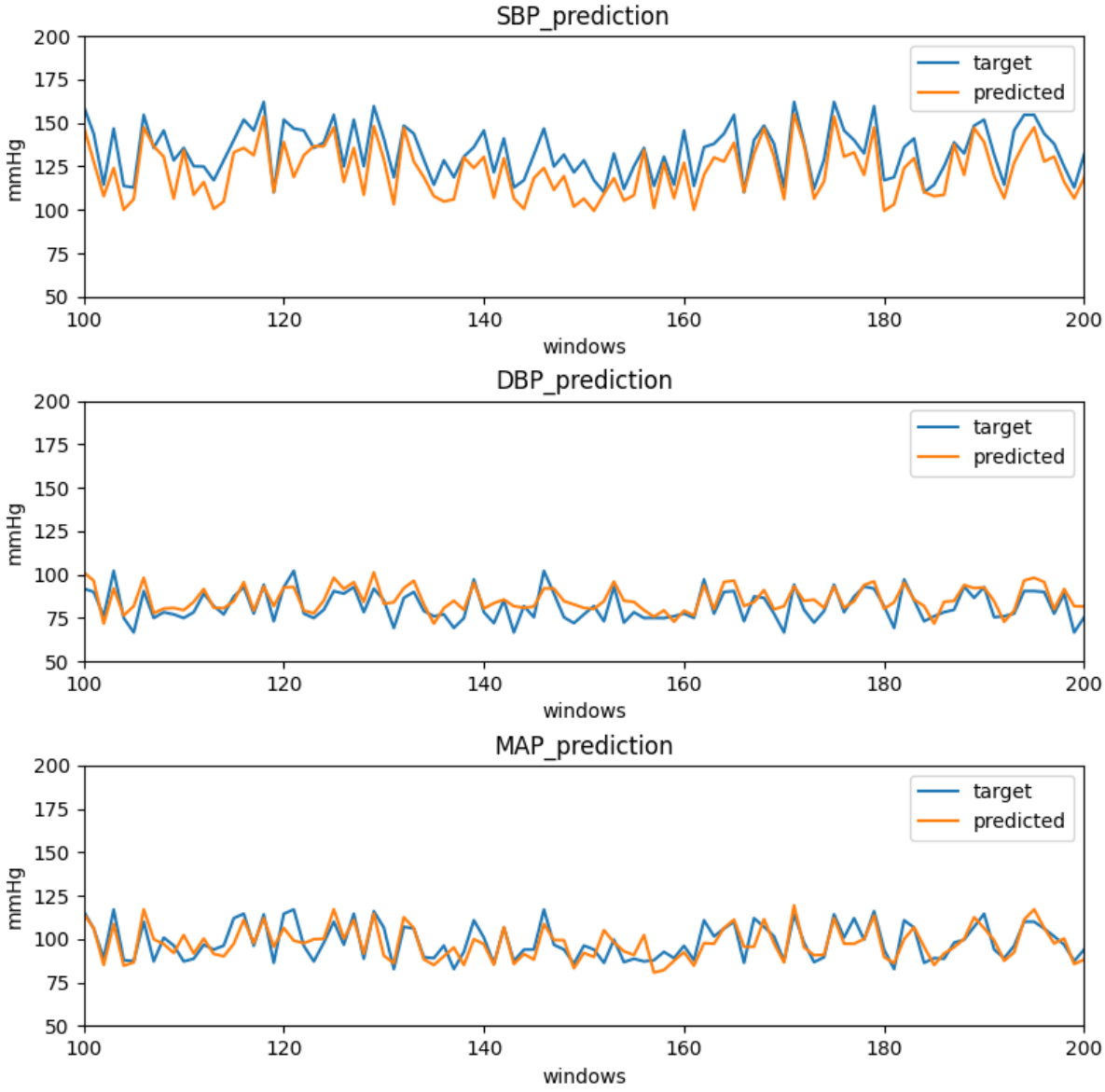

Figure 6.15: Prediction of characteristic parameters for GRU-Net model: SBP, DBP, MBP, STD

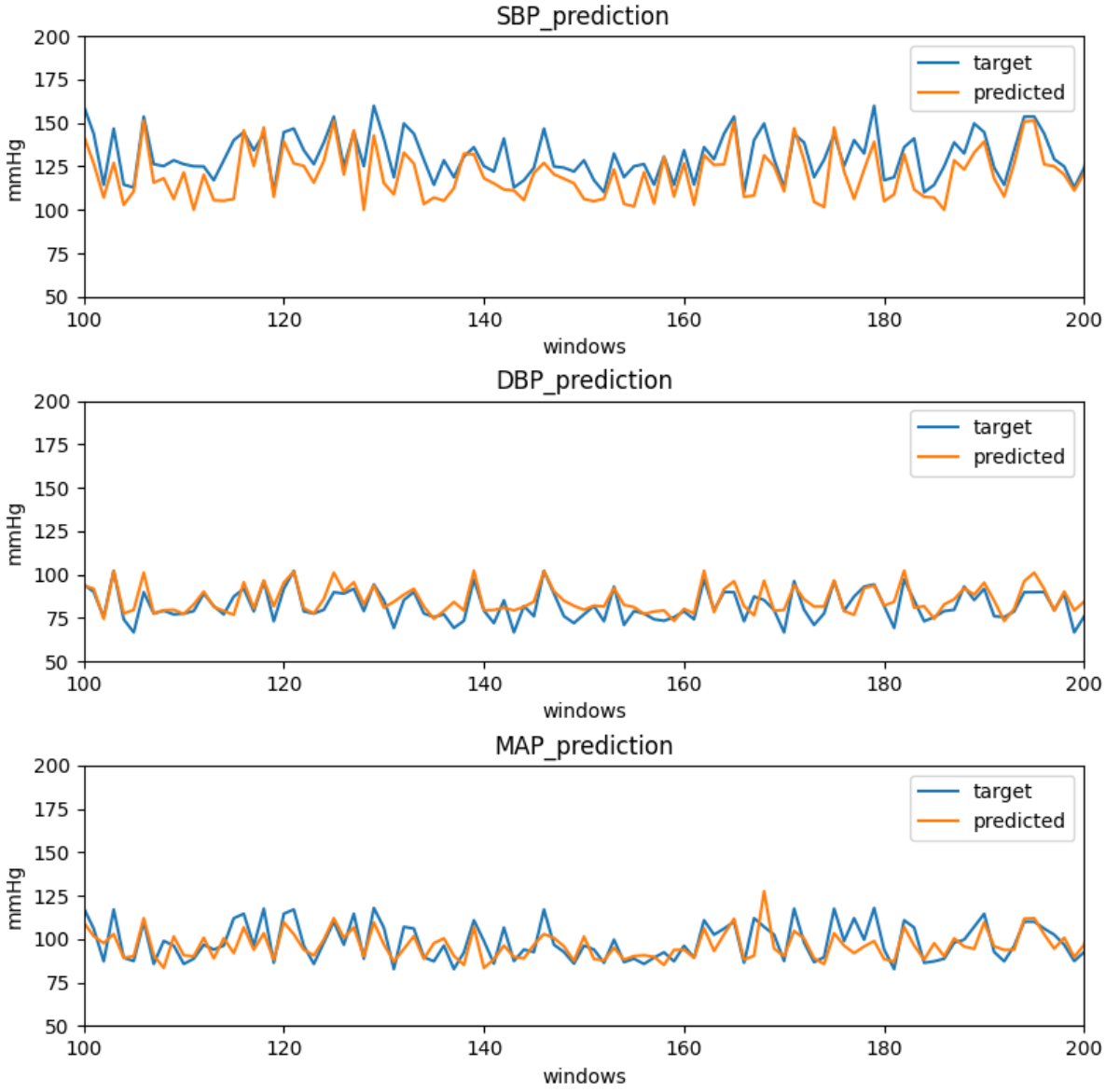

Figure 6.16: Prediction of characteristic parameters for 3GRU-Net model: SBP, DBP, MBP, STD

In the first quadrant of each figure, the predicted values of systolic pressure are displayed, while the second quadrant shows the diastolic pressure, and the third quadrant represents the mean arterial pressure (MAP). The predicted values are shown in orange, while the target values are shown in blue. As observed in the figures, all three models have greater difficulty in predicting systolic pressure values, which are consistently underestimated compared to the target values. However, both the diastolic pressure and mean pressure predictions yield excellent results. Despite the challenges in predicting systolic pressure, the prediction of mean pressure is strong and comparable to the main methods discussed

in the literature. The standard deviation of the predicted signal is also comparable to that of the target signal. This can be observed in Figure 6.16, where it is evident that the reconstructed signal struggles to reach the minimum peak of the target (DBP), but maintains a stable baseline. In Figure 6.17 and 6.18, the error distributions for the U-Net and GRU-Net models are displayed, while Figure 6.19 shows the distribution for the 3GRU-Net model. As observed, all distributions exhibit a Gaussian trend centered around the mean prediction value, indicating good consistency in the predictions.

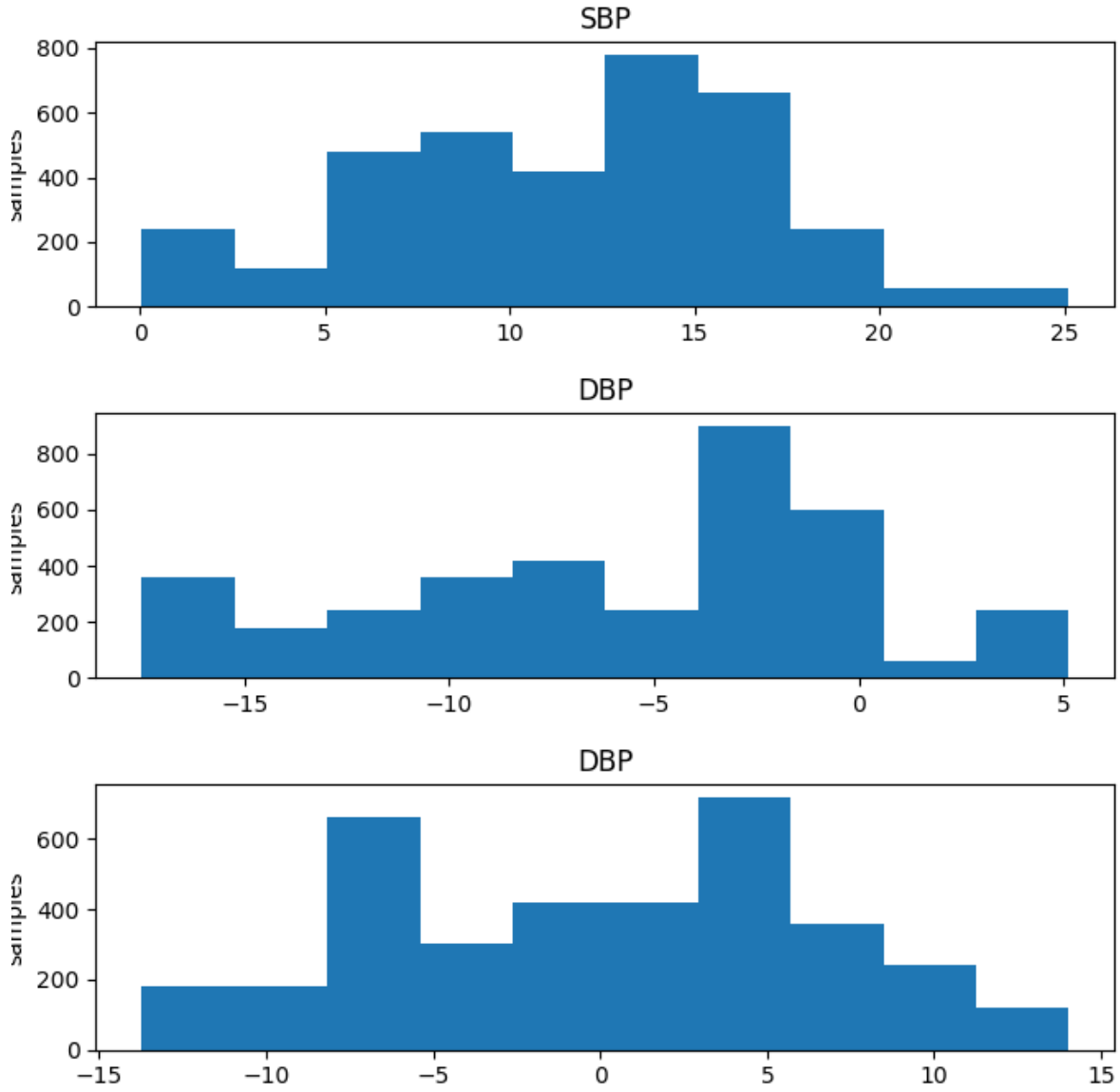

Figure 6.17: Distribution of U-Net errors: SBP, DBP, MBP

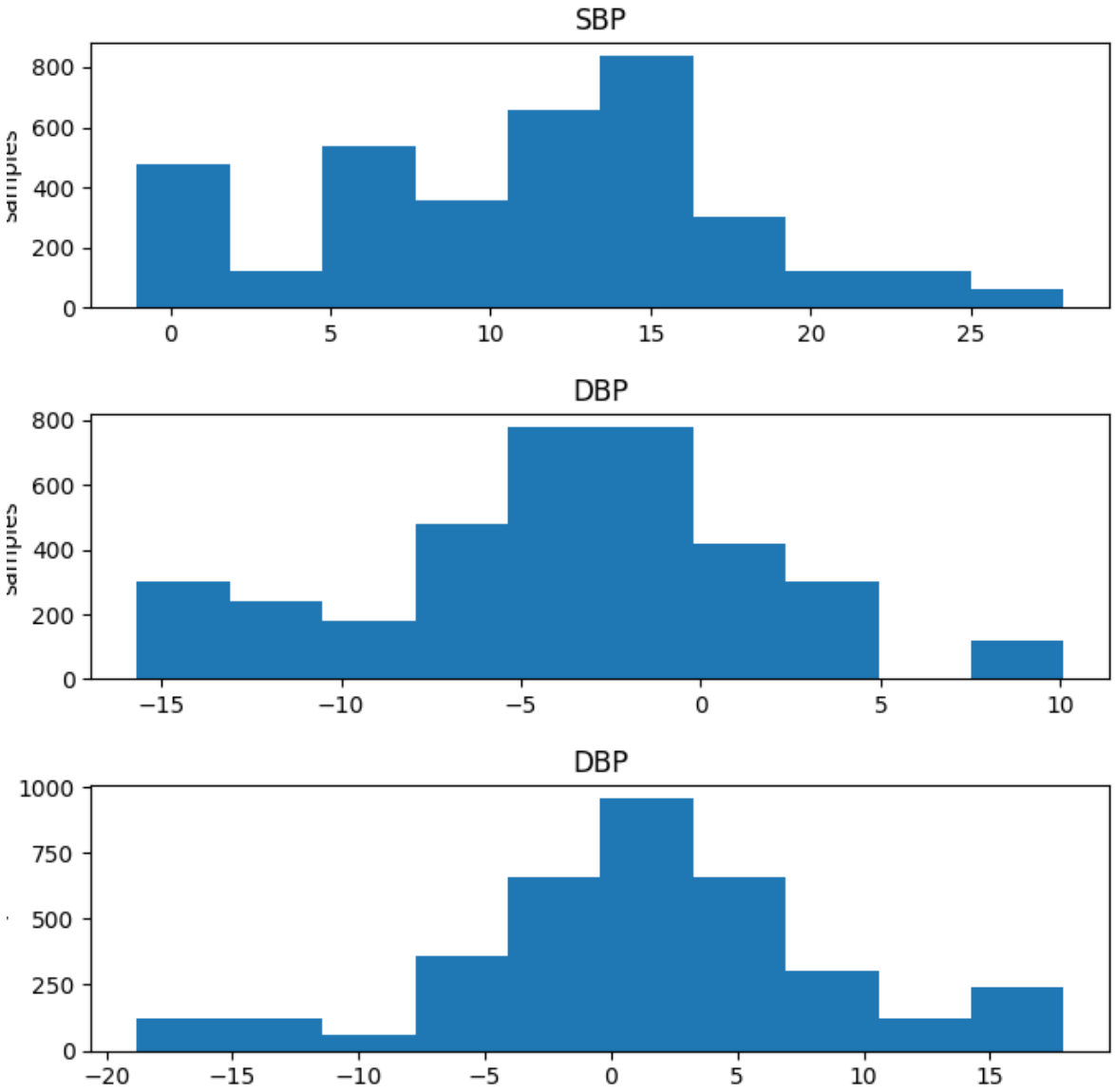

Figure 6.18: Distribution of U-Net errors: SBP, DBP, MBP

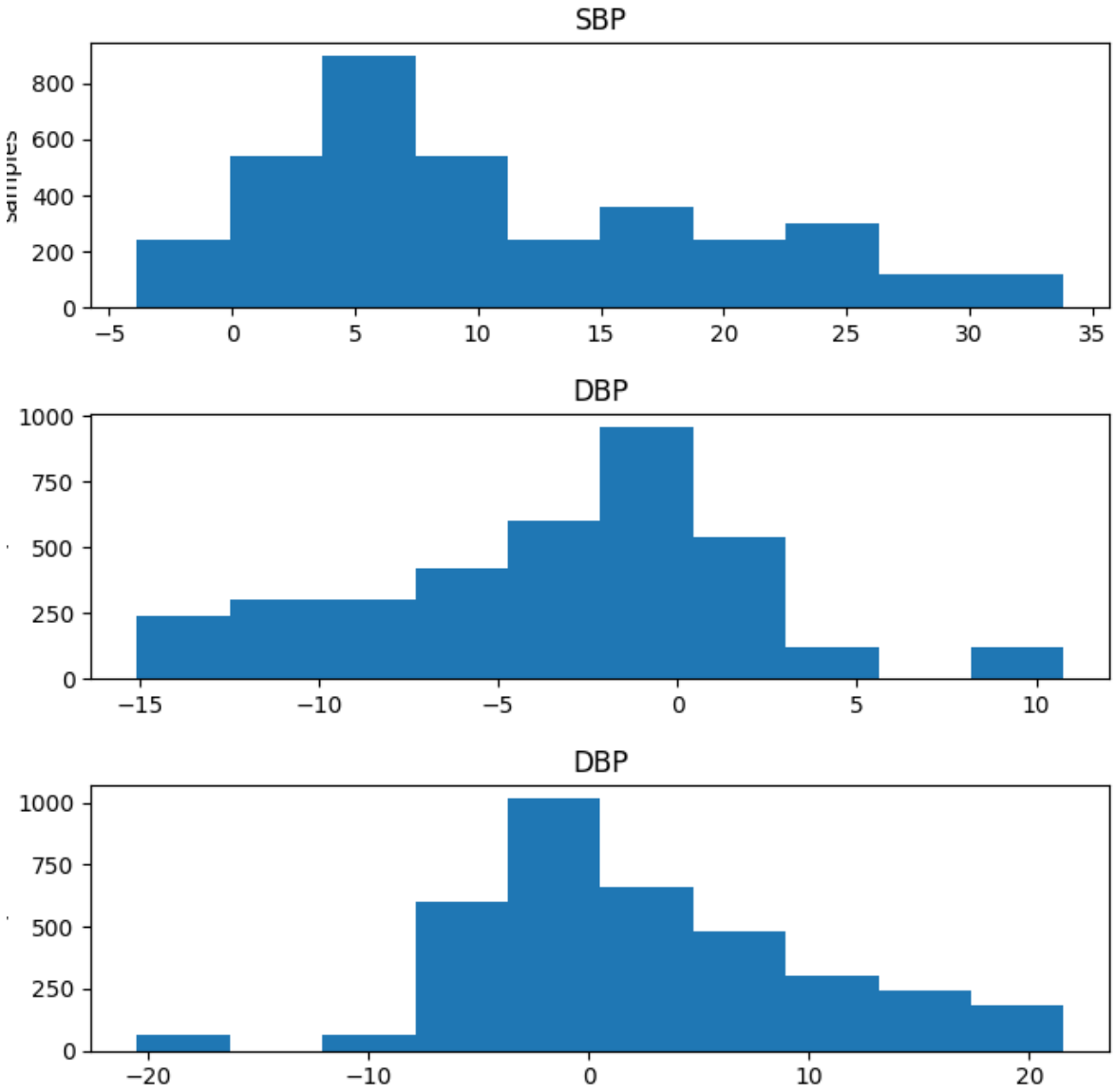

Figure 6.19: Distribution error for 3GRU-Net model: SBP, DBP, MBP

From here, it is possible to clearly highlight which of the three models is the most consistent. Analyzing the most critical parameter, which as seen previously is systolic pressure, it can be observed that the U-Net and GRU-Net models exhibit a concentration of prediction values around 24 mmHg for the U-Net and 15 mmHg for the GRU-Net. On the other hand, the model with three different branches shows a distribution centered around 5 mmHg, as seen in Figure 6.19. Moreover, when examining the error distribution for systolic and mean pressure values, it can be noted that the 3GRU and GRU models are comparable. In Figure 6.20 and 6.21, the mean difference plots are displayed for the U-Net and GRU-Net models, showing the respective values of systolic blood pressure in

the first quadrant, diastolic blood pressure in the second quadrant, and MAP in the third quadrant. Similarly, Figure 6.22 presents the corresponding plots for the 3GRU model. The Bland-Altman plots help to assess the consistency of the measurement method. On the vertical axis, the mean difference between the two measurement methods is depicted, while the horizontal axis represents the values of the analyzed pairs of points. The dashed median line represents the average of the measurement methods being compared.

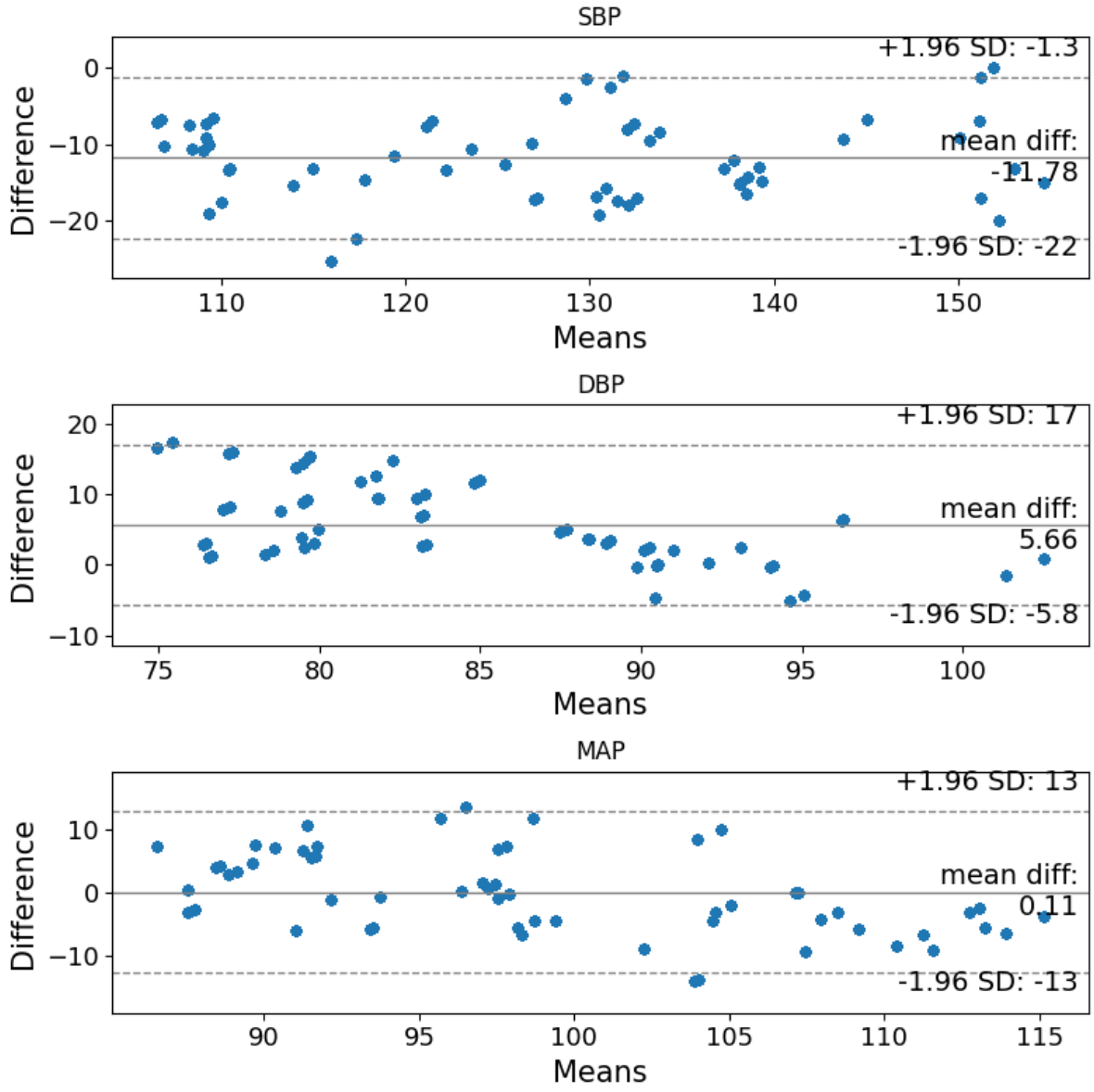

Figure 6.20: Distribution of U-Net errors

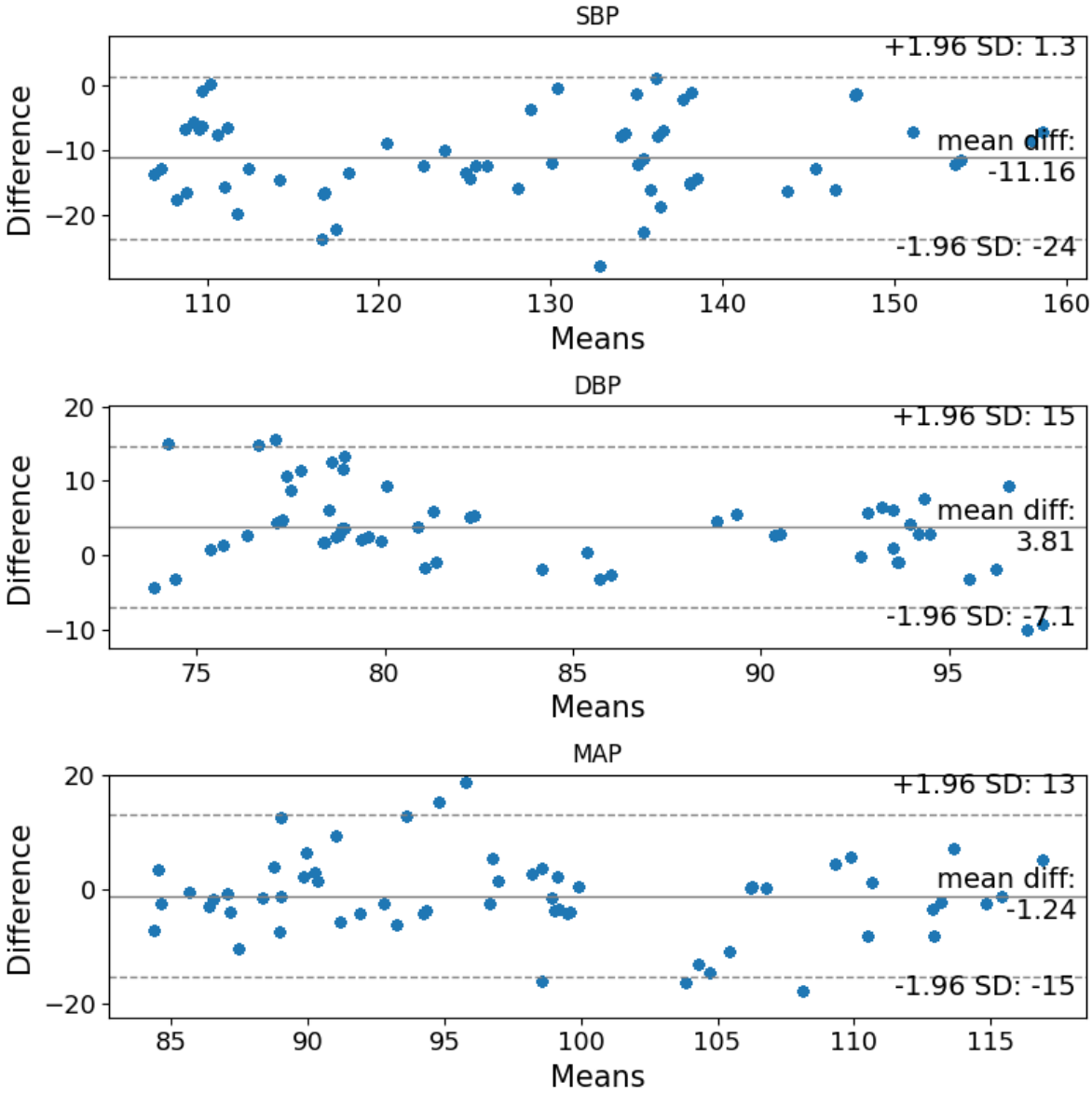

Figure 6.21: Distribution of GRU-Net errors

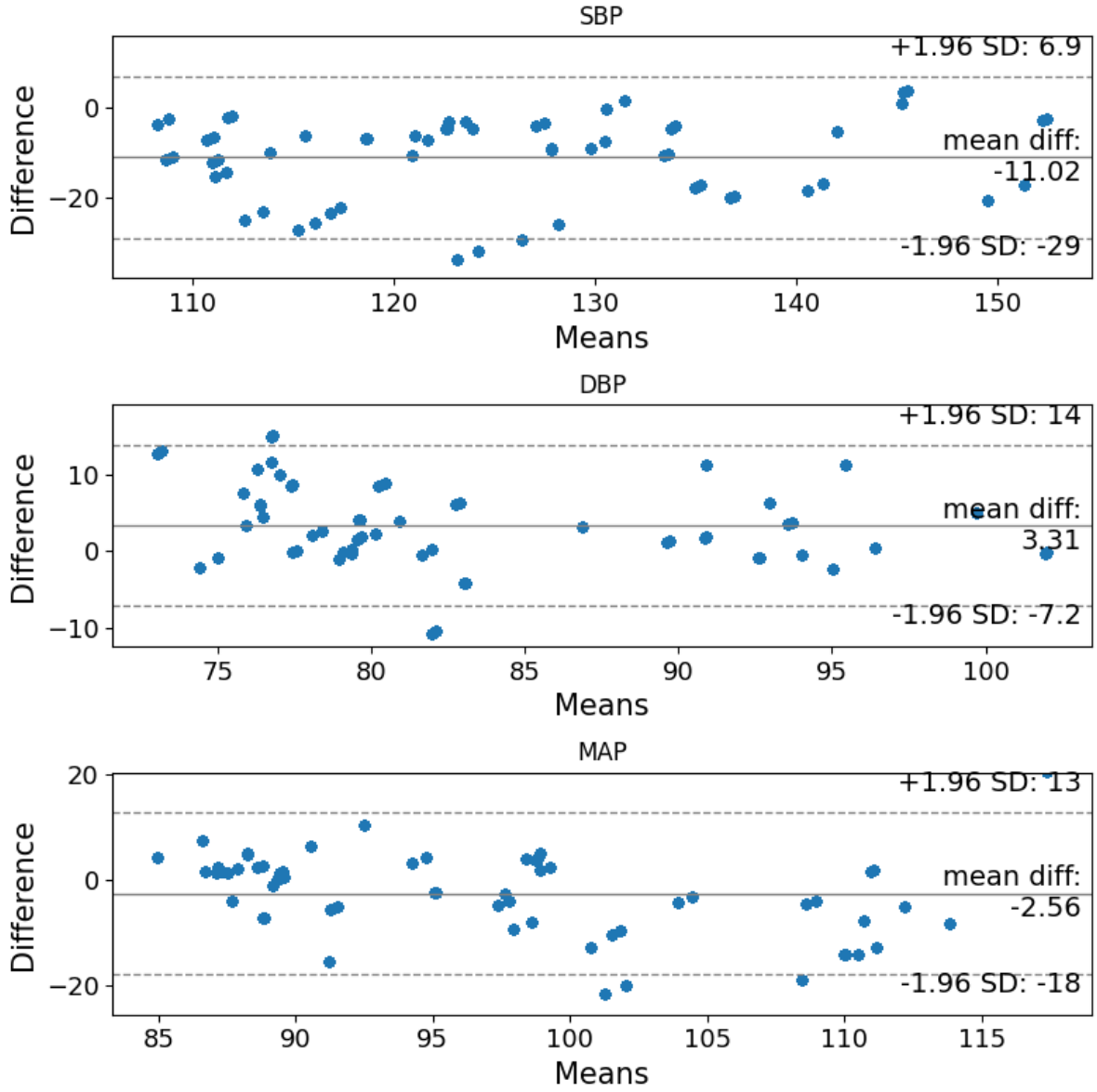

Figure 6.22: Blant Altman error plots for 3GRU-Net model: SBP, DBP, MBP

When examining the critical parameter of systolic blood pressure, it is evident that all three models struggle with its prediction. The mean difference between the two methods is -11.78 for U-Net, -11.16 for GRU-Net, and -11.02 for 3GRU-Net. This reflects the models' tendency to underestimate systolic blood pressure values. Among the three models, 3GRU-Net stands out with a lower value. The majority of values fall within the confidence interval for their respective methods. Analyzing the values of diastolic and mean blood pressure, all three models demonstrate similar performance, with small mean differences between the methods, as shown in Figures 6.20, 6.21 6.22. From this analysis, it is evident that the models offer good performance for the prediction of the DBP and

MAP. However, the difficulty in predicting systolic blood pressure values, as observed in this analysis, may stem from the high standard deviation of the input systolic pressure values, which hover around 18.90 mmHg compared to the diastolic and mean pressure values of 12.07 and 13.71 mmHg, respectively. The model attempts to predict the mean pressure, which is proportional to the standard deviation of the input signal. In this case, the high oscillation of values poses challenges for prediction. However, the models perform better in predicting diastolic and mean blood pressure values. Analyzing the morphology of the predicted signals with the three models and studying the standard deviation of the predicted signal can provide an evaluation of the network's reconstruction quality. Figure 6.23 illustrates the prediction of a chunk from the test set, with the U-Net's predicted waveform in orange and the target signal in blue. As observed, the signal predicts diastolic pressure well, but the model struggles to predict systolic peaks accurately, resulting in an altered shape compared to the target. Additionally, some noise is introduced in the reconstruction.

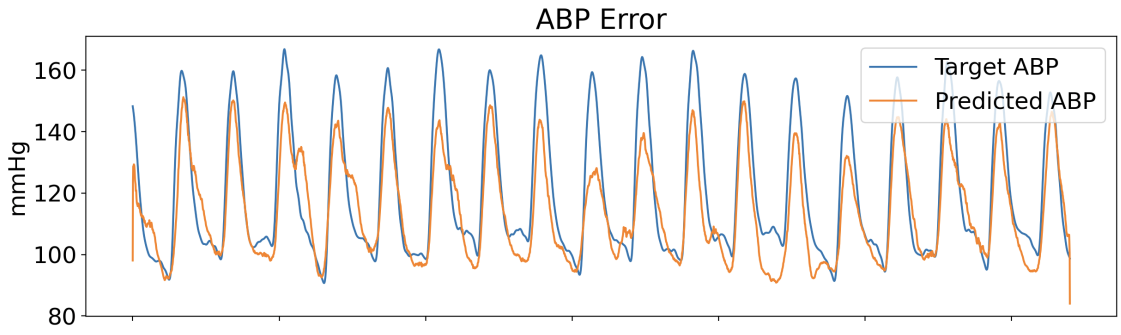

Figure 6.23: Prediction of ABP waveform with U-Net model

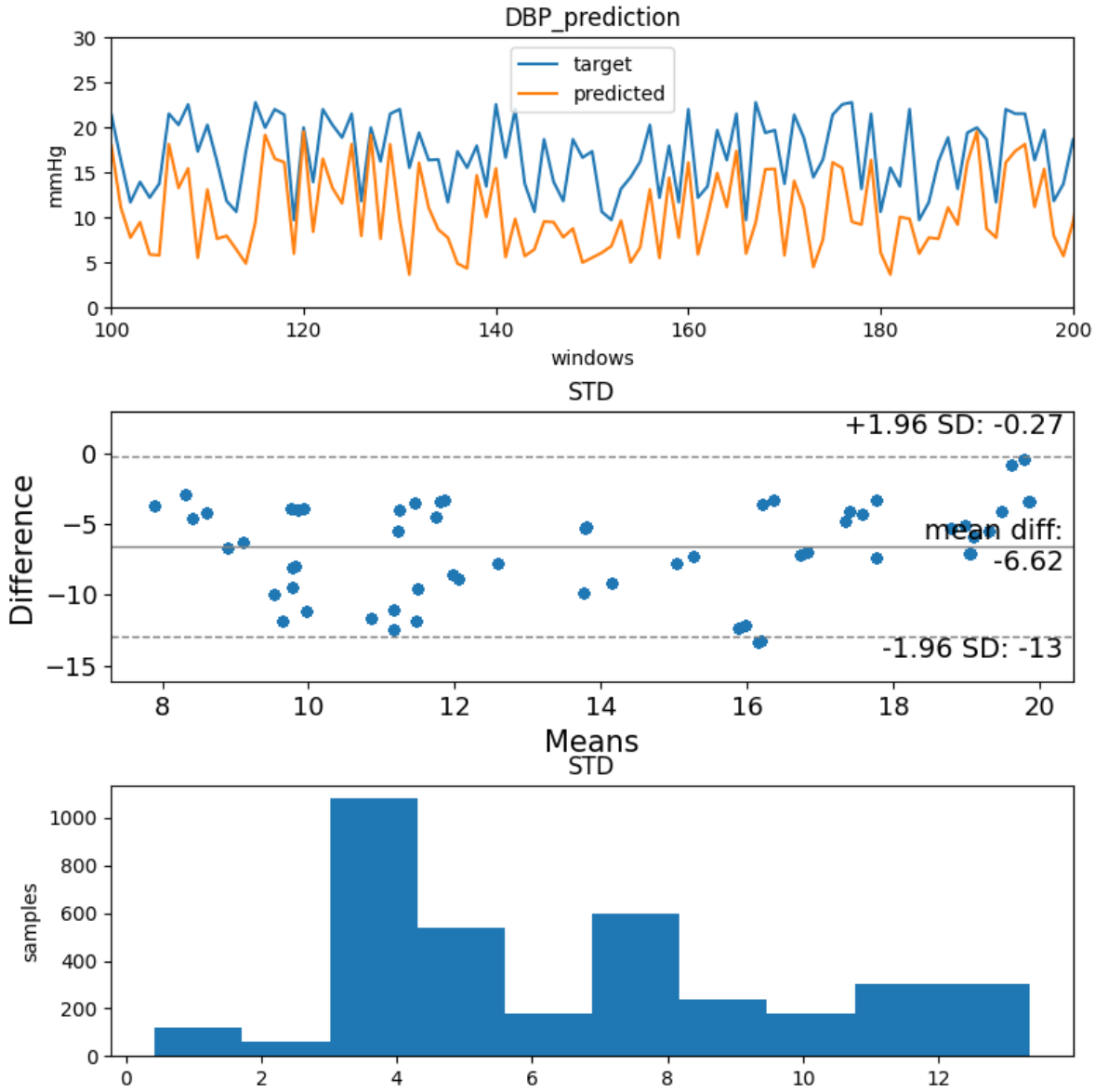

Figure 6.24: STD of U-Net model: In the first quadrant, the prediction of the standard deviation is represented, with the target signal shown in blue. The second quadrant displays the Bland-Altman plot for the standard deviation, and the distribution of the standard deviation is shown in the final quadrant.

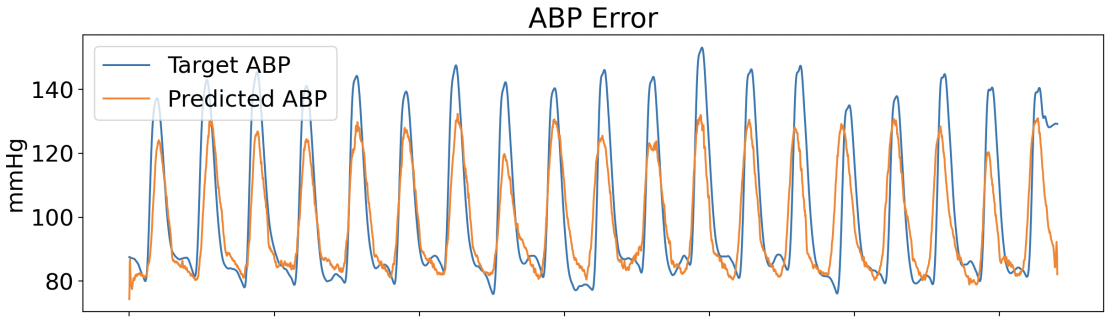

Figure 6.25: Prediction of ABP waveform with GRU-Net model

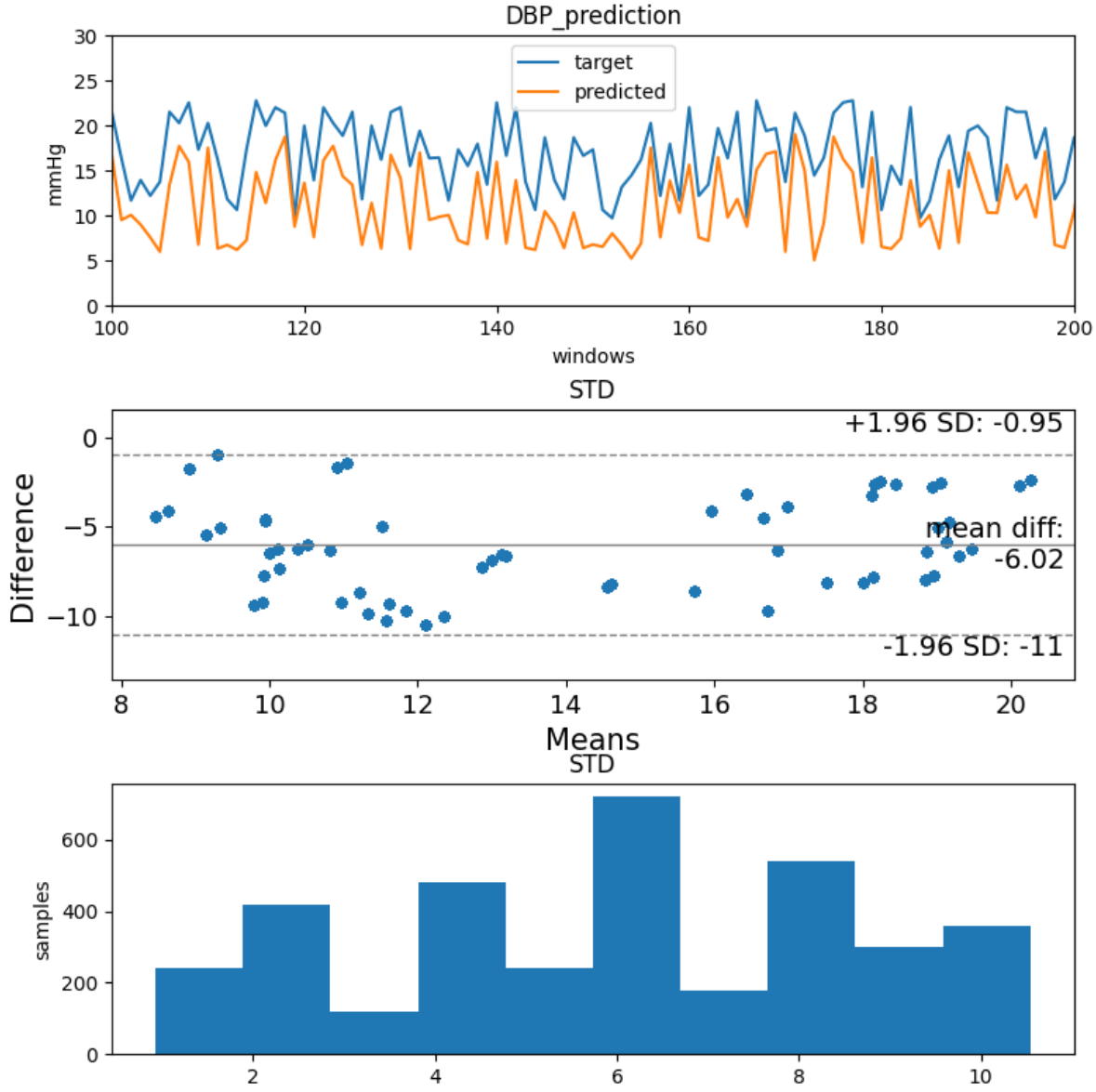

Figure 6.26: STD of GRU-Net model: In the first quadrant, the prediction of the standard deviation and the target signal in blue are depicted. The second quadrant shows the Bland-Altman plot for the standard deviation, and finally, its distribution is presented in the last quadrant.

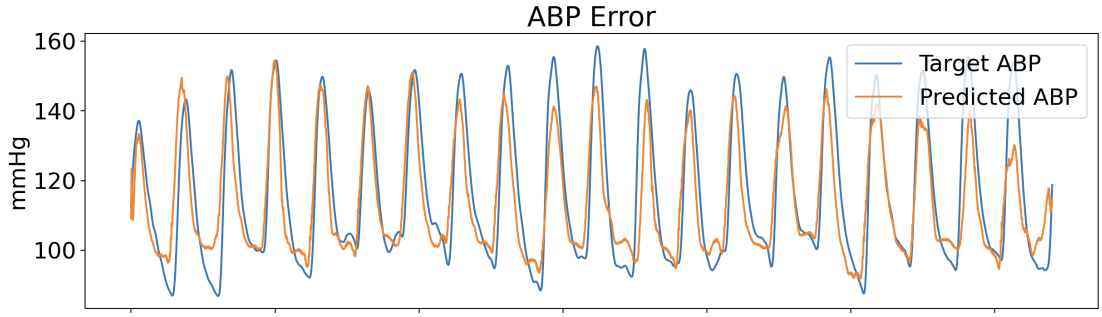

Figure 6.27: Prediction of ABP waveform with 3GRU-Net model

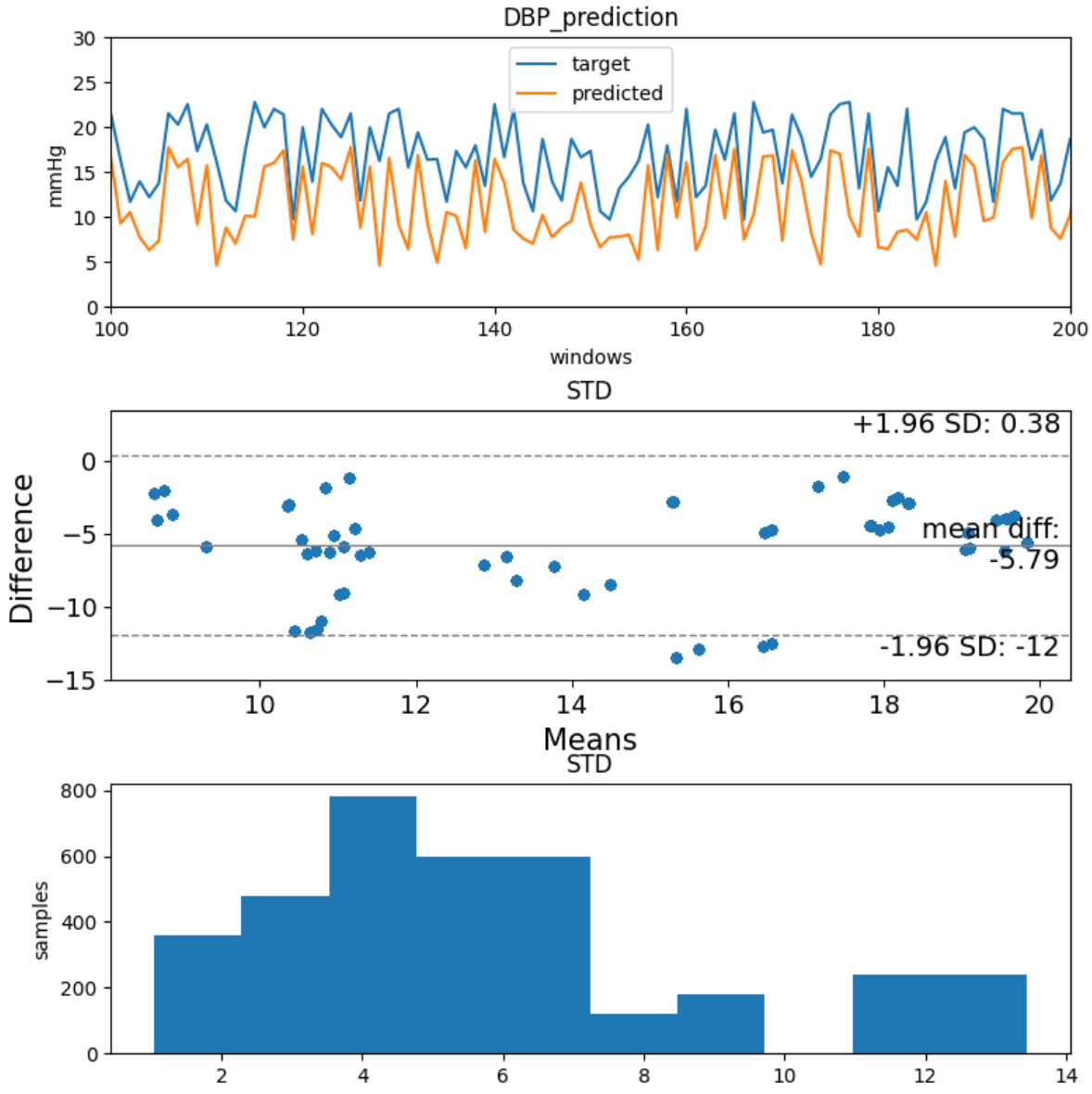

Figure 6.28: STD of 3GRU-Net model: In the first quadrant, the prediction of the standard deviation and the target signal are represented, with the target signal shown in blue. In the second quadrant, the Blant Altman plot for the standard deviation is displayed, and finally, its distribution is shown in the last quadrant.

In Figure 6.24, the analysis of the error on the standard deviation is presented. Specifically, it can be observed that the standard deviation of this model has lower average values compared to the target signal, with a difference highlighted by the Bland-Altman plot of -6.62. The distribution of the error on the standard deviation is not Gaussian and exhibits average values around 4 mmHg. Looking at the image in Figure 6.25, which shows the prediction of the arterial blood pressure (ABP) signal made with the GRU-Net, it can be observed that the noise has decreased and the shift is slightly reduced. In fact, the standard deviation represented in Figure 6.26 has a lower average value compared to the previous model, and the mean difference between the measurement methods is reduced, amounting to -6.02. Analyzing the last model, the 3GRU-Net, which stands out as the best among the three, Figure 6.27 shows that the predicted waveform, represented in orange, is almost overlapping with the target waveform in blue. In particular, the noise is significantly reduced, and the shift is improved. Moreover, it appears to have a better prediction capability for systolic pressure peaks. Figure 6.28 presents an analysis of the standard deviation (STD), which is a key parameter for evaluating the morphology of the predicted signal. The distribution of the error exhibits a Gaussian pattern with a mean value centered around 4 mmHg. Looking at the Blant Altman plot in the second quadrant, we observe a reduced difference between the implemented measurement method and the target, with values of -5.79.

6.1.3. PTT regression models results

Three different regression models based on PTT were implemented for the estimation of arterial blood pressure in the subject-dependent study. Specifically, drawing from various studies found in the literature, three models were developed using Matlab tools:

- Linear model

$$ABP = \alpha * PTT + b \tag{6.1}$$

.

- Inverse model

$$ABP = \alpha * \frac{1}{PTT} + b \tag{6.2}$$

.

- Quadratic model

$$ABP = \alpha * \frac{1}{PTT^2} + b \tag{6.3}$$

.

The main idea of this method is to estimate the parameters α and $\boldsymbol{b}$ for their respective models using linear regression. To accomplish this, a simple algorithm was developed in MATLAB to perform the regression for the three models. Once the parameters are obtained, the corresponding models are tested on the dedicated Test set, from which the values of the main evaluation metrics are derived. Figure 6.29 displays the regression plots for the implemented models. The parameters are computed for both systolic and diastolic pressure. Table 6.13 presents the calculated parameters for the different models along with their respective mean errors computed on the test set.

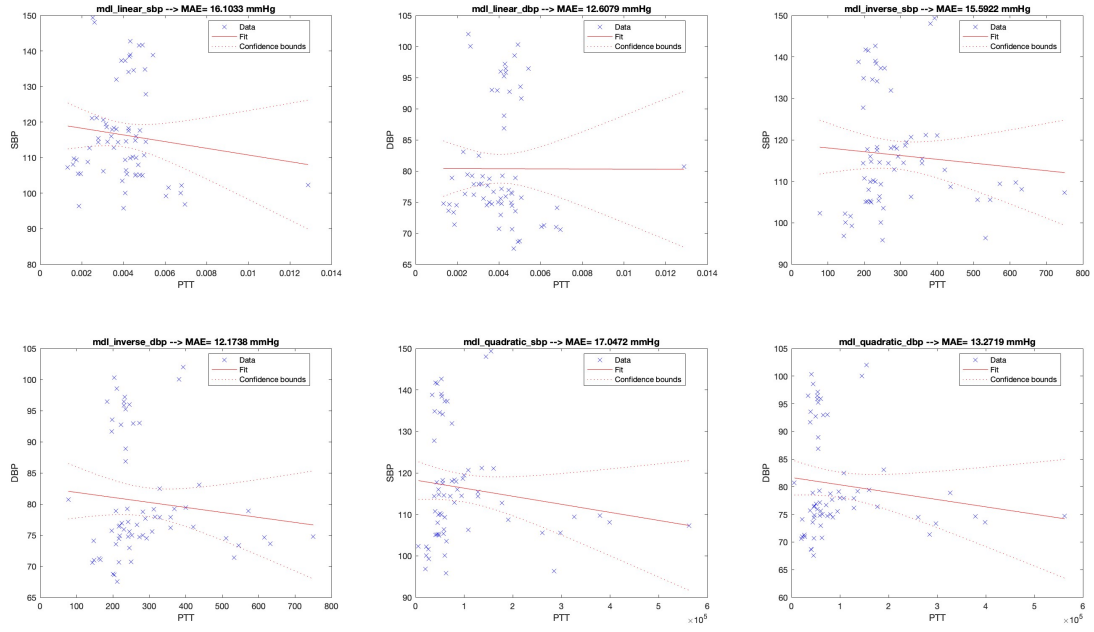

Figure 6.29: Regression plot for the SBP, DBP and MBP values of three different models: linear, inverse, and quadratic

Model	MAE *systolic* [mmHg]	MAE *diastolic* [mmHg]
Linear	16.103	12.607
Inverce	15.592	12.173
Quadratic	17.047	13.271

Table 6.12: Mean Absolute Error for the three different models

As can be seen in Table 6.12, the best results are obtained by the inverse model described by equation 6.2. In Figure 6.29, in the third and fourth quadrants respectively, it can

be observed how the regression line better approximates the systolic and diastolic points compared to the other models. Particularly, most of the samples fall within the confidence interval.

Model	**value**	α(1/mmHg)	**b**(mmHg)	MAE(mmHg)
Linear	SBP	-940.316	120.155	16.103
	DBP	-8.082	80.388	12.607
Inverce	SBP	-0.009	118.972	15.592
	DBP	-0.008	82.671	12.173
Quadratic	SBP	-0.0000194	118.258	17.047
	DBP	-0.000013	81.666	13.271

Table 6.13: Models parameters

The average error obtained with the inverse model, as well as with all three mathematical models, is higher compared to the deep neural network, both for systolic pressure parameters and especially for the calculation of mean diastolic pressure. Specifically, with the 3GRU-Net + ResNet model, the error is 11.356 for systolic pressure and 5.302 for diastolic pressure. Furthermore, the neural network allows for waveform shape estimation and calculation of mean pressure, and it also utilizes moving chunks for prediction. The initial labeling procedure for dataset construction and PTT calculation can be time-consuming and prone to systematic errors.

6.2. Subject-Indipendent analysis

From the previous analysis, it is evident that the 3GRU-Net is the model that provides the best performance in predicting the arterial pressure waveform, as seen from the earlier analysis of the error in calculating the final parameters. This is further supported by the calculation of the BHS for the three models. By using the 3GRU-Net cascaded with the Res-Net, a subject-independent analysis is conducted, utilizing the entire dataset described in the preceding section. Specifically, the values of the input systolic, diastolic, and mean pressure parameters are shown in Table 3.12. It can be observed that the standard deviation calculated on the input parameters is significantly higher compared to the subject00 input dataset in Table 3.13. This indicates a greater difficulty in predicting the target parameters. Figure 6.30 illustrates the trend of the loss function, with values of 303.419 for the training set and 366.035 for the validation set. Meanwhile, Figures

6.31 and 6.32 display the mean absolute error and mean signed error. As observed, the network saturates around values of 15.583 mmHg for the validation set, while it continues to learn up to values of 14.593 mmHg during training. Table 6.15 reports the MAE and loss values of the network. Table 6.14 provides the hyperparameters used for the network. As seen here, the Adam optimizer is utilized, and there are 15 initial filters in the encoder layer.

Models	**Loss function**	**Optimizer**	**Initial Filter**	**GRU Units**	**Epochs**
3GRU-Net+ResNet	MSE	Adam	15/5	1	1200

Table 6.14: 3GRU-Net+ResNet initialization parameters for the complete model

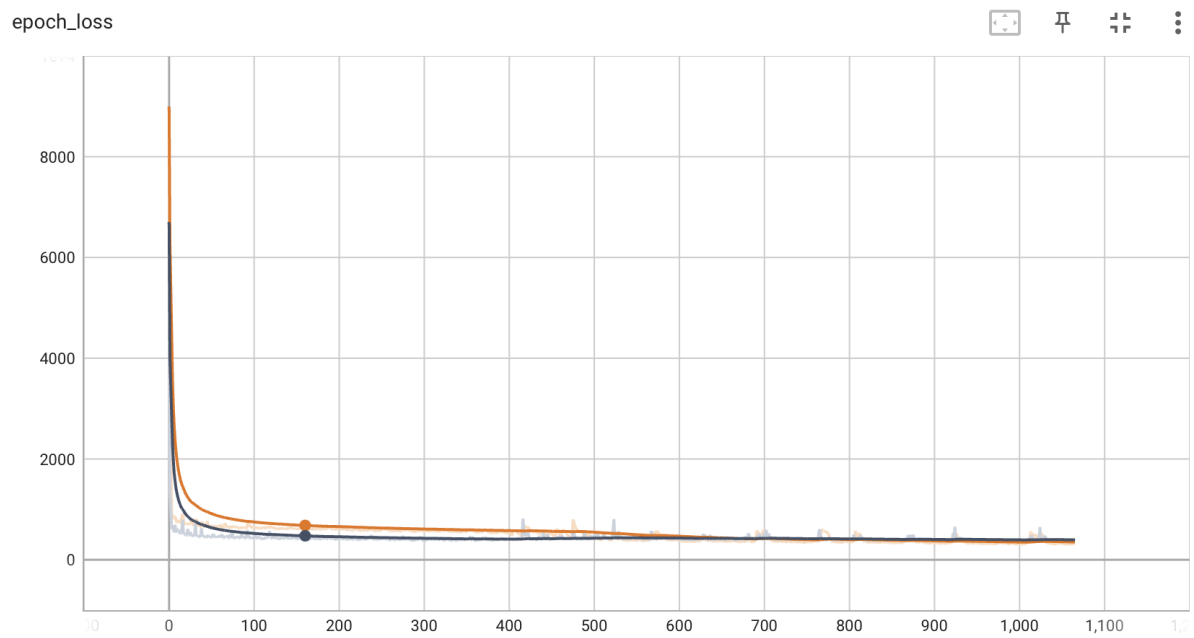

Figure 6.30: Trend of loss function for 3GRU-Net with all subjects: orange for 3GRU training, black for 3GRU-Net validation

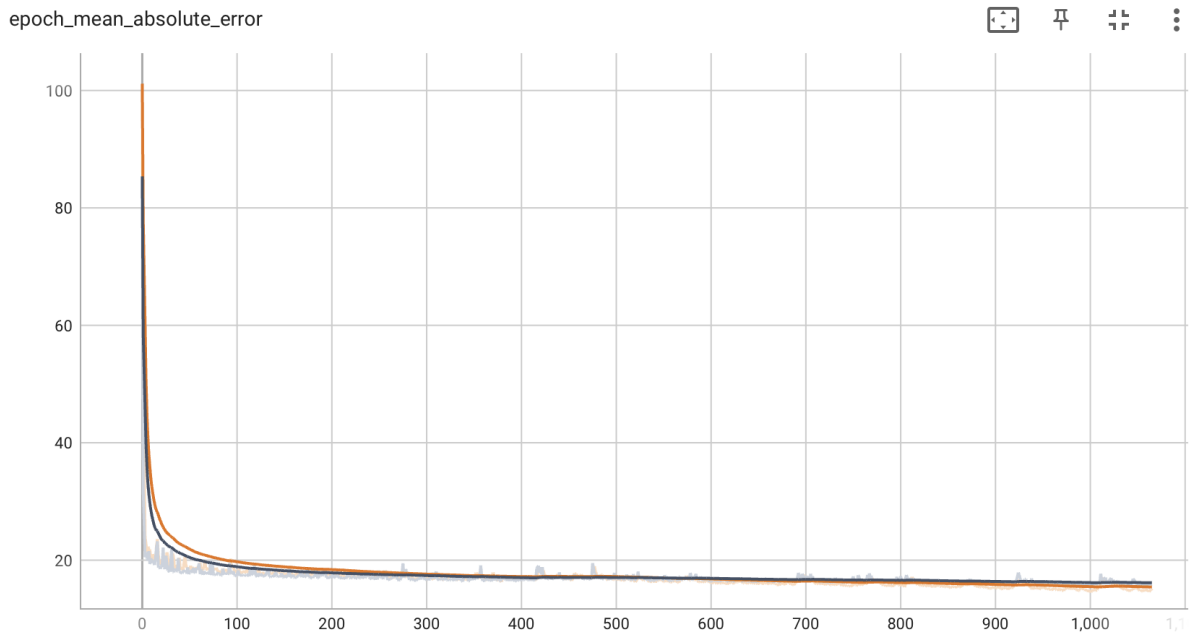

Figure 6.31: Trend of MAE function for 3GRU-Net with all subjects: orange for 3GRU training, black for 3GRU-Net validation

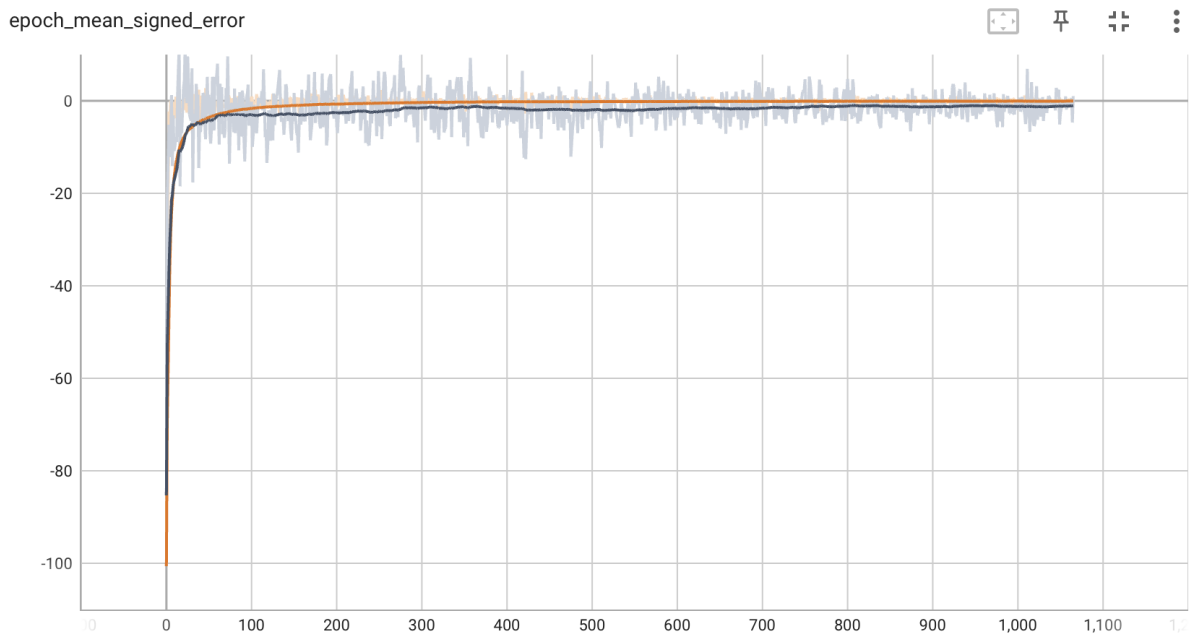

Figure 6.32: Trend of mean signed error function for 3GRU-Net with all subjects: orange for 3GRU training, black for 3GRU-Net validation

3GRU-Net+ResNet			
Training set		**Validation set**	
Loss value	**MAE [mmHg]**	**Loss value**	**MAE [mmHg]**
303.419	14.593	366.035	15.583

Table 6.15: 3GRU-Net+ResNet parameters errors for the complete model

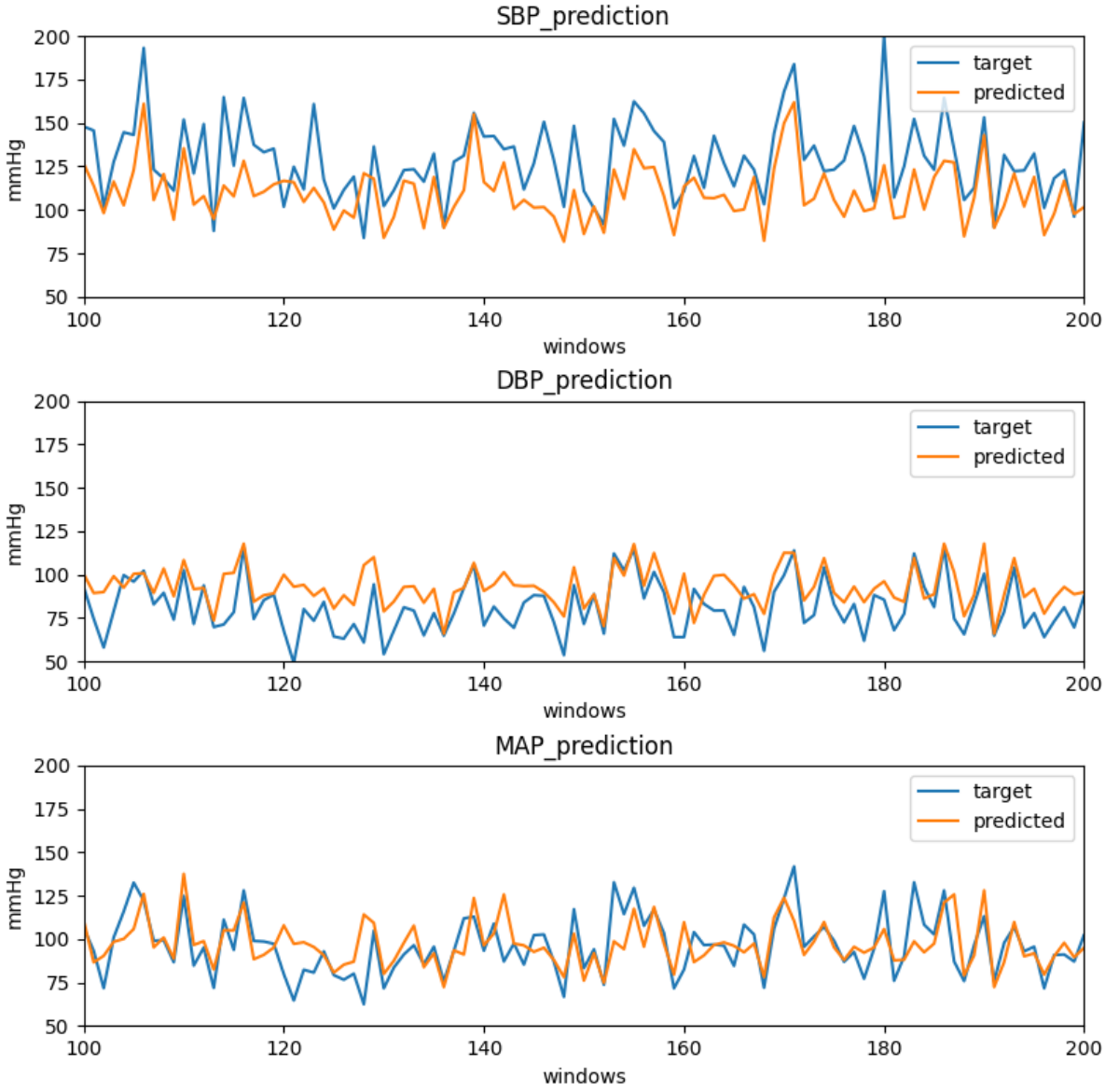

Figure 6.33: Prediction of characteristic parameters for the 3GRU-Net model with all subjects: SBP, DBP, MBP, STD

By analyzing the predicted systolic, diastolic, and mean pressure using the same procedure described earlier, a more detailed picture of the network's performance can be obtained. In particular, Figure 6.33 displays the predicted values of systolic pressure in the first quadrant, diastolic pressure in the second quadrant, and mean pressure in the third quadrant. As observed, similar results are obtained compared to the earlier subject-dependent analysis. Specifically, systolic pressure is consistently underestimated, while diastolic and mean pressure exhibits a higher error compared to the previous results of the subject-dependent analysis.

	MAE + STD [mmHg]	**MSE + STD [mmHg]**	**RMSE + STD [mmHg]**
SBP	22.59 ± 12.83	675.57 ± 15.50	25.99 ± 12.90
DBP	12.53 ± 8.73	233.31 ± 10.33	15.27 ± 8.58
MAP	9.34 ± 8.70	165.01 ± 12.83	12.84 ± 8.81
STD	10.98 ± 4.85	144.61 ± 4.90	12.02 ± 4.89

Table 6.16: Parameters computation for 3GRU-Net over the Test set for all subjects

In Table 6.16, the results of the errors for the respective parameters calculated on the predicted target signal using the model are presented. In Figure 6.34, the distribution of errors is shown, indicating a Gaussian distribution with the mean centered around 20 mmHg for systolic pressure, 11 mmHg for diastolic pressure, and 1.5 mmHg for mean pressure.

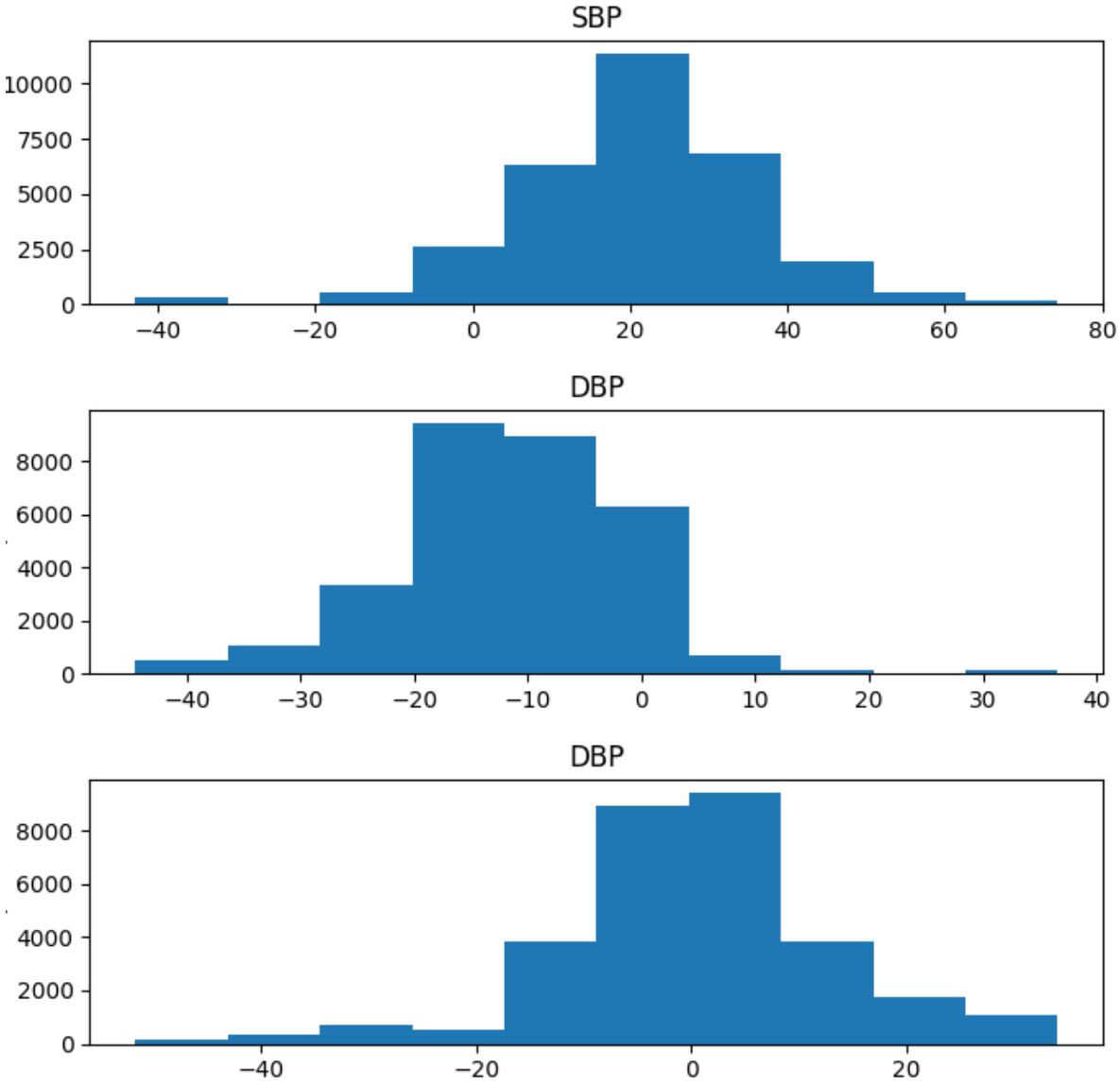

Figure 6.34: Distribution of characteristic parameters for the 3GRU-Net model with all subjects: SBP, DBP, MBP, STD

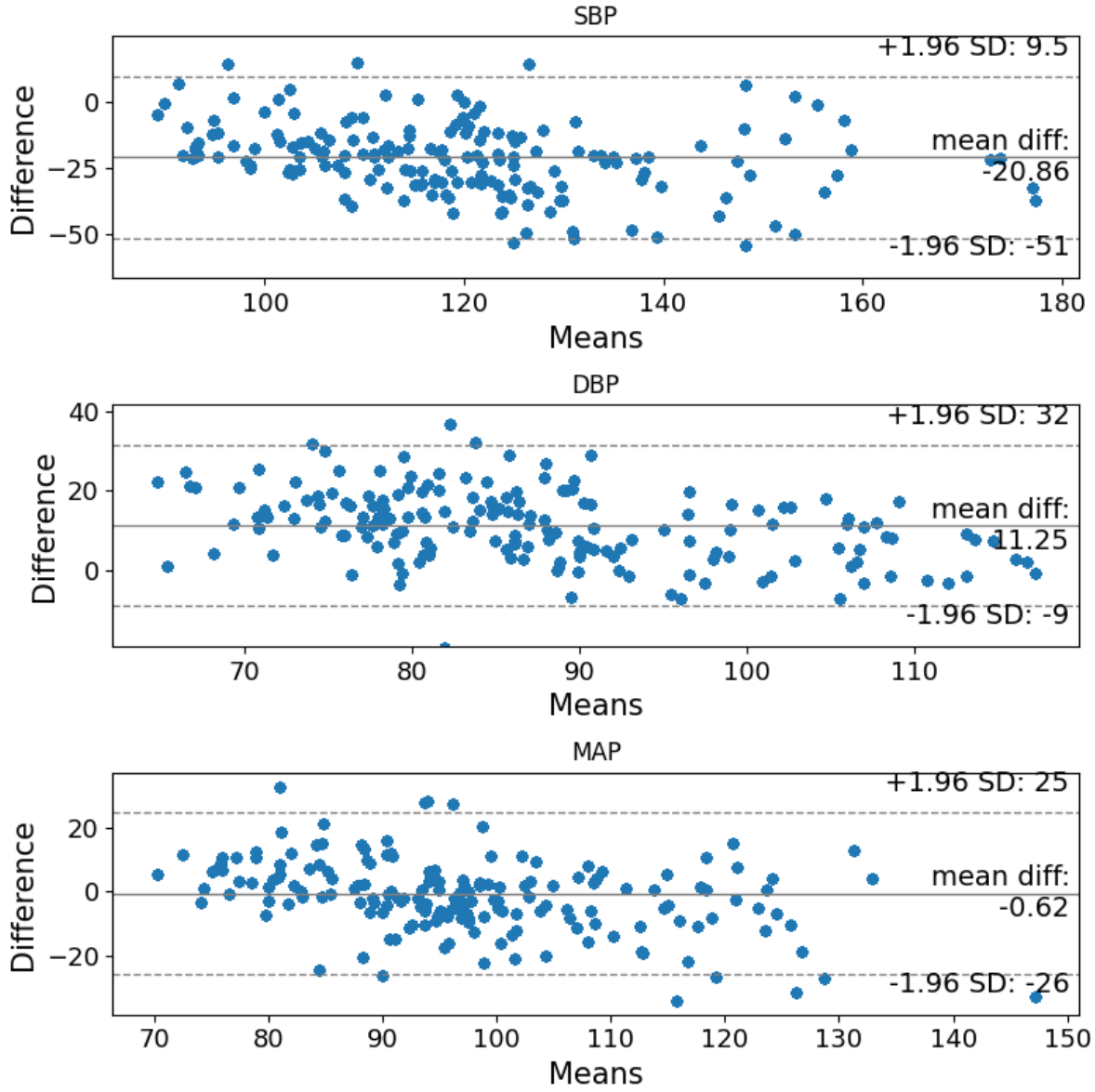

Figure 6.35: Prediction of characteristic parameters for the 3GRU-Net model with all subjects: SBP, DBP, MBP, STD

In Figure 6.35, the Bland-Altman plots are presented, which provide an estimation of the mean difference between the two measurement methods used. Specifically, it can be observed that for all parameters, the majority of points fall within the confidence interval highlighted by the two dashed lines in their respective plots. Analyzing the mean difference across the three parameters, it is evident that systolic pressure exhibits a significantly higher mean difference, indicating a large disparity between the two methods in calculating this parameter, further confirming its critical nature.

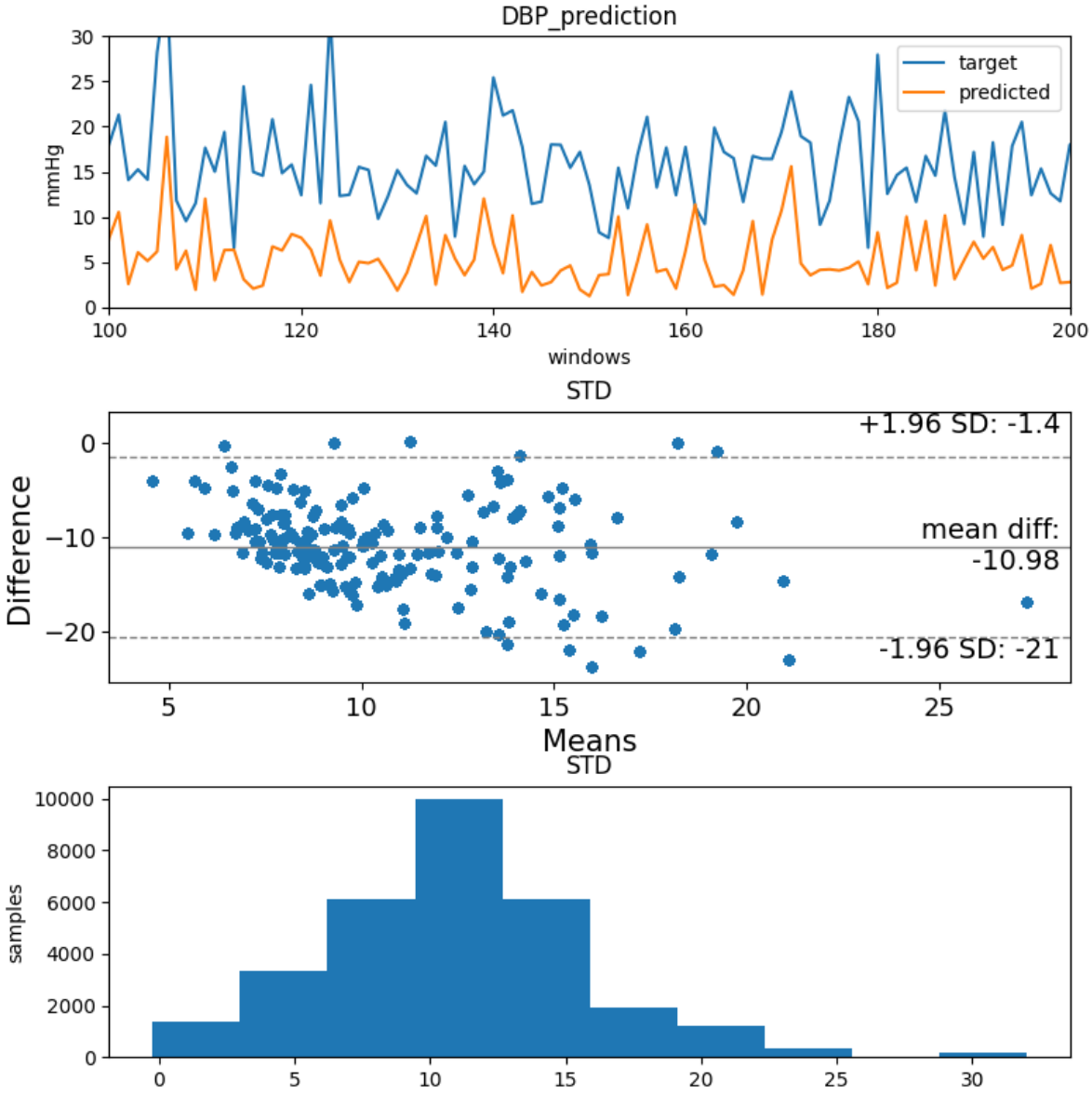

Figure 6.36: Standard deviation analysis between the predicted and target signals

By evaluating the standard deviation of the signal, it is possible to assess how closely the predicted waveform aligns with the target signal. Figure 6.36 presents an analysis of the standard deviation calculated on both signals. In the first quadrant, we find the prediction of the standard deviation, which, as observed, has a considerable mean difference, indicating that the reproduced waveform often exhibits greater variability compared to the target. In the second quadrant, the Bland-Altman plot is displayed, while the error distribution is shown in the third quadrant.

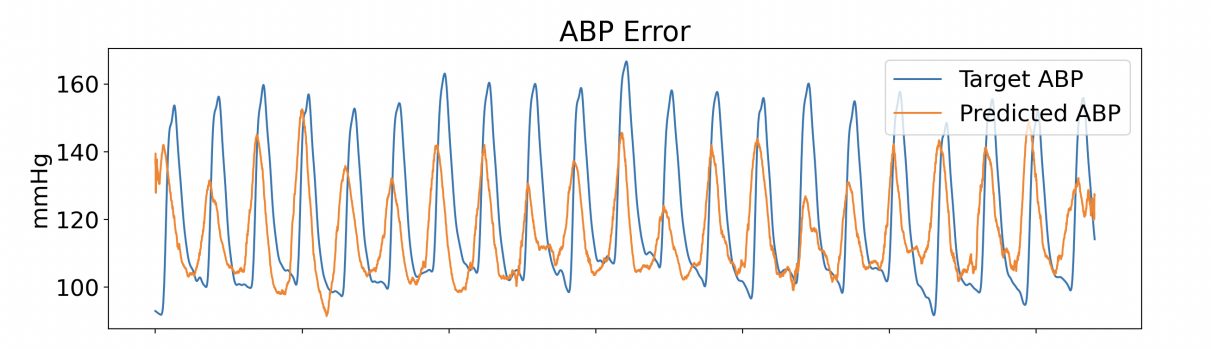

Figure 6.37: prediction waveform example: in orange the predicted signal and in blue the target one

In Figure 6.37, an example of prediction on a chunk of the test set is shown. As observed, there is high variability in the signal and slight noise present. However, the prediction for some chunks appears to be very accurate, likely due to the high quality of the input signal.

6.3. BHS Computation

To conclude the analysis of the methods, an evaluation index is calculated following the standards of The British Hypertension Society (BHS). This allows for an objective assessment based on the BHS standards, enabling the classification of the device/method used for blood pressure monitoring. In particular, this index has become a widely-used evaluation metric, calculated based on the absolute error obtained. Specifically, the percentages of cumulative error are calculated, considering three different ranges: less than 5 mmHg, less than 10 mmHg, less than 15 mmHg, and greater than 15 mmHg. Based on the total errors calculated on the test set, the percentage of errors falling within the aforementioned limits is determined. Table 6.17 presents the various classifications based on the achieved cumulative error percentages.

	Cumulative Error Percentage		
BHS	**< 5 mmHg**	**< 10 mmHg**	**< 15 mmHg**
Grade A	60%	85%	95%
Grade B	50%	75%	90%
Grade C	40%	65%	85%
U-Net	**< 5 mmHg**	**< 10 mmHg**	**< 15 mmHg**
SBP	20%	41.66%	68.33%
DBP	20.01%	80%	86%
MAP	20.02%	83.33%	98%
GRU-Net	**< 5 mmHg**	**< 10 mmHg**	**< 15 mmHg**
SBP	21.66%	41.66%	88.33%
DBP	21.67%	81.66%	91.66%
MAP	21.69%	75%	86.66%
3GRU-Net	**< 5 mmHg**	**< 10 mmHg**	**< 15 mmHg**
SBP	33.33%	55.00%	88.50%
DBP	33.34%	83.33%	98.33%
MAP	33.36%	80%	91.70%

Table 6.17: Classification of the device based on BHS standard

As observed in the table, based on the results of the BHS index calculation, it can be noted that among the three models, the closest one to meet the standards is the third model, which utilizes three distinct branches based on the frequency band of the input signals. However, despite this, all three models fail to meet the standards set by the British Hypertension Society.

	Cumulative Error Percentage		
3GRU-Net	**< 5 mmHg**	**< 10 mmHg**	**< 15 mmHg**
SBP	8.57%	15.43%	29.72%
DBP	8.59%	42.86%	63.43%
MAP	8.61%	64.57%	82.86%

Table 6.18: Classification of the device based on BHS standard for all subject model

The British Hypertension Society (BHs) index is also calculated for the 3GRU-Net model used in the subject-independent analysis. The results of the calculation for systolic, diastolic, and mean arterial pressures are presented in Table 6.18. It can be observed that

the obtained results for this analysis are significantly lower compared to those obtained in the subject-dependent study, as shown in Table 6.17. In fact, the model fails to accurately calculate all three parameters, especially with a decrease in the percentage of error accumulation below 5%. This can be attributed to the relatively high mean error committed by the model.

7 | Discussion

7.1. Main Findings

Limitations associated with traditional methods of arterial pressure measurement, such as the reliance on invasive monitoring techniques like catheter-based measurements or the inability to obtain continuous measurements like with a sphygmomanometer, have prompted studies to explore alternative techniques for monitoring this fundamental physiological parameter for early identification of what is known as a silent killer. As described in the introduction, the most commonly used alternative techniques in medicine rely on mathematical models and the recording of signals such as PPG and ECG, from which systolic, diastolic, and mean arterial pressure parameters can be derived through PTT calculation and specific regression models. However, these techniques are computationally expensive and require extensive preprocessing due to the identification of specific fiducial points for PTT calculation. In this research, as previously mentioned, a regression model is developed that incorporates linear, inverse, and logarithmic regressions. This model serves as a reference and comparison to the described artificial intelligence techniques. Specifically, it is calculated only for subject-dependent analysis as this type of analysis is sensitive to the subject's physiological parameters. There are also measurement methods that allow for continuous analysis of pressure and its waveform, such as the method developed by Penaz [44], which estimates continuous blood pressure signals using a finger cuff based on the previously described volume clamp technique. However, the main limitations of this technique lie in the instrumentation used, which is not easily applicable for measurements during movement due to its poor portability. As a result, various research branches have focused on the use of artificial intelligence algorithms based on neural networks that primarily utilize PPG and its derivatives or ECG signals, or a combination of both. These algorithms are based on deep neural network models that enable an end-to-end approach, eliminating the need for fiducial point detection. The main limitation of these techniques is that they are primarily tested on specific datasets such as MIMIC and are not validated under real-world conditions. In this work, the developed deep learning models are tested under real-world conditions using a dataset constructed

through an approved data acquisition phase at Politecnico di Milano, simulating a real clinical protocol. The employed device allows for simple and continuous signal collection during both rest and movement phases. One notable aspect of this approach is the ability to analyze and monitor arterial pressure during both rest and movement, enabling monitoring during stress tests or physical activities. This is particularly significant considering that ambulatory blood pressure monitoring requires the patient to remain stationary during the acquisition procedure. With the Soundi® device, it is possible to record a set of signals that includes physiological signals such as ECG, PCG, and SCG, as well as non-physiological signals like acceleration, PPG, and external temperature. From the analysis of the results previously conducted, it can be observed that the three developed models, particularly the one with three different branches corresponding to the frequency content of the input signals, perform quite well for subject-dependent analysis. However, equally satisfactory results are not achieved for the analysis of the entire dataset, which encompasses all patients for subject-independent analysis. Since the protocol involved both a movement phase and a rest phase, the decision was made to analyze the data by combining both phases, thereby considering the signals during pedaling as well. This leads to an overall increase in the standard deviation of the pressure, which is also evident with the Finapress device often producing pressure values that are physiologically outside the clinical range. During the pedaling phase, it is noted that certain signals recorded with the PPG exhibit better quality, resulting in excellent prediction performance.

Analyzing the prediction results with the corresponding input signal bank, it is observed that the prediction is better when there is higher quality in the PPG and ECG signals, like in Figure 7.1 in which there is a simple interface developed in python in order to evaluate the predicted model with corresponding input PPG and ECG signal. In Figure 7.2 is possible to look at the different chunks in which the PPG has bedder quality with respect to the others. How we can see the prediction computed by the model is different from the target one, only the systolic pressure is right approximates due to the fact that the position of the plethysmographic sensor is a critical point for the Soundi® device.

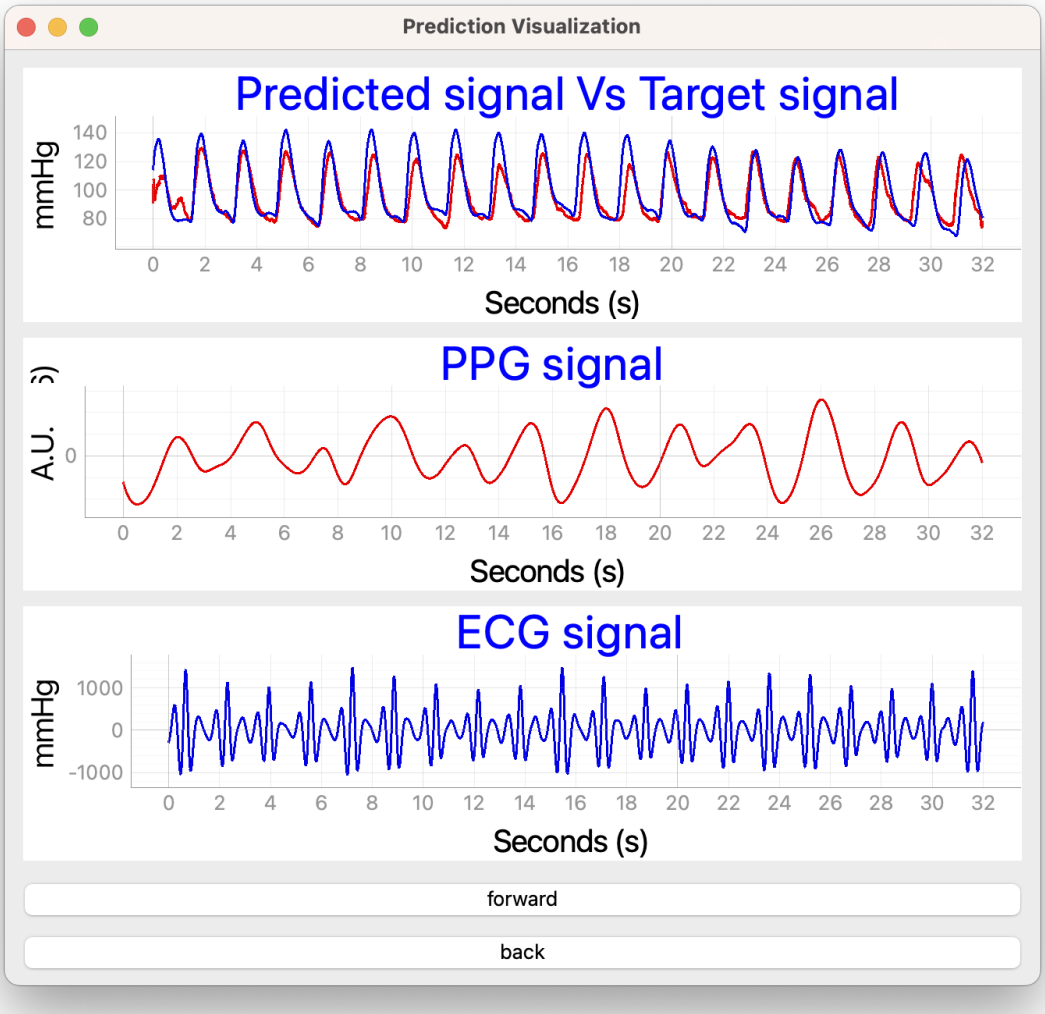

Figure 7.1: Python interface to visualize the predicted signal with target one and corresponding PPG and ECG signals.

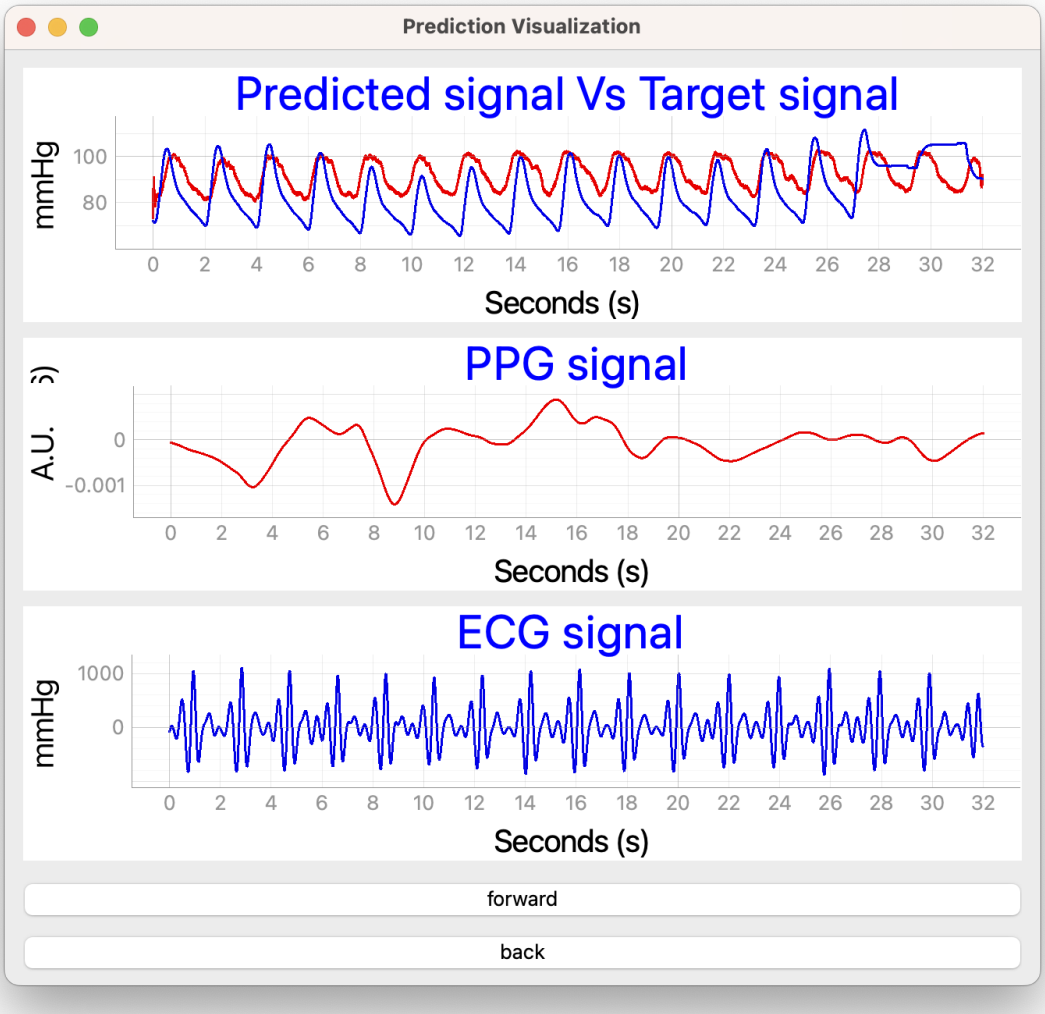

Figure 7.2: Python interface to visualize the predicted signal with target one and corresponding PPG and ECG signals.

The positioning of the device to ensure proper placement of the PPG sensor proves to be particularly challenging as it can vary from person to person, depending on factors such as gender and skin color, which can influence the reflected optical power. For the deep learning models U-Net, GRU, and 3GRU, the BHS index is also calculated, which allows for the classification of the method/device for arterial pressure monitoring based on the accumulation error for different parameters. The 3GRU model achieves higher BHS values but still does not fall within the classifications identified by the British Hypertension Society. Furthermore, for subject-dependent analysis, a comparison can be made with the methods presented in the literature, but it should be considered that the

developed method here utilizes a dataset collected under real-world conditions, including the associated systematic errors and protocol considerations, which are not present in the MIMIC dataset.
In the literature, several studies have attempted to reproduce the blood pressure signal using deep learning techniques, with the main ones being reported in Table 7.1.

Studies	Used signals	SBP(mmHg)	DBP (mmHg)	MBP (mmHg)	STD (mmHg)
Lin et al.	PPG, VPG, APG	4.59	2.47	/	1.78
Wang et al.	PPG	3.95	2.14	/	4.28
Madhuri et al.	PPG	3.97	2.30	/	0.06
Our study	Signal-bank	8.816	3.17	3.15	10.510

Table 7.1: Comparison of studies

However, these studies use only PPG and/or ECG for prediction, while in this study a method using a bank of signals was proposed. As seen, the values are comparable for the calculation of diastolic pressure and mean pressure, while the error is greater for the prediction of systolic pressure.

7.2. Limits

The main limitations primarily concern the dataset acquisition phase. The reference instrumentation used for arterial pressure monitoring generated high variability in the acquired pressure signals. In fact, the temperature of the hands during the placement of the cuff with the plethysmograph on the index finger could influence the signal quality due to temperature-induced vasoconstriction or vasodilation. This resulted in physiologically altered pressure ranges even after calibration, introducing high variability in the input dataset that is reflected in the predictions. Even the connections of the headset during the movement phase create sensor displacements that result in inaccurate pressure acquisition. Additionally, the positioning of the Soundi® device sometimes posed challenges as the correct position could vary depending on the individual's gender, sweating and other features affecting the quality of signal monitoring, especially the PPG. For this reason, multiple recordings were performed for different subjects.

There are structural issues related to the acquisition of signals used for training the network. In particular, the performance was evaluated under real-world conditions where signal quality is not ideal and there is a large variability in measurements due to device-related issues. In various measurements, it was observed that the quality of signals varies depending on the subject, particularly the PPG signal, which is of fundamental impor-

tance as demonstrated in the previous ablation study. Specifically, it was found that the quality of this signal is correlated with the patient's gender due to different physical characteristics, skin color that can influence transmitted optical power, and the presence of fat layers at the Soundi® placement site and level of sweating. Furthermore, after the preprocessing procedure, the size of the dataset is significantly reduced due to the aforementioned issues, resulting in the elimination of many signal windows. The inclusion of segments during the movement phase in the analysis can introduce errors, particularly in signals such as PPG, which are noticeably attenuated.

7.3. Further Improvments

- **Dataset expansion**: One of the first steps to consider is the enlargement of the dataset and the development of an accurate and proper procedure for the placement of the sensor (e.g., Finapres). Additionally, exploring alternative protocols that improve the utilization of Finapres could be beneficial.
- **Validation with a different dataset**: Performing validation with an independent dataset can help assess the performance and robustness of the networks. This would provide additional evidence on the generalization capabilities of the models.
- **Integration of additional signals**: Exploring the inclusion of other physiological or non-physiological signals in the analysis could potentially enhance the accuracy and reliability of the predictions. This could involve investigating the relevance and impact of different signals on arterial blood pressure waveform reconstruction.
- **Focus on specific dataset segments**: Instead of analyzing the entire dataset, focusing solely on resting periods could provide insights into the network's performance during specific physiological states. This targeted analysis may help identify areas for improvement and optimize the network for particular scenarios.

With these improvements, it is possible to enhance the neural network's performance, reliability, and applicability for continuous arterial blood pressure calculation.

8 | Conclusion

In this master's thesis, developed in collaboration with engineer Mattia Sarti and Biocubica s.r.l, who provided the device used for signal monitoring, an "End-To-End" approach is proposed for the continuous calculation of arterial blood pressure waveform. This approach utilizes three deep learning models. Additionally, a regression model based on pulse transit time (PTT) on Subject00 records is developed using mathematical models. The aim of the project is to reconstruct the arterial blood pressure waveform continuously by utilizing a bank of physiological signals and not, relying on a loss function that maximizes point-to-point prediction by the network. In particular, a subject-dependent study is conducted, and the results obtained with the best-proposed model are compared with those obtained using PTT regression models and with literature that computes the BHS index. The results demonstrate the good performance of the model for subject-dependent analysis, approaching clinical standards defined by the British Hypertension Society. Then thanks to the fact that the Soundi® doesn't need the initial calibration phase, a subject-independent analysis was performed. In this case, the performance is lower compared to subject-dependent analysis, as the complete dataset exhibits high variability in input blood pressure, making it challenging for the model to make accurate predictions. Further ablation studies could be conducted to enhance the architecture's complexity and refine the selected hyperparameters. Enhanced performance could lead to the development of a monitoring model that utilizes key physiological and non-physiological signals for arterial blood pressure reconstruction. Given the ease of recording these signals, this could be a revolutionary aspect of non-invasive arterial pressure monitoring. Therefore, the development of a technique capable of calculating arterial pressure parameters through the creation of a regression model using a deep neural network, without the need for initial calibration like most techniques, is a major advantage as it enables rapid measurement once the network is trained. This is one of the key strengths of this end-to-end approach compared to conventional techniques for acquiring pressure through PPG, such as the Finapress, which requires initial calibration on the subject under analysis to calibrate the pressure. By refining and integrating the model with Soundi®, it is possible to monitor blood pressure without the need for device calibration, allowing measurements to be taken

even during movement.

Bibliography

[1] *2019 5th Iranian Conference on Signal Processing and Intelligent Systems (ICSPIS).* IEEE. ISBN 9781728153506.

[2] *2019 5th Iranian Conference on Signal Processing and Intelligent Systems (ICSPIS).* IEEE. ISBN 9781728153506.

[3] Il monitoraggio battito-battito della pressione arteriosa finometer ® pro. URL `www.sedaitaly.it`.

[4] A global brief on hypertension | a global brief on hyper tension, 2013. URL `www.who.int`.

[5] J. Allen. Photoplethysmography and its application in clinical physiological measurement. *Physiological Measurement*, 28, 3 2007. ISSN 13616579. doi: 10.1088/0967-3334/28/3/R01.

[6] T. Athaya and S. Choi. An estimation method of continuous non-invasive arterial blood pressure waveform using photoplethysmography: A u-net architecture-based approach. 2021. doi: 10.3390/s21051867. URL `https://doi.org/10.3390/s21051867`.

[7] S. Aziz, M. U. Khan, M. Alhaisoni, T. Akram, and M. Altaf. Phonocardiogram signal processing for automatic diagnosis of congenital heart disorders through fusion of temporal and cepstral features. doi: 10.3390/s20133790. URL `www.mdpi.com/journal/sensors`.

[8] S. Baker, W. Xiang, and I. Atkinson. A hybrid neural network for continuous and non-invasive estimation of blood pressure from raw electrocardiogram and photoplethysmogram waveforms. *Computer Methods and Programs in Biomedicine*, 207, 8 2021. ISSN 18727565. doi: 10.1016/j.cmpb.2021.106191.

[9] R. C. Block, M. Yavarimanesh, K. Natarajan, A. Carek, A. Mousavi, A. Chandrasekhar, C. S. Kim, J. Zhu, G. Schifitto, L. K. Mestha, O. T. Inan, J. O. Hahn, and R. Mukkamala. Conventional pulse transit times as markers of blood pres-

sure changes in humans. *Scientific Reports*, 10, 12 2020. ISSN 20452322. doi: 10.1038/s41598-020-73143-8.

[10] J. M. Bote, J. Recas, and R. Hermida. Evaluation of blood pressure estimation models based on pulse arrival time. *Computers and Electrical Engineering*, 84, 6 2020. ISSN 00457906. doi: 10.1016/j.compeleceng.2020.106616.

[11] D. Castaneda, A. Esparza, M. Ghamari, C. Soltanpur, and H. Nazeran. A review on wearable photoplethysmography sensors and their potential future applications in health care. 2018. doi: 10.15406/ijbsbe.2018.04.00125. URL `http://medcraveonline.com`.

[12] P. Castiglioni. Ii. system description.

[13] F. S. Cattivelli and H. Garudadri. Noninvasive cuffless estimation of blood pressure from pulse arrival time and heart rate with adaptive calibration. pages 114–119, 2009. ISBN 9780769536446. doi: 10.1109/BSN.2009.35.

[14] J. Cheng, Y. Xu, R. Song, Y. Liu, C. Li, and X. Chen. Prediction of arterial blood pressure waveforms from photoplethysmogram signals via fully convolutional neural networks. *Computers in Biology and Medicine*, 138, 11 2021. ISSN 18790534. doi: 10.1016/j.compbiomed.2021.104877.

[15] K. Cho, B. van Merrienboer, C. Gulcehre, D. Bahdanau, F. Bougares, H. Schwenk, and Y. Bengio. Learning phrase representations using rnn encoder-decoder for statistical machine translation. 6 2014. URL `http://arxiv.org/abs/1406.1078`.

[16] C. P. Chua and C. Heneghan. Continuous blood pressure monitoring using ecg and finger photoplethysmogram. pages 5117–5120. IEEE, 8 2006. ISBN 1-4244-0032-5. doi: 10.1109/IEMBS.2006.259612.

[17] C. H. Chuang, K. Y. Chang, C. S. Huang, and T. P. Jung. Ic-u-net: A u-net-based denoising autoencoder using mixtures of independent components for automatic eeg artifact removal. *NeuroImage*, 263, 11 2022. ISSN 10959572. doi: 10.1016/j.neuroimage.2022.119586.

[18] J. Chung, C. Gulcehre, K. Cho, and Y. Bengio. Empirical evaluation of gated recurrent neural networks on sequence modeling. 12 2014. URL `http://arxiv.org/abs/1412.3555`.

[19] M. Drozdzal, E. Vorontsov, G. Chartrand, S. Kadoury, and C. Pal. The importance of skip connections in biomedical image segmentation. 8 2016. URL `http://arxiv.org/abs/1608.04117`.

[20] G. Du, X. Cao, J. Liang, X. Chen, and Y. Zhan. Medical image segmentation based on u-net: A review. *Journal of Imaging Science and Technology*, 64, 3 2020. ISSN 19433522. doi: 10.2352/J.ImagingSci.Technol.2020.64.2.020508.

[21] I. Goodfellow, Y. Bengio, and A. Courville. *Deep Learning*. MIT Press, 2016. ISBN 9780262035613. URL `https://books.google.co.in/books?id=Np9SDQAAQBAJ`.

[22] J. Granados, F. Tavera, J. M. Velázquez, G. López, R. T. Hernández, and A. Morales. Acoustic heart. interpretation of phonocardiograms by computer. volume 582. Institute of Physics Publishing, 2015. doi: 10.1088/1742-6596/582/1/012057.

[23] V. Hartmann, H. Liu, F. Chen, Q. Qiu, S. Hughes, and D. Zheng. Quantitative comparison of photoplethysmographic waveform characteristics: Effect of measurement site. *Frontiers in Physiology*, 10, 2019. ISSN 1664042X. doi: 10.3389/fphys.2019.00198.

[24] N. Hasanzadeh, M. M. Ahmadi, and H. Mohammadzade. Blood pressure estimation using photoplethysmogram signal and its morphological features. *IEEE Sensors Journal*, 20:4300–4310, 4 2020. ISSN 15581748. doi: 10.1109/JSEN.2019.2961411.

[25] K. He, X. Zhang, S. Ren, and J. Sun. Deep residual learning for image recognition. 12 2015. URL `http://arxiv.org/abs/1512.03385`.

[26] Y. Y. Hsieh, C. D. Wu, S. S. Lu, and Y. Tsao. A linear regression model with dynamic pulse transit time features for noninvasive blood pressure prediction. pages 604–607. Institute of Electrical and Electronics Engineers Inc., 2016. ISBN 9781509029594. doi: 10.1109/BioCAS.2016.7833867.

[27] D. Hughes, C. Babbs, L. Geddes, and J. Bourland. Measurements of young's modulus of elasticity of the canine aorta with ultrasound. *Ultrasonic Imaging*, 1:356–367, 10 1979. ISSN 0161-7346. doi: 10.1177/016173467900100406.

[28] N. Ibtehaz and M. S. Rahman. Multiresunet : Rethinking the u-net architecture for multimodal biomedical image segmentation. 2 2019. doi: 10.1016/j.neunet.2019.08.025. URL `http://arxiv.org/abs/1902.04049http://dx.doi.org/10.1016/j.neunet.2019.08.025`.

[29] N. Ibtehaz, S. Mahmud, M. E. H. Chowdhury, A. Khandakar, M. A. Ayari, A. Tahir, and M. S. Rahman. Ppg2abp: Translating photoplethysmogram (ppg) signals to arterial blood pressure (abp) waveforms.

[30] G. Iglesias, E. Talavera, Ángel González-Prieto, A. Mozo, and S. Gómez-Canaval. Data augmentation techniques in time series domain: A survey and taxonomy. 6 2022.

doi: 10.1007/s00521-023-08459-3. URL http://arxiv.org/abs/2206.13508http://dx.doi.org/10.1007/s00521-023-08459-3.

[31] C. Ilies, M. Bauer, P. Berg, J. Rosenberg, J. Hedderich, B. Bein, J. Hinz, and R. Hanss. Investigation of the agreement of a continuous non-invasive arterial pressure device in comparison with invasive radial artery measurement. *British Journal of Anaesthesia*, 108:202–210, 2012. ISSN 14716771. doi: 10.1093/bja/aer394.

[32] S. Ioffe and C. Szegedy. Batch normalization: Accelerating deep network training by reducing internal covariate shift. 2 2015. URL http://arxiv.org/abs/1502.03167.

[33] Y. Kurylyak, S. M. IEEE, F. Lamonaca, M. Ieee, D. Grimaldi, and S. M. IEEE. A neural network-based method for continuous blood pressure estimation from a ppg signal.

[34] X. Li, X. Sun, Y. Meng, J. Liang, F. Wu, and J. Li. Dice loss for data-imbalanced nlp tasks. 4 2019. doi: 10.48550/arXiv.1911.02855. URL http://arxiv.org/abs/1911.02855.

[35] Y. Liang, Z. Chen, R. Ward, and M. Elgendi. Photoplethysmography and deep learning: Enhancing hypertension risk stratification. *Biosensors*, 8, 10 2018. ISSN 20796374. doi: 10.3390/bios8040101.

[36] Y. Ma, J. Choi, A. Hourlier-Fargette, Y. Xue, H. U. Chung, J. Y. Lee, X. Wang, Z. Xie, D. Kang, H. Wang, S. Han, S. K. Kang, Y. Kang, X. Yu, M. J. Slepian, M. S. Raj, J. B. Model, X. Feng, R. Ghaffari, J. A. Rogers, and Y. Huang. Relation between blood pressure and pulse wave velocity for human arteries. *Proceedings of the National Academy of Sciences of the United States of America*, 115:11144–11149, 10 2018. ISSN 10916490. doi: 10.1073/pnas.1814392115.

[37] M. A. Mehrabadi, S. A. H. Aqajari, A. H. A. Zargari, N. Dutt, and A. M. Rahmani. Novel blood pressure waveform reconstruction from photoplethysmography using cycle generative adversarial networks. 1 2022. URL http://arxiv.org/abs/2201.09976.

[38] F. Miao, Z. D. Liu, J. K. Liu, B. Wen, Q. Y. He, and Y. Li. Multi-sensor fusion approach for cuff-less blood pressure measurement. *IEEE Journal of Biomedical and Health Informatics*, 24:79–91, 1 2020. ISSN 21682208. doi: 10.1109/JBHI.2019.2901724.

[39] M. R. Mohebbian, A. Dinh, K. Wahid, and M. S. Alam. Blind, cuff-less, calibration-free and continuous blood pressure estimation using optimized inductive group

method of data handling. *Biomedical Signal Processing and Control*, 57, 3 2020. ISSN 17468108. doi: 10.1016/j.bspc.2019.101682.

[40] S. L. Oh, E. Y. Ng, R. S. Tan, and U. R. Acharya. Automated beat-wise arrhythmia diagnosis using modified u-net on extended electrocardiographic recordings with heterogeneous arrhythmia types. *Computers in Biology and Medicine*, 105:92–101, 2 2019. ISSN 18790534. doi: 10.1016/j.compbiomed.2018.12.012.

[41] G. Parati, J. E. Ochoa, C. Lombardi, and G. Bilo. Assessment and management of blood-pressure variability. *Nature Reviews Cardiology*, 10:143–155, 2013. ISSN 17595010. doi: 10.1038/nrcardio.2013.1.

[42] J. Park, H. S. Seok, S. S. Kim, and H. Shin. Photoplethysmogram analysis and applications: An integrative review, 3 2022. ISSN 1664042X.

[43] A. Paviglianiti, V. Randazzo, S. Villata, G. Cirrincione, and E. Pasero. A comparison of deep learning techniques for arterial blood pressure prediction. *Cognitive Computation*, 14:1689–1710, 9 2022. ISSN 18669964. doi: 10.1007/s12559-021-09910-0.

[44] J. Penaz. Criteria for set point estimation in the volume clamp method of blood pressure measurement. *Physiol. Res*, pages 415–425, 1992.

[45] K. Qin, W. Huang, and T. Zhang. Deep generative model with domain adversarial training for predicting arterial blood pressure waveform from photoplethysmogram signal. *Biomedical Signal Processing and Control*, 70:102972, 9 2021. ISSN 17468094. doi: 10.1016/j.bspc.2021.102972.

[46] O. Ronneberger, P. Fischer, and T. Brox. U-net: Convolutional networks for biomedical image segmentation. 5 2015. URL `http://arxiv.org/abs/1505.04597`.

[47] I. Silva. Physionet 2010 challenge: A robust multi-channel adaptive filtering approach to the estimation of physiological recordings. 2010. URL `http://www.physionet.org`.

[48] K. Tegtmeyer, G. Brady, S. Lai, R. Hodo, and D. Braner. Placement of an arterial line. *New England Journal of Medicine*, 354:e13, 4 2006. ISSN 0028-4793. doi: 10.1056/NEJMvcm044149.

[49] P. Verdecchia, G. Schillaci, C. Borgioni, A. Ciucci, I. Zampi, R. Gattobigio, N. Sacchi, and C. Porcellati. White coat hypertension and white coat effect similarities and differences, 1995. URL `https://academic.oup.com/ajh/article/8/8/790/305431`.

[50] C. Wang, F. Yang, X. Yuan, Y. Zhang, K. Chang, and Z. Li. An end-to-end neural network model for blood pressure estimation using ppg signal, 2020.

[51] J. Wang, R. Li, R. Li, K. Li, H. Zeng, G. Xie, and L. Liu. Adversarial de-noising of electrocardiogram. *Neurocomputing*, 349:212–224, 7 2019. ISSN 18728286. doi: 10.1016/j.neucom.2019.03.083.

[52] R. Wang, W. Jia, Z.-H. Mao, R. J. Sclabassi, and M. Sun. Cuff-free blood pressure estimation using pulse transit time and heart rate. doi: 10.1109/ICOSP.2014.7014980.

[53] D. B. Wax, H.-M. Lin, and A. B. Leibowitz. Invasive and concomitant noninvasive intraoperative blood pressure monitoring observed differences in measurements and associated therapeutic interventions, 2011. URL `www.anesthesiology.org`.

[54] R. Yamashita, M. Nishio, R. K. G. Do, and K. Togashi. Convolutional neural networks: an overview and application in radiology, 8 2018. ISSN 18694101.

[55] Z.-B. Zhou, T.-R. Cui, D. Li, J.-M. Jian, Z. Li, S.-R. Ji, X. Li, J.-D. Xu, H.-F. Liu, Y. Yang, and T.-L. Ren. Wearable continuous blood pressure monitoring devices based on pulse wave transit time and pulse arrival time: A review. *Materials*, 16: 2133, 3 2023. doi: 10.3390/ma16062133.

List of Figures

List of Tables

List of Abbreviations

Abbr.	Meaning	Abbr.	Meaning
ABP	*Arterial Blood Pressure*	SBP	*Systolic Blood Pressure*
DBP	*Diastolic Blood Pressure*	MAP	*Mean Arterial Pressure*
CNN	*Convolutional Neural Network*	GAN	*Generative Adversarial Network*
GRU	*Gated Recurrent Unit*	DNNs	*Deep Neural Networks*
CVD	*Cardiovascular Disease*	HBPM	*olter blood pressure monitor*
PWV	*Pulse Wave Velocity*	PTT	*Pulse Transit Time*
PAT	*Pulse Arrival Time*	PEP	*Pre-Ejection Period*
ECG	*Electrocardiogram*	PPG	*Photoplethysmography*
PCG	*Phonocardiogram*	SCG	*Seismocardiogram*
CT	*Computed Tomography*	LSTM	*Long Short-Term Memory*

Acknowledgements

I want to thank Professor Pietro Cerveri for allowing me to participate in this project and for the time dedicated to me during the development of the work. I especially thank Dario, Caterina, and Alberto who accompanied me on this journey, helping me grow and welcoming me into the Biocubica family. Lastly, I would like to thank Mattia Sarti for the time we spent together developing our model and for his fundamental contribution to the realization of the project.